A systems biology analysis of acetate metabolism and photosynthesis in *Chlamydomonas reinhardtii*

A thesis submitted to The University of Manchester for the degree of Doctor of Philosophy

2015

Stephen P. Chapman

List of contents

Word Count: 41696

List of figures

List of tables

List of abbreviations:

ΔpH	Proton gradient
1,3DPG	1,3-bisphosphoglycerate
3PG	3-phosphoglycerate
6PG	6-phosphogluconate
6PGL	6-phosophoglucolactone
ACS	Acetyl-CoA synthase
ATPase	ATP synthase
CEF	Cyclic electron flow
Chl *a*	Chlorophyll *a*
COBRA	Constraint-based reconstruction and analysis
Cyt b_6f	Cytochrome b_6f complex
DHAP	Dihydroxyacetone phosphate
FBA	Flux balance analysis
FD	Ferredoxin
FNR	Ferredoxin–$NADP^+$ reductase
FVA	Flux variability analysis
G3P	Glyceraldehyde 3-phosphate
G6P	Glucose 6-phosphate
GAPDH	Glyceraldehyde phosphate dehydrogenase
GEM	Genome scale model
LEF	Linear electron flow
LHC	Light harvesting complex
MDH	Malate dehydrogenase
MOMA	Minimisation of metabolic adjustment
OEC	Oxygen evolution complex
OPPP	Oxidative pentose phosphate pathway

PC	Plastocyanin
PEP	Phosphoenolpyruvate
PGK	Phosphoglycerate kinase
PSI	Photosystem I
PSII	Photosystem II
PQ	Plastoquinone
PQH_2	Plastoquinol
PTOX	Plastid terminal oxidase
ROOM	Regulatory on-off minimisation
Ru5P	Ribulose 5-phosphate
RUBP	Ribulose bisphosphate
TAG	Tri-acyl glyceride
TCA	Tricarboxylic acid cycle
TPT	Triose phosphate translocator

Abstract

The green alga *Chlamydomonas reinhardtii* can be grown phototrophically using light as an energy source or mixotrophically using reduced carbon in the form of acetate in addition to light. Acetate, despite increasing biomass, also inhibits photosynthesis as compared to cells grown phototrophically. A better understanding of acetate assimilation and how it regulates photosynthesis would enable a more efficient conversion of carbon into valuable products such as biofuels. In this thesis constraint-based modelling techniques are used in conjunction with a genome-scale model of the organism and experimental data to understand this phenomenon.

Using flux balance analysis we show that the preferred route of acetate assimilation is likely to be via the enzyme acetyl-CoA synthase, and that exogenous acetate feeds into a modified tricarboxylic acid cycle, which bypasses the CO_2 evolution steps. This is consistent with experimental data and explains increases in biomass with mixotrophic growth on acetate in comparison to phototrophic metabolism.

Using a cycle decomposition algorithm with a mass-consistent adaptation of the model we were able to examine the role of cycles that further theoretically explain the down-regulation of photosynthesis observed when cells are grown in the presence of acetate. These results suggest that acetate modulates changes in the oxidative pentose phosphate pathway and increases mitochondrial respiration activity.

Label-free proteomics was used to quantify 2951 polypeptides with various roles including the assimilatory route of acetate, photosynthesis, the Calvin–Benson cycle, central carbon metabolism and oxidative phosphorylation. We show how acetate assimilation induces a shift in central carbon metabolism to activate the oxidative pentose phosphate pathway. This results in the cycling of electrons around Photosystem I, which accounts for the down-regulation of photosynthesis.

Declaration

I declare that no portion of the work referred to in the thesis has been submitted in support of an application for another degree or qualification of this or any other university or other institute of learning.

Copyright statement

Acknowledgements

Blimey, this was an adventure. I feel incredibly fortunate for the experiences that I have gained whilst conducting this research. Firstly I'd like to thank my supervisors, Giles Johnson and Jean-Marc Schwartz and my advisor Jon Pittman for giving up a lot of their time and for their constant supervision. I also have to thank Marcelo Trindade dos Santos and Mauricio Kritz for a more than fantastic collaboration; the 6 months I spent in Brazil were a dream come true. Tudo legal! I also have to thank Mick Follows for inviting me and for funding a trip to the MIT; I was introduced to some amazing minds. A special mention goes out the lab members of the Johnson and Schwartz labs that have made this PhD such an enjoyable experience, you know who you are. Let me also thank the funding bodies behind this project, the BBSRC and FAPERJ. I must also thank the Doctoral Training Centre for their acceptance. Ronan and Julian, many thanks for your help and support with the proteomic side of things. I also feel the need to thank my examiners for their support, time and patience.

A good number of friends outside academia also should get a mention; despite now living 'abroad', I owe you all big time. Jibbernation Phil and Libbenge, you have both been there from the start.

I would like to thank the staff at IBERS, Aberystwyth University for helping me settle into my new role, and I couldn't possibly continue without acknowledging my favourite swimming partner, Katja.

1. General Introduction

Recent concerns over fossil fuel depletion have re-ignited research into the use of micro-algae to produce sustainable bio-fuel (Hannon et al., 2010). In addition to renewable energy production, it is well established that micro-algae can produce a plethora of biotechnologically important metabolites which include therapeutic proteins (Almaraz-Delgado et al., 2014), methane liberated from anaerobic digestion of algal biomass (Zhang et al., 2014) and bio-hydrogen (Ghirardi et al., 2000a). In addition, the premise of algal-derived biofuel is heightened by increased photosynthetic efficiencies resulting in elevated yields of biofuel as seen in **Figure 1.1** (Chen et al., 2010). Despite high theoretical predictions, algal oil production is prohibitively expensive due to the extensive processing needed for algal concentration, harvesting, and lipid extraction. Previous work has provided many insights into how mass culture conditions can be manipulated to increase oil yields.

Cell growth and metabolism of phototrophic organisms ultimately depend on the reactions of photosynthesis. Through photosynthesis, algae fix CO_2 using light energy to produce molecules that can later be metabolised to provide the cell with ATP, reducing power and carbon skeletons contained within biomass. Cells grown in the presence of supplementary acetate to induce mixotrophic growth have been observed to down-regulate photosynthesis. Therefore understanding the regulation of photosynthesis is of upmost importance in our attempts to increase algal biomass.

The overall aim of this thesis is to understand this regulation of photosynthesis using a combination of experimental and computational methodologies.

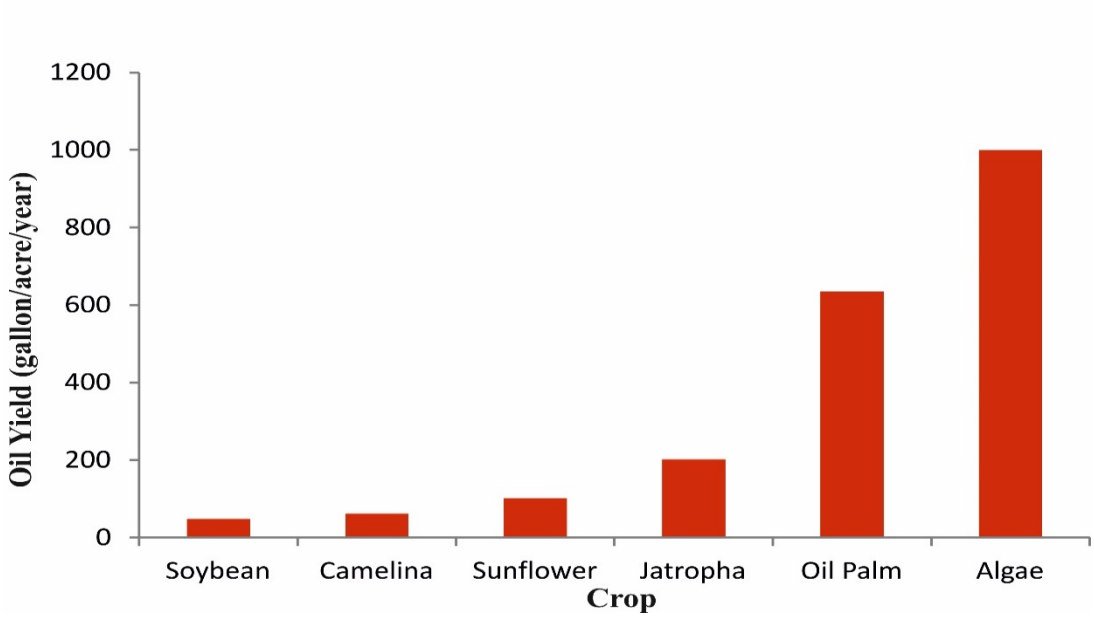

Figure 1.1 |Comparison of oil yields from different producers

Microalgae can potentially produce over 1000 gallons of biodiesel per acre of land every year, an amount that is significantly higher than that of soybeans and other oil-producing crops. The algal oil yields given in this Figure are based on experimentally demonstrated biomass productivity in photo bioreactors. Reproduced from (Chen et al., 2010).

1.1 *Chlamydomonas reinhardtii* as a model organism

C. reinhardtii, a unicellular microalga belonging to the *Chlorophyceae* class, has been used as a model organism for more than half a century in order to study a wide range of cellular functions including photosynthesis.

The organism in its natural environment of soil and fresh water is typically ~10 μm in diameter and consists of a cell wall, a nucleus, mitochondria, two anterial flagella, an eye spot and a single chloroplast (**Figure 1.2**) (Harris, 2001). A typical doubling rate of 6-8 hours under laboratory conditions and a well understood haploid lifecycle strengthen its utility as a model species. The genome of *C. reinhardtii* was found to contain 17 chromosomes, with all three genomes (nuclear, chloroplast and mitochondrial) being well annotated. The 121 MB nuclear genome is complemented by chloroplast and mitochondrial genomes that contain approximately 200,000 and 16,000 base pairs respectively (Merchant et al., 2007). A large number of mutant strains have been identified, including mutants void in key photosynthetic

reactions and complexes (Spreitzer and Mets, 1981), CO_2 uptake (Hanson et al.), carbon fixation (Spreitzer and Mets, 1981) and chlorophyll biosynthesis (Grovenstein et al., 2013).

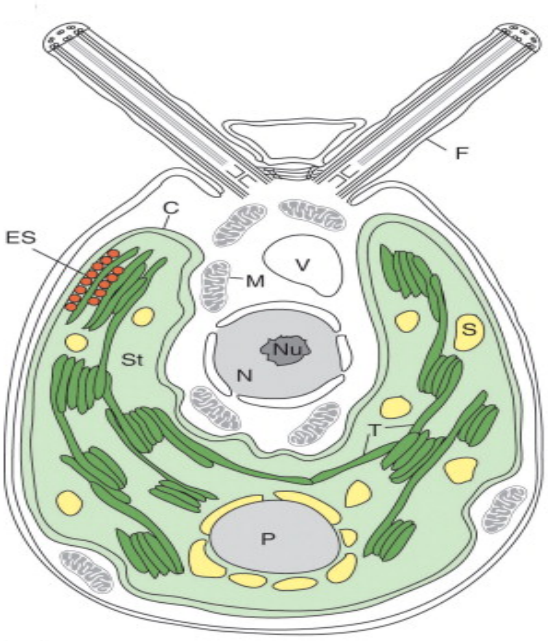

Figure 1.2 |The structure of *Chlamydomonas reinhardtii*

Labelled is the nucleus (N) within the nucleolus (Nu). This is surrounded by the single chloroplast (C) that houses the stroma (St) and eye-spot (ES) associated with the inner membrane of the chloroplast. Within the stroma are thylakoid membranes (T), starch grains (S) and the pyrenoid (P). The cytoplasm contains vacuoles (V) whilst the two flagella (F) can be seen pointing from the apical portion of the cell. Taken from Dent et al., (2001).

1.2 *C. reinhardtii* as a model organism for the study of photosynthesis

In addition to making an excellent genetic model, another valuable characteristic of *C. reinhardtii* is its ability to perform photosynthesis across a wide range of conditions including different light intensities and nutrient availability. *C. reinhardtii* is a facultative phototrophic organism; in addition to growing by means of photosynthesis it can also grow 'mixotrophically', exploiting inorganic carbon supplemented into the growth media, and 'heterotrophically', in the dark using only an organic carbon such as acetate (Morales-Sanchez et al., 2015). Introduction of acetate to culture medium results in elevated growth rates; however, acetate has been shown to give rise to a decrease in the capacity for photosynthetic oxygen evolution (Roach et al., 2013, Johnson and Alric, 2012, Plancke et al., 2014). This photosynthetic down-regulation with inorganic carbon suggests a strong metabolic interaction between photosynthetic and non-photosynthetic carbon metabolism. To develop an efficient phototrophic process of biofuel production, this interaction between photosynthetic and non-photosynthetic metabolism must be understood. To date, many investigations have been undertaken attempting to understand the physiology of *C.*

reinhardtii, generating a detailed description of the regulation of photosynthesis for the organism.

1.3 Oxygenic photosynthesis

Algal photosynthetic function is highly comparable to that of higher vascular plants with respect to its compartmentalisation within the chloroplast and its function to provide reducing power and ATP to drive metabolism. Light harvesting occurs within the thylakoid membranes inside the chloroplast. As with higher plants, *C. reinhardtii* contains many thylakoids stacked together to form grana (Engel *et al.,* 2015).

As proposed by Hill and Bendall (1960) and presented in **Figure 1.3**, the classic Z scheme of photosynthesis describes the light-dependent reactions of photosynthesis, in which light energy oxidises water producing molecular oxygen and hydrogen ions. The hydrogen in this case has lost an electron, resulting in the release of a proton. This proton is then passed through a series of carrier proteins via the reduction and oxidation of electron acceptors, before finally producing reducing power in the form of NADPH through a Linear Electron Flow (LEF). In so doing, a proton gradient (ΔpH) is generated across the thylakoid membrane that is in turn used to drive the production of ATP. These products are used to fuel the dark reactions of photosynthesis, which involve the fixation of CO_2 into metabolism.

1.3.1 Light reactions of photosynthesis: linear electron flow

The capture of light by oxygenic organisms involves the coordinated activity of two distinct photosystems. Photosystem I (PSI) and photosystem II (PSII) each consist of a reaction centre encoded by respective PSA and PSB genes associated to a light harvesting complex of integral membrane proteins and encoded by LHCA or LHCB genes respectively.

PSII, or water-plastoquinone oxidoreductase, can be regarded as the first protein complex in the light reactions of photosynthesis. The PSII core complex is composed of chlorophyll *a* (Chl a) and β-carotene bound to polypeptides D1 (PsbA) and D2 (PsbD), surrounded by an antenna complex. The core antenna complex, composed of CP43 (PsbC) and CP47 (PsbB), binds Chl a and β-carotene. This is further complemented by a variable amount of light harvesting complexes (LHCB) that bind Chl a, Chl b and xanthophylls. Antenna proteins

absorb light energy and transfer it to the reaction centre. On the luminal side of the reaction centre is an oxygen-evolving complex (OEC), which acts as the active site for the oxidation of water. The OEC is composed of the extrinsic polypeptides OEE1 (PsbO), OEE2 (PsbP) and OEE3 (PsbQ), as well as a cluster of manganese ions and calcium and chloride ions. Absorption of light by a special pair of Chl a in the reaction centre, termed P680, results in an electron being transferred from the luminal to the stromal side of the membrane. The oxidised P680 is then re-reduced by the OEC, with electrons being extracted from water. During the oxidation of two molecules of water, four electrons are transferred to the reaction centre of PSII and a molecule of oxygen is produced. As a result, 4 protons are released into the thylakoid lumen. Charge separation involves an electron being transferred from P680 to the primary electron-acceptor molecule, pheophytin. This in turn reduces a plastoquinone, Q_A, which further transfers an electron to a second plastoquinone, Q_B. Once Q_B has been reduced twice and protonated by hydrogen ions from the chloroplast stroma, plastoquinol (PQH_2) is released into the membrane.

PQH_2 is the substrate for the next electron carrier protein, the cytochrome b_6f complex (*Cyt* b_6f). The crystal structure of the *Cyt* b_6f of *C. reinhardtii* has been previously determined to contain a dimer, with each monomer composed of 8 subunits (Stroebel et al., 2003). The *Cyt* b_6f functions to mediate the transfer of electrons towards the core reaction centre of the second photosystem, PSI via either Plastocyanin (PC) or a cytochrome c6 in *Chlamydomonas* (Juergens et al., 2015) facilitated by an iron sulphur cluster. Following electron movement in a 'cyclic' or 'non-cyclic' manner, the *Cyt* b_6f is additionally responsible for generating a proton gradient that drives ATP synthesis by pumping two protons from the stroma into the thylakoid lumen.

The reaction centre core of PSI consists of a heterodimer of PsaA and PsaB proteins that bind the primary donor, P700, a pair of Chl a molecules with a peak absorption at 700 nm (Hankamer et al., 2001). When light energy is transferred to P700 from the antenna complex, an electron is excited to a higher energy level, designated as P700*. This transfers an electron to a modified chlorophyll acceptor, A_0. A_0 then reduces a secondary electron acceptor, A_1; a phylloquinone. A_1 in turn reduces the Fe-S centres, F_x, F_a and F_b. These reduce the soluble Fe-S protein ferredoxin (Fd). Feredoxin reduces NADP, a reaction catalysed by ferredoxin-NADP-reductase (FNR), producing NADPH.

The synthesis of ATP occurs as a result of proton movement across the thylakoid membrane. During the linear electron flow described above, *Cyt* b_6f accepts electrons from PSII and, via PC or cytochrome b6, passes them to PSI. In so doing, protons are pumped across the thylakoid membrane into the lumen. Additionally, cycling of electrons back to the PQ pool within *Cyt* b_6f generates additional ΔpH (Q-cycle). ATP synthase (ATPase) catalyses the conversion of ADP and inorganic phosphate into ATP, using the flow of protons as they pass through a channel located in the membrane spanning the CF_0 domain as a driving force. Proton translocation through the proton channel drives the rotation of the second domain, CF_1, located on the stromal face of the membrane. Rotation of the CF_1 is linked to a sequential change in shape of the enzyme, resulting in the binding and phosphorylating of ADP and releasing ATP into the stroma of the chloroplast (Allen, 2003).

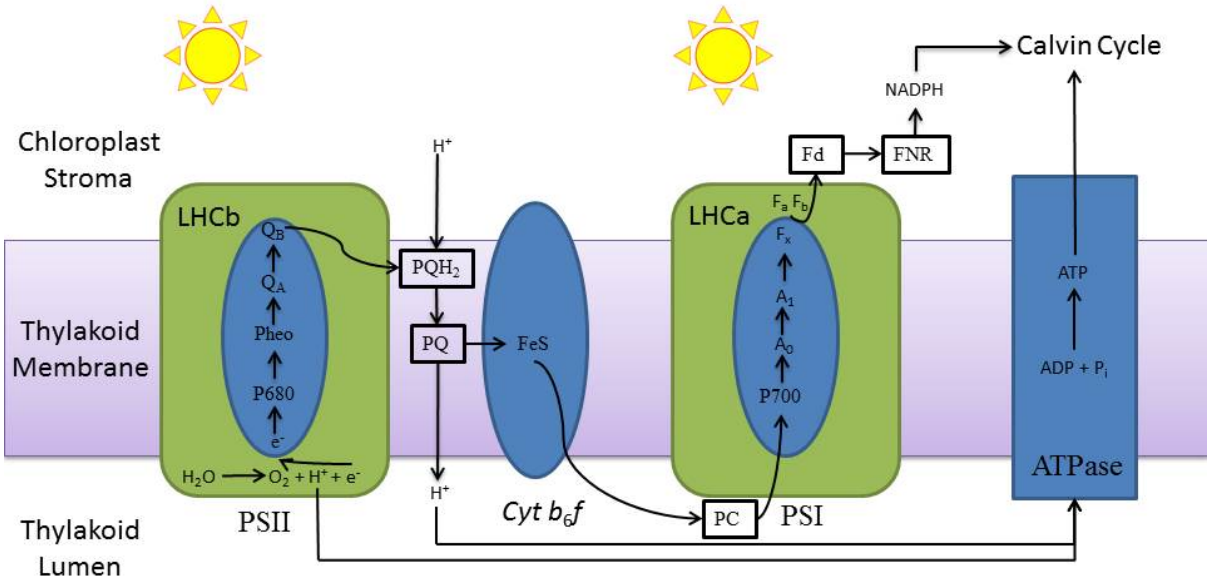

Figure 1.3 |A schematic model of the light reactions of photosynthesis during linear electron flow

In linear electron flow, electrons are passed along an electron transport chain resulting in the production of ATP and NADPH from the oxidation of water. Abbreviations: *Cyt* b_6f: Cytochrome b_6f complex, FeS: Iron, Sulphur complex, Fd: Feredoxin, FNR: Feredoxin – NADP-reductase, LHCa: light harvesting complex associated to PSI, LHCb: light harvesting complex associated to PSII, PC: Plastocyanin, Pheo: Pheophytin, PSI: Photosystem I, PSII, Photosystem II, PQ: Plastoquinone.

1.3.2 Light reactions of photosynthesis: cyclic electron flow

In addition to LEF as described above, another mechanism of electron flow has been described, namely Cyclic Electron Flow (CEF) (**Figure 1.4**). CEF involves the transfer of electrons from photosystem I to the plastoquinone pool via unknown electron carriers, then back to photosystem I via the *Cyt* b_6f. At least two distinct pathways have been proposed to account for CEF, these being the PGR5- and NDH-dependent pathways (Johnson, 2011). One role of CEF is thought to be that of protecting against photo damage to PSII at high light intensities (Johnson et al., 2014a). The way in which CEF plays a protective role is by sustaining an increased pH gradient across the thylakoid lumen, in order to trigger processes of non-photochemical quenching, which regulate photon absorption (Johnson, 2011).

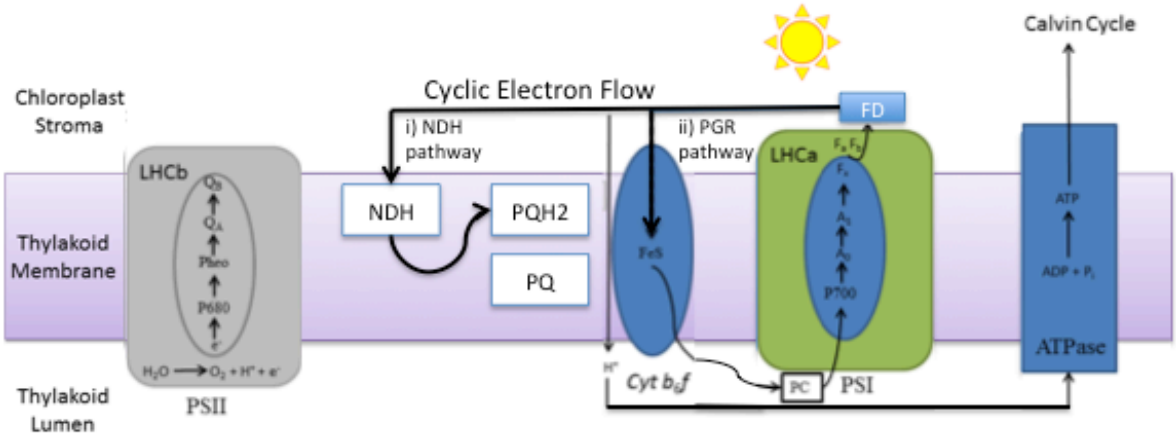

Figure 1.4 |A schematic model of the light reactions of photosynthesis sustaining a cyclic electron flow

In a cyclic electron flow electrons are injected back into the electron transport chain and mediated by feredoxin in either a NDH pathway (i) or PGR pathway (ii). As such, ferredoxin –NADP-reductase is no longer the recipient of electrons, resulting in the regulation of NADPH synthesis. **Abbreviations:** *Cyt* b_6f: Cytochrome b_6f complex, FeS: Iron, Sulphur complex, Fd: Feredoxin, LHCa: light harvesting complex associated to PSI, LHCb: light harvesting complex associated to PSII, PC: Plastocyanin, Pheo: Pheophytin, PSI: Photosystem I, PSII, Photosystem II, PQ: Plastoquinone.

1.3.3 The Mehler reaction

In addition to LEF and CEF between the photosystems, there are several additional electron transport pathways that have been described. The Mehler reaction (Mehler, 1951) is one such example. Reactive oxygen species (ROS), generated in oxygen-rich environments, are

potentially damaging towards proteins, lipids and nucleic acids. The major site of ROS production is PSI (Pospíšil, 2009). The Mehler reaction involves reduction of oxygen by PSI to produce ROS. Superoxide from this reduction is converted into H_2O_2 by the activity of superoxide dismutase. Through the action of the ascorbate peroxidase pathway, the H_2O_2 is scavenged and turned into H_2O and O_2 (Makino et al., 2002). Since electrons were initially donated by a water molecule and transferred to oxygen to produce a water molecule, this reaction is also called the water-water cycle. It is believed that the Mehler reaction generates ΔpH across the thylakoid membrane at times when PSI electron accepters are limited (Strizh, 2008). This process may be costly to the cell however, as it involves generation of damaging superoxide radicals.

1.3.4 Plastid terminal oxidase

In addition to the Mehler reaction, Plastid Terminal Oxidase (PTOX) is a protein that may also compete with LEF. PTOX is present on the thylakoid membrane of plants, cyanobacteria and *C. reinhardtii*. The function of PTOX is to catalyse the oxidation of the plastoquinone pool and transfer the electrons to two water molecules. Similar to the role of the Mehler reaction and CEF, PTOX is believed to serve a photo-protective role by acting as an alternative electron sink at times when the plastoquinone pool is over-reduced. In this way, activation of PTOX is thought to protect PSII from oxidative damage.

1.3.5 Light independent reactions of photosynthesis: carbon fixation

The primary pathway of carbon fixation in algae is through the carbon reduction (Calvin–Benson, or reductive pentose phosphate) cycle in the chloroplast stroma. The Calvin–Benson cycle utilises the products of light dependent reactions to fix atmospheric CO_2 into carbon skeletons that are used for starch and sucrose biosynthesis (**Figure 1.5**). The cycle consists of three phases, with the first phase being initiated by the enzyme Rubisco, which fixes CO_2 into Ribulose Bisphosphate (RUBP). The unstable 6-carbon molecule thus formed immediately breaks down to form two molecules of 3-phosphoglycerate (3PG). The second phase of the cycle involves a reduction of both molecules of 3PG into glyceraldehyde 3-phosphate (G3P) using ATP and NADPH synthesised from the light reactions (Raines, 2003). The final phase of the Calvin–Benson cycle involves regeneration of RUBP from a series of reactions

requiring at least nine other enzymes. It is the regeneration of RUBP, which requires ATP that closes the cycle.

G3P, a triose phosphate, is the first metabolically accessible product of photosynthesis. The presence of important triose phosphates has been observed in both the chloroplast and cytosolic compartments in *C. reinhardtii* and serves many purposes such as synthesis of lipids, carbohydrates and amino acids (Johnson and Alric, 2013). Triose phosphate can be shuttled between the two compartments via a triose-phosphate/phosphate translocator (TPT). Starch and sucrose are normally thought of as the two most immediate products of triose phosphate, both of which require the generation of hexose sugars via an aldolase reaction. Starch is a short-term carbon storage compound that can be stored to high levels in the chloroplast (Johnson and Alric, 2012). In the absence of light, at night time for example, starch can be degraded to provide a fixed source of carbon for respiration. The synthesis of starch is also represented in **Figure 1.5**.

Sucrose synthesis occurs in the cytosol and triose phosphate is trafficked out of the chloroplast through the action of the TPT. Sucrose synthesis occurs from the condensation reaction of G3P and dihydroxyacetone phosphate (DHAP) to form fructose 1,6-bisphosphate, proceeding to sucrose. For higher plants, the main function of sucrose metabolism is to transport carbon from source to sink organs and has been observed to regulate photosynthesis (Paul and Foyer, 2001, Smith and Stitt, 2007). For *C. reinhardtii* however, with the absence

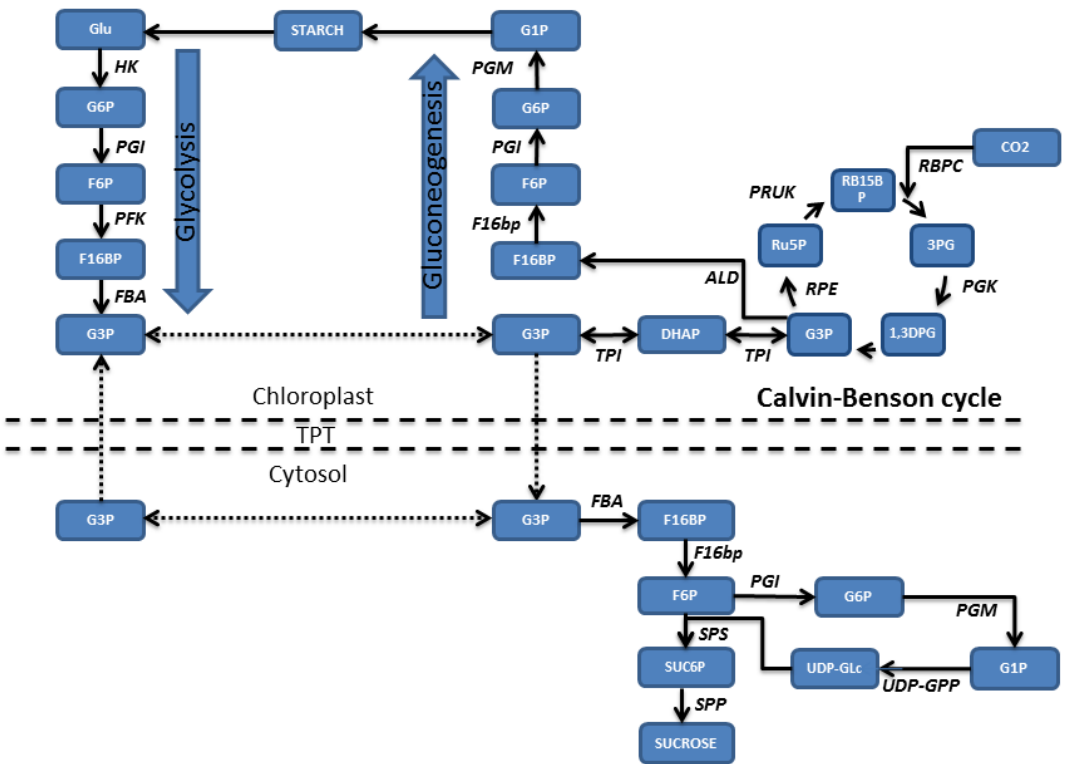

of distinct sink organs, the role of sucrose metabolism is unclear.

Figure 1.5 |The light independent reactions of photosynthesis; carbon fixation to starch and sucrose synthesis

CO_2 is fixed through the action of Rubisco into the Calvin–Benson cycle, with triose phosphate entering primary carbon metabolism into starch within the chloroplast, or alternatively sucrose in the cytosol. At night time, starch is degraded and provides a source of energy for respiration. The triose-phosphate transporter facilitates the movement of triose phosphate between compartments. **Abbreviations:** 1,3DPG: 3-Phospho-D-glyceroyl phosphate, ALD: Fructose bisphosphate aldolase, DHAP: Dihydroxyacetone phosphate, F6P: fructose 6-phosphate, F16BP: Fructose1,6 bisphosphate, F16bp: Fructose1,6 bisphosphatase, FBA: Fructose bisphosphoaldose, G1P: Glucose 1-phosphate, G3P: Glyceraldehyde 3-phosphate, G6P: Glucose 6 phosphate, Glu: Glucose, HK: Hexokinase, PFK: Phosphofructokinase, PGI: Glucose-6-phosphate Isomerase, PGK: Phosphoglycerate kinase, PGM: Phosphoglucomutase, PRUK: Phosphoribulokinase, RB15BP: Ribulose 1,5-bisphosphate, RBPC: Rubisco, RPE: Ribulose-5 phosphate 3-epimerase, Ru5P: Ribulose 5-phosphate, SUC6: Sucrose 6-phosphate, SPP: Sucrose phosphate phosphatase, SPS: Sucrose phosphate synthase, TPI: Triose-phosphate isomerase, TPT: Triose-phosphate transporter, UDP-GLc: UDP-glucose, UDP-GPP: UDP-glucose pyrophosphorylase.

Alternative glycolytic pathways exist to provide a level of metabolic flexibility. The Oxidative Pentose Phosphate Pathway (OPPP) is one such pathway in which glucose 6-phosphate is oxidised to 6-phosphoglucolactone and then to ribulose 5-phosphate. These oxidative steps produce two NAPDH molecules and one molecule of CO_2 for every 6-carbon molecule that enters the pathway. Higher plants have duplicated the glycolytic and OPPP in the chloroplast and cytosol. For *C. reinhardtii* however, the glycolytic pathway is compartmentalised. Metabolic steps that account for glyceraldehyde 3-phosphate production from glucose occur exclusively in the chloroplast, whereas the steps that include pyruvate production are localised in the cytosol (Johnson et al., 2013).

In addition to starch synthesis, fixed CO_2 can also enter a fatty acid synthesis pathway, ultimately producing triacylglycerides (TAGs) that accumulate within *C. reinhardtii*. In this pathway, triose phosphate from the light independent reaction of photosynthesis is converted to pyruvate within the chloroplast. Pyruvate dehydrogenase converts the newly formed pyruvate into acetyl-CoA, liberating a molecule of CO_2. Acetyl-CoA carboxylase further converts acetyl-CoA and a molecule of bicarbonate to malonyl-CoA, which is considered the first committed step in fatty acid and TAG synthesis (Radakovits et al., 2010). Malonyl-CoA is converted into malonyl-ACP, which enters a fatty acid synthesis cycle producing acetyl-ACP which is converted to free fatty acids via fatty acyl-ACP thioesterase. The newly

synthesised free fatty acids are exported to the cytosol and converted to acetyl-CoA with addition of a molecule of CoA. It is here, within the cytosol, that step-wise elongation reactions produce TAG lipid bodies.

1.4 Growth on alternative carbon sources

In addition to the phototrophic growth explained above and in contrast to higher plants, *C. reinhardtii* can exploit reduced carbon sources. Sources which can be used include exogenous acetate and other small organic molecules, but not sugars such as glucose for which there is no transporter (Johnson and Alric, 2013). Such pathways mean that models developed for higher plants cannot be applied directly to algae, which show a higher metabolic diversity, thus requiring the development of a more detailed understanding on a case-by-case basis.

The incorporation of acetate into metabolism has been suggested to occur in *Chlamydomonas* through one of two steps, both of which require ATP. The first is a direct conversion catalysed by the enzyme acetyl-CoA synthase (ACS):

(1) Acetate + ATP + CoA→Acetyl-CoA + AMP + p_i

Alternatively, a two-step reaction may occur involving acetate kinase (AK) and phosphate acetyltransferase (PAT) (Heifetz et al., 2000b):

(1) Acetate +ATP <==> Acetyl phosphate + ADP
(2) Acetyl phosphate + CoA <==> Acetyl-CoA + p_i

Acetyl-CoA is then believed to enter one of two possible cycles: the glyoxylate cycle that occurs in a membrane-bound organelle called the glyoxysome (a specialised type of peroxisome, also termed 'microbody') (Dal'Molin et al., 2011); or alternatively, a modified tricarboxylic acid (TCA) cycle might occur in the mitochondrion involving similar reactions to the glyoxylate cycle but taking place in a distinct location (**Figure 1.6**), (Johnson and Alric, 2012, Heifetz et al., 2000b). Glyoxysomes are believed to enhance growth, by feeding intermediate metabolites straight into carbohydrate synthesis through gluconeogenesis. Although well established in higher plants (Beevers, 1982) the location and existence of glyoxysomes in *C. reinhardtii* has been contested, especially in studies addressing acetate metabolism. In one study, the transcript levels of genes that encode glyoxylate cycle-specific

enzymes were measured. These included malate synthase, malate dehydrogenase, isocitrate lyase (ICL) and citrate synthase, all of which increased with acetate metabolism (Hayashi, 2015). In the same study, the size and number of peroxisomes were also measured. Acetate had the marked effect of increasing peroxisome volume, which was not observed when cells were grown on other inorganic carbon sources. The results from this study suggest that peroxisome-like bodies, presumed to be glyoxysomes, in *C. reinhardtii* are involved with acetate metabolism via the glyoxylate cycle. In contrast to the above study, Singh et al. (2014), used labelled acetate in the growth medium of cells and showed evidence for its assimilation into the mitochondria. In the same study, the authors used a mitochondrial inhibitor to uncouple ATP production from electron transport, hence inhibiting ATP production arising from oxidative phosphorylation. The results of this experiment indicated that inhibitor treated cells, under mixotrophic conditions, were still able to assimilate acetate in the mitochondria but were unable to metabolise it further.

A key distinguishing feature between the TCA cycle and the glyoxylate cycle is the presence of the enzymes isocitrate dehydrogenase and ICL. In the TCA cycle, ICL is missing whilst isocitrate dehydrogenase converts isocitrate to α-ketogluterate. The glyoxylate cycle however contains ICL, which converts isocitrate to succinate and glyoxylate. The TCA cycle results in production of reductant that feeds into the respiratory chain. In contrast, there is no such association with the glyoxylate cycle. Heifetz et al., (2000) used radioactive ^{13}C labelling to investigate acetate assimilation. They showed that the assimilation of acetate occurs through the glyoxylate cycle. They also showed that photosynthetic carbon fixation is reduced by almost 50% when cells are supplemented with acetate. The location of ICL and the presence of glyoxysomes were not discussed in this study.

In another study, mutants devoid of the enzyme ICL and grown in the presence of acetate showed a marked decrease of acetate assimilation, with enzymes of the glyoxylate cycle being down regulated whilst enzymes of the TCA cycle were upregulated. This study confirms the role of the glyoxylate cycle in acetate assimilation and highlights the non-essential role of this glyoxysome-located enzyme since mixotrophic cultures were still capable of sub-optimal growth as compared to wild type (Plancke et al., 2014).

The assimilatory route of acetate presents alternative possibilities that have deeper implications with respect to respiration and global metabolism. At present there is no accepted solution and one aim of this research is to provide insight into the assimilatory route

of acetate and its deeper consequences for metabolism, which could account for a down-regulation of photosynthesis.

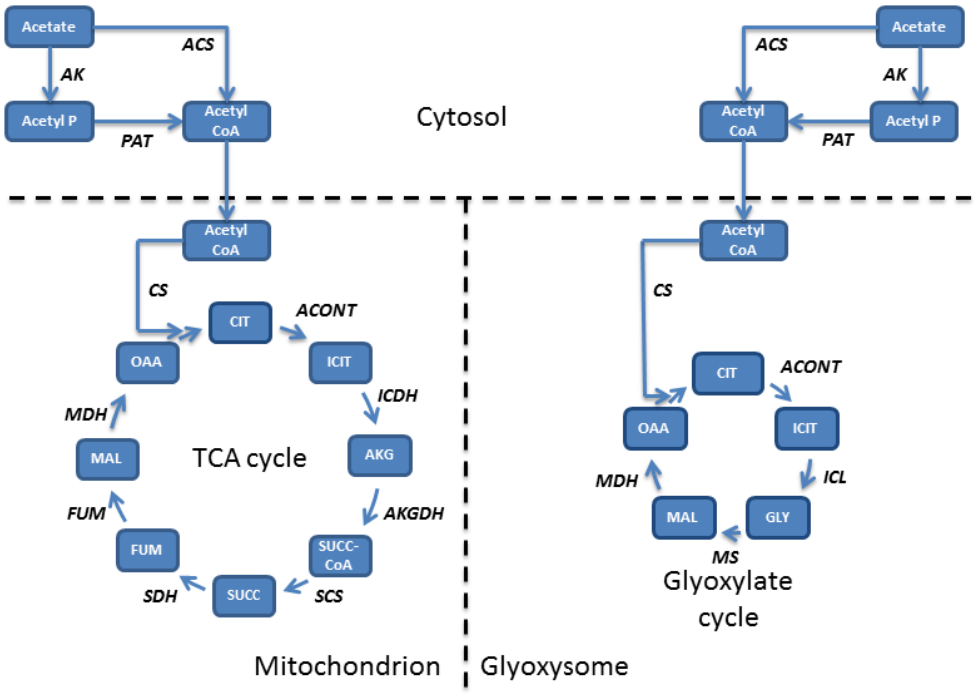

Figure 1.6 |Acetate uptake and assimilatory routes

A simplified schematic diagram showing acetate uptake and assimilation and its involvement with either the TCA cycle or the glyoxylate cycle. **Abbreviations:** Acetyl P: Acetyl phosphate, ACONT: Aconitate hydratase, ACS: Acetyl synthase, AK: Acetate kinase, AKG: α-ketogluterate, AKGDH: α-ketogluterate dehydrogenase, CIT: Citrate, CS: Citrate synthase, FUM: fumarate hydratase, GLY: Glyoxylate, ICDH: Isocitrate dehydrogenase, ICIT: Isocitrate, ICL: Isocitrate lyase, MAL: Malate, MDH: Malate dehydrogenase, MS: Malate synthase, OAA: Oxaloacetate, PAT: Phosphate acetyltransferase, SCS: Succinyl-CoA synthetase, SDH: Succinate dehydrogenase, SUCC: Succinate, SUCC-CoA: Succinyl CoA.

1.5 The interaction between carbon metabolism and light reactions of photosynthesis

The first experiments to investigate a relationship between metabolism and photosynthesis occurred in the 1950's. A variety of mechanisms have since been described in the literature which attempt to provide a further understanding of how carbon metabolism can regulate photosynthesis. These involve alternative electron flows (Johnson, 2011), inter-organelle metabolite transport (Johnson and Alric, 2013), and acclimation responses to changes in the environment (Johnson and Alric, 2012).

1.5.1 Cyclic electron flow increases ATP production

Photosynthesis is a tightly regulated process and needs to be maintained to produce the correct ATP: NADPH, as required by the demands from metabolism. In addition, NADPH is a potent reductant, capable of reducing many cellular structures resulting in the production of toxic oxygen species. Cyclic Electron Flow (CEF) involves the production of ATP without producing reducing equivalents. In addition to playing a role in regulating light harvesting, as discussed above (**Section 1.3.2**), CEF functions to regulate the balance of ATP/NAPDH production resulting from the photosynthetic reactions.

1.5.2 The malate shunt modulates chloroplastic NADPH

C. reinhardtii contains a chloroplast surrounded by multiple mitochondria (Harris, 2001). The shuttling of metabolites between these compartments could also shuttle reductant in or out of the chloroplast. One example is the malate shunt in which malate and oxaloacetate are moved between the chloroplast and mitochondrion. Malate dehydrogenase (MDH) converts chloroplastic oxaloacetate into malate using NAPDH derived from photosynthetic electron transport. Malate can move to the mitochondrion via malate oxaloacetate translocators, where it is converted back into oxaloacetate by MDH, producing NADH. In this way, excess reductant produced by photosynthesis can be consumed in the mitochondria and used to balance ATP: NADPH across the cell. The malate shunt may operate in two directions, either allowing consumption of excess NAPDH produced by the chloroplast in the mitochondrion or, as discussed previously, supplying reducing power (NADPH) to boost photosynthesis (Scheibe, 2004). The existence of the malate shunt has been demonstrated previously in *C. reinhardtii* (Cardol et al., 2011).

1.5.3 Fate of triose-phosphate can regulate cytosolic and chloroplast ATP

As seen in **Figure 1.7**, the fate of triose phosphate has also been shown to regulate the production of ATP in the chloroplast, thereby regulating photosynthesis (Boschetti and Schmid, 1998). To meet the metabolic demands imposed by the organism, the shuttling of triose-phosphates between the chloroplast and cytosol can occur through the TPT. In times where NAPDH and ATP are both limiting, glyceraldehyde phosphate dehydrogenase (GAPDH) has been reported to oxidise G3P into 1,3-bisphosphoglycerate (1,3DPG) using pools of inorganic phosphate, whilst phosphoglycerate kinase (PGK) will dephosphorylate

1,3DPG back into G3P (Klein et al., 1983). When NAPDH and ATP are in excess, the same enzymes can catalyse the reverse reactions and these conversions can occur simultaneously within the chloroplast and cytosol. Since G3P production from 3PG requires ATP and NADH, and the conversion of G3P into 3PG liberates NADH and ATP; translocation of triose phosphate can result in the net translocation of ATP and NADH between compartments.

Photosynthesis results in the production of ATP and NADPH, fuelling the production of chloroplastic G3P. Through the TPT, newly formed G3P can be exported to the cytosol, releasing NAPH and ATP into the cytosol. During acetate assimilation under mixotrophic growth conditions, the feeding of acetate into the TCA cycle would support ATP production from oxidative phosphorylation, resulting in the export of ATP from the mitochondria into the cytosol. An abundance of cytosolic ATP would therefore reverse the activity of PGK, increasing 1,3DPG, exporting G3P back into the chloroplast and releasing NAPDH (and ATP). A down-regulation of photosynthesis can be expected to occur in this situation in order to prevent NAPDH accumulation.

Despite the wealth of knowledge that has been gained in identifying such mechanisms, which might explain the down-regulation of photosynthesis, a lot of unknowns still remain. Very little is known, for example, as to whether the above processes are active synchronously or asynchronously, or if other mechanisms exist that have yet to be elucidated. The complex nature of metabolism and photosynthesis presents additional challenges such as understanding how the interconnectivity of pathways may feed back and regulate other pathways.

For relatively simple pathways, radio-isotope labelling methods, measuring carbon flux through various pathways have been proved to be a valuable asset. By way of example, identification of the Calvin–Benson cycle were identified following the introduction of labelled CO_2 (Calvin, 1962). Despite being a powerful approach to elucidate many different pathways, radio-isotope labelling presents limitations in that, as the labelled atoms spread through metabolism from a point of introduction, they can be transferred though multiple pathways and therefore it is no longer possible to trace them. This is especially true where cycles are occurring. As such, further approaches to analyse metabolism on a global scale must be introduced.

To understand the regulation of metabolism, we need to adapt strategies that take the global perspectives into account; a holistic systems biology approach is therefore essential. Computational biology, through metabolic modelling and theoretical exploration, provides a powerful basis to address such critical scientific questions.

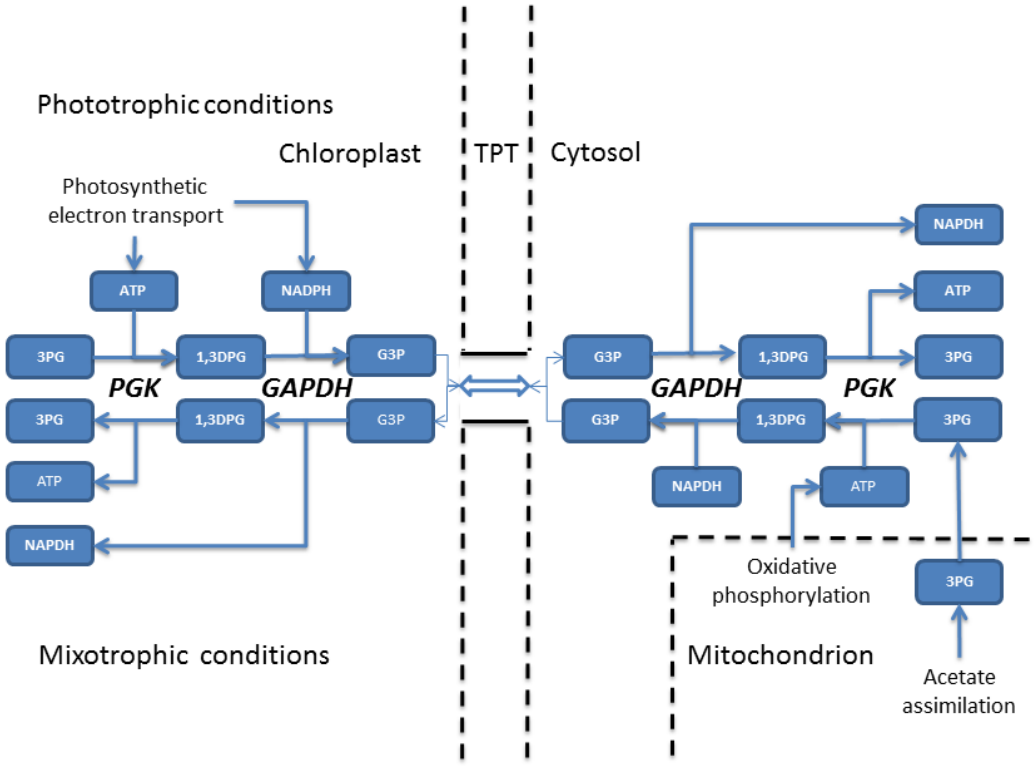

Figure 1.7 |A schematic representation of the triose phosphate pathway

Phototrophic conditions result in increased production of ATP and NADPH. In such conditions, activity of the enzymes phosphoglycerate kinase (PGK) and glyceraldehyde phosphate dehydrogenase converts 3-phophoglycerate (3PG) into 1,3-bisphospheglycerate (1,3DPG) and glyceraldehyde 3-phosphate (G3P) respectively using photosynthetically derived ATP and NADPH. G3P is exported through the TPT into the cytosol. Oxidation of Cytosolic G3P into 1,3DPG by GAPDH and dephosphorylation of 1,3DPG into 3PG releases NAPDH and ATP into the cytosol. Mixotrophic growth may result in high cytosolic ATP and NAPDH levels, causing the reverse of the above. Starting in the cytosol, the conversion of 3PG into G3P requires ATP and NAPDH. Transport of cytosolic G3P into the chloroplast and the eventual conversion into 3PG would thereby release ATP and NADPH into the chloroplast, feeding back on the reactions of photosynthesis to maintain ATP: NADPH.

1.6 Using systems biology to understand global metabolism

Recent advances in the development of high throughput 'omic techniques, such as microarrays and liquid or gas chromatography coupled to mass spectroscopy have resulted in knowledge of the genome, proteome, transcriptome and metabolome. This combination of 'omic data and advances in computational analytical methods allows for a greater understanding of the data, which in turn allows for the generation of networks (Bruggeman and Westerhoff, 2007). Networks are typically defined as a set of nodes representing genes, proteins and metabolites, and a set of directed or undirected edges connecting each node. Ultimately, edges represent the interactions between the connecting nodes. By representing metabolism via networks and applying fundamental principles that govern life, the prediction of metabolic consequences can be calculated. The ability to model and predict the metabolome will ultimately give phenotypic descriptions and address the alterations of the metabolome required to present a particular phenotype.

1.7 Metabolic modelling

Modelling metabolic networks can be undertaken using a variety of approaches, including kinetic, logic and stoichiometry-based methods (Machado et al., 2011). Classical kinetic modelling approaches describe the rate of change in the concentration of a metabolite based on the kinetic properties of individual enzymes, using the corresponding experimentally derived parameters (e.g., rate constant, maximum reaction velocity and dissociation constants) (Resat et al., 2009). Metabolic networks (typically fewer than 50 reactions) can be modelled using kinetics (Baghalian et al., 2014). The ability to model particular metabolic pathways such as glycolysis has given a greater understanding of how metabolic steps with the most stringent control over the system can regulate metabolism (Smallbone et al., 2013). The TCA cycle has also been kinetically modelled, giving further information about alternative cycles that could exist (Sweetlove et al., 2010).

One of the largest kinetic models that have been built is *e*-photosynthesis, representing C3 photosynthesis as performed by wheat, rice and soybean crops (Zhu et al., 2013). This model consists of 50 differential rate equations that account for light absorption, hydrolysis, LEF between PSII and PSI, and proton translocation from the lumen to the stroma resulting in ATP and NAPDH synthesis. In addition, CEF was included and carbon fixation up to sucrose synthesis was also represented in the model. Through kinetic modelling, the authors

demonstrated the capability of *e*-photosynthesis to accurately predict qualitative and quantitative experimental data. Increases of photon flux led to the prediction of increased oxygen evolution, luminal pH and increased chlorophyll fluorescence, in line with experimental evidence (Sargent, 1940, Steinberg-Yfrach et al., 1998, Osborne et al., 1997).

The use of kinetic modelling is, however, limited to current biochemical knowledge regarding the reactions being modelled. All parameters, such as enzyme concentrations and their kinetic properties must be accurately estimated in experimental conditions that mimic that of the cell to give meaningful results. This is a costly process in terms of time and money. Available kinetic data for accurate simulation of networks are scarce, limiting the scope of kinetic modelling. Another emerging feature of networks is that control of a system is now believed to be an inherent property of the whole system, since metabolic control can be distributed among various metabolic steps (Westerhoff et al., 2009). The greater the number of metabolic interactions that exist, the more that metabolic regulation can be dispersed. By choosing to model selected pathways, we are ultimately choosing to ignore any regulating steps at the level of the metabolome.

1.7.1 Genome scale models using flux balance analysis

Metabolism is derived from the enzymes encoded by the genome. A GEnome scale Model (GEM) represents all known metabolic reactions in an organism and is reconstructed primarily from genomic information and the literature. Knowledge of metabolite stoichiometry and localisation, along with biomass composition and energy requirements can be integrated into a stoichiometric model of metabolism (Santos et al., 2011). As such, GEMs cover the whole metabolism of an organism in a top-down modelling approach. The assumption that many pathways will operate at a steady state means that, despite GEMs sharing with kinetic modelling the need to know metabolite stoichiometry, other kinetic parameters associated with the reactions can be ignored. A steady-state description here means that the concentration of a given metabolite is constant in time, since its production and consumption rate are equal (Yizhak et al., 2010). By calculating steady-state rates through the reactions that catalyse the production of a metabolite, metabolic fluxes can be predicted. Metabolic flux is typically defined as the amount of metabolite being converted by a particular enzyme per unit time and per gram (dry cell weight) of cells. GEM can give a detailed analysis of the metabolic potential of the organism using constraint-based modelling

approaches that calculate the flux through any reaction contained within the model. As a result, GEMs have proven useful for assessing the essentiality of metabolic steps (Henry et al., 2006), improving metabolic engineering strategies by simulating gene knockouts (Kennedy et al., 2009, Matsuda et al., 2011), and for elucidating metabolism giving rise to observed physiological traits (Dal'Molin et al., 2011).

Computational tools have been developed to analyse the system properties of GEMs. Flux Balance Analysis (FBA) is one approach for the study of such metabolic networks (Orth et al., 2010). FBA employs a liner programming optimisation method to determine the flux through a network at steady state which optimises a defined objective function (e.g. maximal biomass) under a set of imposed physiochemical constraints (e.g. substrate constituents, uptake rates and product secretion rates).

As represented in **Figure 1.8**, the first step of FBA is to mathematically represent a metabolic network in the form of a stoichiometric matrix (**S**), composed of rows of metabolites (***n***) and reactions (***m***) as columns. For each reaction within the matrix, metabolites that are consumed in that particular reaction are given a negative stoichiometric coefficient, whilst products are represented by a positive coefficient. The next step involves defining an objective function (***Z***) that is biologically relevant to the problem being studied. For predicting growth, for example, maximisation of biomass might be the best objective function, since biomass reactions contain all nucleic acids, proteins, lipids, etc, that are required for cell division. Another example of an objective function could be the optimal production of a target metabolite of interest or the minimisation of nutrient use. The reaction that is deemed suitable as the objective function can either be maximised or minimised on the assumption that selective processes during evolution guide any systems towards an optimal state.

A further critical step involved with FBA is the application of constraints upon the matrix. Constraints are represented as metabolite stoichiometry and as upper and lower reaction bound for all reactions. These bounds define maximum and minimum allowable fluxes of reactions whilst metabolite stoichiometry constraints ensures mass balance, such that at steady state the total amount of any metabolite production is equal to its consumption. For the constrained matrix (**S**), the overall reaction flux vector (**v**) in matrix **S** at steady state equals zero (**Sv = 0**) ensuring a global mass balance.

The final step involves optimising the objective function, a function that satisfies the steady state assumption using linear programming. The many flux solutions that could exist are limited by the constraints imposed on the system, resulting in the allowable flux entering a theoretical phenotypic solution space, as depicted in **Figure 1.8(e)**. The phenotypic solution space can be thought of mathematically as the complete metabolic capability of a particular genotype, constrained by matrix **S**. The null space of **S** is typically large, and it represents the flexibility that a cell has in determining the use of its metabolic capabilities (Valma & Palsson, 1994). Analysis of the pathways carrying the greatest flux gives an indication of the metabolic pathways most likely to have been used in order to achieve a given objective.

1.7.2 Flux Variability Analysis

In theory, this phenotypic solution space contains all possible flux combinations that the cell can use. FBA identifies one optimal solution in the presence of co-existing alternative optimal solutions. By using the principles that drive FBA whilst constraining the objective function at a given value, it is possible to calculate the range of possible minimal and maximal fluxes for each reaction in the network that give rise to the same optimal objective using a method called Flux Variability Analysis (FVA) (Gudmundsson and Thiele, 2010). As a result all alternative reactions that could carry a flux can be sought, giving rise to alternative pathways that still conform to the phenotypic phase plane.

A number of computational tools have been produced to analyse the fluxes resulting from a GEM using a constraint-based approach. Becker et al., (2007) developed a Constraint-Based Reconstruction and Analysis (COBRA) toolbox, a software package running from within the MATrix LABoratory (MATLAB) environment. COBRA allows for the quantitative prediction of both steady-state and dynamic optimal growth behaviour cellular flux and remains the most widely used software to date (Becker et al., 2007).

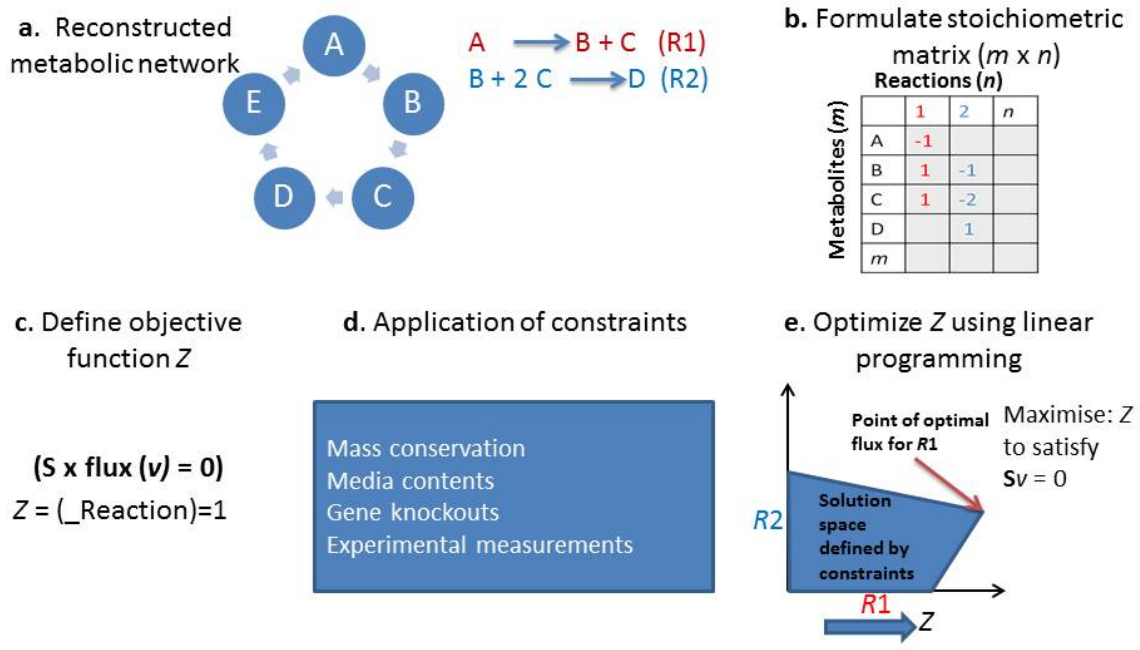

Figure 1.8 |Basics of COBRA functionality

(a) Reconstructed metabolic pathways are represented as lists of ordered reactions. **(b)** Metabolic reactions are represented as a stoichiometric matrix (**S**). **(c)** Definition of an objective function ***Z*** that is relevant to the problem being studied, i.e. biomass. The objective function will have a position of 1 during simulation of growth. **(d)** Constraints are applied to reactions to resemble environmental conditions. **(e)** Linear programming can be employed to identify a particular flux distribution that maximises or minimises the selected objective function whilst complying to the constraints imposed by the reaction bounds. Reproduced from Orth et al. (2010).

1.8 Advances made with metabolic models of *C. reinhardtii*

GEMs have been constructed for many organisms including bacteria (Durot et al., 2009), cyanobacteria (Vu et al., 2012), yeast and photosynthetic organisms such as plants (de Oliveira Dal'Molin et al., 2010, Saha et al., 2011) and microalgae (Dal'Molin et al., 2011, Chang et al., 2011, Boyle and Morgan, 2009).

The first FBA model of *C. reinhardtii,* developed by Boyle and Morgan (2009), consists of 484 reactions and 454 metabolites divided between the chloroplast, mitochondrion and cytosol. Under phototrophic growth simulations, the model predicted the majority of flux resulting from carbon fixation into the Calvin–Benson cycle as expected. NADPH, resulting from LEF, was consumed in the production of triose phosphate and exported to the cytosol to meet the demands of ATP and NADPH outside the chloroplast. Mixotrophic simulations suggested an inhibition of carbon fixation through Rubisco led to acetate assimilation into a complete TCA cycle at low light levels. As light increased however, carbon fixation was

active resulting in acetate assimilation into the glyoxylate cycle. Higher light levels result in increased flux through LEF, producing more NAPDH than needed for biomass synthesis and allowing for the fixation of carbon. Despite qualitative and quantitative insights into carbon metabolism, the model did not account for CEF and remains an incomplete model, since the authors did not consider a compartmentalised glyoxylate cycle. In addition, the model contains an under representation of known reactions and metabolites as compared to other FBA models.

AlgaGEM, a genome-scale metabolic network model of *C. reinhardtii* represents a more complete GEM, accounting for 1725 reactions involving 1862 metabolites (Dal'Molin et al., 2011). This model included a microbody to house the glyoxylate cycle, in addition to the cytoplasm, mitochondrion, chloroplast and nucleus. AlgaGEM closely resembles that of AraGEM, a GEM of *Arabidopsis thaliana* (de Oliveira Dal'Molin et al., 2010), with 85% of reactions being identical between the two models. Designed to investigate maximum hydrogen production in *C. reinhardtii*, heterotrophic simulations suggested acetate assimilation into both the glyoxylate and TCA cycles. In this study, the CEF was associated with maximum hydrogen production only. Under mixotrophic conditions, the presence and activation of CEF resulted in a decrease of hydrogen production. The authors concluded that hydrogen itself is able to accept excess electrons when CEF is inhibited, providing a regulatory role of the reaction. This study has shown how predictive modelling can be used to address how physiological manipulations can give rise to emergent traits. However, the role of acetate and its effects on photosynthesis were not addressed. Furthermore, its similarity to AraGEM may present a limitation in its use.

A further GEM of *C. reinhardtii*; *i*RC1080 has been developed to investigate light-driven metabolism (Chang et al., 2011). This model accounts for 2190 reactions encoded by 1080 genes, 1068 metabolites and 10 compartments, including a glyoxysome covering a total of 83 subsystems. At time of publication, this model contained more than 32% of estimated genes with known metabolic functions, which remains a significant increase over previous reconstructions. Another key feature of this model is centrality of the chloroplast, accounting for over 30% of reactions in the model and displaying the importance of the chloroplast in carbon metabolism. Furthermore, the model was able to qualitatively predict correct oxygen evolution and growth rate with varying light sources and photon flux, thus displaying a

greater coverage of the photosynthetic reactions. For these reasons, *i*RC1080 represents a better model to investigate the effects of acetate on metabolism and photosynthesis.

1.9 Research aims

When cultures of *C. reinhardtii* are grown in the presence of acetate, they experience a down-regulation of photosynthetic oxygen evolution. Any study that attempts to investigate this regulation of photosynthesis associated with mixotrophic growth can start to address how metabolic manipulations can increase photosynthesis. This project aims to uncover fundamental biological mechanisms underlying the regulation of photosynthesis seen in *C. reinhardtii*, by integrating genome-scale metabolic reconstructions and *in vivo* and *in vitro* experimental validations.

In the first data chapter, a GEM of *Chlamydomonas*; *i*RC1080 is used to quantitatively predict the down-regulation of photosynthesis by acetate using a combination of FBA and FVA to investigate changes in metabolism that occur when cultures of the alga are grown phototrophically or mixotrophically. This work involved both curation of the published model to correct errors in certain reactions, and also the application of FVA and essentiality analysis, which have not previously been applied to models of this species. Experimental data and information from the literature were used to further validate model predictions. This work has recently been published in Frontiers in Plant Science (Chapman et al., 2015).

Following on from this, a novel modelling approach is used which attempts to address how dynamic fluxes can be associated with biochemical reactions in the network by using an algorithm initially designed to study fluxes from ecological trophic networks (**Chapter 3**). The aim of this work was to partition fluxes obtained from the previous modelling work into cyclic and acyclic sub-networks. As a pre-requisite, a mass-consistent version of the model needed to be implemented to reveal the role of cyclic fluxes in driving and maintaining metabolic fluxes arising from acetate addition. Examination of the role of cycles has given further insights to explain photosynthetic down-regulation. This work has been submitted for publication and is under review with Biosystems.

The final approach compares model predictions with a global analysis of the proteome for cultures of *C. reinhardtii* grown under the two conditions. The use of proteomics provides a direct readout of the metabolic acclimation mechanisms that are present in the cell. This work

aimed to quantify in relative terms which metabolic pathways are subject to change when acetate is introduced to culture media. This has given an indication of the predictive quality of the GEM, adding another level of model validation. Furthermore, discrepancies between proteomic data and the model's predictions have been introduced into the model to further improve the predictive scope of the model.

References for this chapter can be found in **Chapter 6**.

2. Flux balance analysis reveals acetate metabolism modulates cyclic electron flow and alternative glycolytic pathways in *Chlamydomonas reinhardtii*

Stephen Chapman, Caroline M. Paget, Giles N. Johnson, Jean-Marc Schwartz*

University of Manchester, Faculty of Life Sciences, Manchester, UK

*** Correspondence:** Dr Jean-Marc Schwartz, University of Manchester, Faculty of Life Sciences, Michael Smith Building, Oxford Road, Manchester, M13 9PT, UK

jean-marc.schwartz@.manchester.ac.uk

Keywords: glycolysis, mixotrophic growth, metabolic model, photosynthesis, green algae, flux balance analysis, acetate metabolism, cyclic electron flow

Author contributions: All work presented in this chapter was conducted by the lead author. Dr. Paget was responsible for providing training with the COBRA toolbox and Dr Johnson and Dr Schwartz were responsible for supervision over the experimental and computational sections respectively.

Abstract

Cells of the green alga *Chlamydomonas reinhardtii* cultured in the presence of acetate perform mixotrophic growth, involving both photosynthesis and organic carbon assimilation. Under such conditions, cells exhibit a reduced capacity for photosynthesis but a higher growth rate when compared to phototrophic cultures. A better understanding of the down-regulation of photosynthesis would enable more efficient conversion of carbon into valuable products like biofuels.

In this study, Flux Balance Analysis (FBA) and Flux Variability Analysis (FVA) have been used with a genome scale model of *C. reinhardtii* to examine changes in intracellular flux distribution in order to explain their changing physiology. Additionally, a reaction essentiality analysis was performed to identify which reaction subsets are essential for a given growth condition. Our results suggest that exogenous acetate feeds into a modified tricarboxylic acid cycle, which bypasses the CO_2 evolution steps. This explains an increase in biomass which is consistent with experimental data. In addition, reactions of the oxidative pentose phosphate and glycolysis pathways, inactive under phototrophic conditions, show substantial flux under mixotrophic conditions. Importantly, acetate addition leads to an increased flux through cyclic electron flow (CEF), but results in a repression of CO_2 fixation via Rubisco, explaining the down-regulation of photosynthesis. However, although CEF enhances growth on acetate, it is not essential; impairment of CEF results in alternative metabolic pathways being increased.

We have demonstrated how the reactions of photosynthesis interconnect with carbon metabolism on a global scale, and how systems approaches play a viable tool in understanding complex relationships at the scale of the organism.

2.1 Introduction

Photosynthesis uses light energy to fix atmospheric CO_2 into organic molecules, which are incorporated into carbon skeletons that can be used to produce biomass or broken down to provide ATP and reducing power. *Chlamydomonas reinhardtii* has been widely used as a model organism to study photosynthesis (Harris, 2001). However, more recently it has received attention as a potential system for producing biofuels (Hannon et al., 2010). *C. reinhardtii* is a facultative phototrophic organism; it can use light and atmospheric CO_2 as the sole carbon source but can also grow mixotrophically when supplemented with additional inorganic carbon, such as acetate. Mixotrophic growth typically results in an enhanced biomass, however this is at a cost of reduced photosynthetic capacity (Johnson and Alric, 2012, Plancke et al., 2014).

It has been widely reported that providing cells with acetate results in an inhibition of photosynthesis (Johnson and Alric, 2013, Johnson et al., 2014b, Plancke et al., 2014). Assimilation of acetate might occur via either the glyoxylate or the tricarboxylic acid (TCA) cycle, providing carbon skeletons and reducing equivalents to drive metabolism (Roach et al., 2013). A key requirement of this suggested assimilation is a source of ATP since the incorporation of acetate into metabolism can occur along one of two pathways, both requiring ATP: either a direct conversion with acetyl CoA synthase (ACS) or a pathway involving acetate kinase (ACK) and phosphate acetyltransferase (PAT) (Johnson and Alric, 2013). The optimal functioning of photosynthesis depends on there being a balance in the stoichiometry of the products of electron transport, namely NAPDH and ATP. Assimilation of acetate is liable to disturb this balance, consuming ATP and producing reducing equivalents. It has been suggested that this imbalance results in a re-routing of the photosynthetic electron transport chain, from linear flow, involving both Photosystem (PS) II and PSI, to a cyclic flow, only involving PSI. This cycling of electrons around PSI results in the generation of ATP without producing NADPH, giving rise to a decrease in oxygen evolution (Munekage et al., 2008). To gain a further understanding of this photosynthetic acclimation response to acetate, we need to investigate how acetate is integrated into metabolism at an organismal level. The availability of a full genome sequence for this species (Merchant et al., 2007) means that we can now adopt a systems level approach to understanding how acetate modulates metabolism. All known metabolic pathways encoded by the genome of *C.*

reinhardtii have been mapped in a global representation of its metabolism. With this knowledge, several methods for analysing metabolism have been developed.

One of the most popular methods for analysing metabolic pathways is constraint-based modelling, which includes the techniques of Flux Balance Analysis (FBA) and Flux Variability Analysis (FVA) for the prediction of metabolite flux through a metabolic network reconstruction (Orth et al., 2010). Flux-based modelling allows for the inclusion of realistic constraints imposed upon the system, for example maximal nutrient uptake/excretion rates. As a result, growth rates and production of biotechnologically important metabolites can be predicted using constraint-based methods in conjunction with genome-scale models (GEM), which contain all known metabolic information (Schilling et al., 1999). FBA was first used by Boyle and Morgan (2009) to address carbon metabolism in a small-scale model of *C. reinhardtii.* More recently, two GEMs of this organism were presented and used for prediction of metabolic fluxes in different growth conditions (Dal'Molin et al., 2011, Chang et al., 2011).

The AlgaGEM model, which was derived from a previous model of *Arabidopsis thaliana* (de Oliveira Dal'Molin et al., 2010), showed substantial evidence for the accurate prediction of hydrogen production during a heterotrophic growth regime. They analysed the competition between hydrogen production and the photosynthetic pathway of cyclic electron flow, thereby showing the importance of optimising photosynthetic regulation for biofuel production. *i*RC1080, the other published and validated GEM of *C. reinhardtii,* was assembled following a bottom-up approach and specifically validated by examining the effects of different light spectral ranges and intensities on metabolic and photosynthetic reactions (Chang et al., 2011). The centrality of the chloroplast and the complexity of photosynthetic reactions make this model optimal for the prediction of biomass and light usage under phototrophic and mixotrophic growth conditions. In addition, starch and other carbon sinks can accumulate as biomass within *i*RC1080, giving indicative *in silico* results that can explain the photosynthetic responses to acetate. For these reasons, the *i*RC1080 model was chosen for our study.

The aim of this work was to examine how metabolic fluxes change in response to acetate addition. We have investigated the functioning and regulation of photosynthesis in *C.*

reinhardtii in silico to assess photosynthetic down-regulation using flux modelling techniques and validated against experimental evidence. FBA and FVA were then used to calculate flux distribution for both phototrophic and mixotrophic growth. Furthermore, a reaction essentiality analysis was performed to investigate which reactions are essential to explain observed traits. We show that the ATP requirement for acetate assimilation is indeed obtained by a re-routing of electrons around PSI, consistent with qualitative experimental published data (Munekage et al., 2008, Johnson and Alric, 2013), and an increased activity of central carbon metabolic pathways is associated to mixotrophic growth on acetate.

2.2 Material and methods

2.2.1 Model curation

As the photosynthetic reactions are of particular importance, all photosynthetic reactions in the model were validated and corrected where necessary. Specifically, we corrected the cyclic electron flow reactions, in which flux towards plastocyanin was re-directed towards cytochrome b_6f, in line with published data (Alric, 2014). In addition to this, we included the movement of protons from the stroma to the lumen that occurs as a result of CEF (Johnson, 2011), which was otherwise missing in the original model (for complete SBML model, see **supplementary file 2.1**).

2.2.2 Flux balance analysis

Flux Balance Analysis (FBA) was performed using a pre-existing model of *C. reinhardtii* metabolism, *i*RC1080 (Chang et al., 2011). Since it was necessary to obtain an optimal flux state and resulting global flux distribution that accounts for maximal cell growth, maximisation of biomass was used as the objective function for FBA. It was shown by the authors of the *i*RC1080 model (Chang et al., 2011) that the hypothesis of maximisation of biomass adequately reflects experimental conditions, which are the same conditions we are using and which are expected to favour growth.

Flux predictions were compared between acetate-fed conditions and cells grown phototrophically. For phototrophic growth, the model inputs were represented by experimental nutrients and light uptake (constraints found in **supplementary file 2.2** and **2.3**) as a base model, and the addition of acetate to this model represented mixotrophic growth. Additional constraints imposed on the system included constraining the dry weight of an actively metabolising algal cell (Mitchell et al., 1992), known starch degradation rates in the light (Levi and Gibbs, 1984), and the light induced inhibition of the enzymes protochlorophyllide reductase (Cahoon and Timko, 2000), phosphofructokinase, glucose-6-phosphate-1-dehydrogenase, glucose 6-phosphate dehydrogenase (Mustroph et al., 2013) and fructose-bisphosphate aldolase (Murakami et al., 2005). The resulting fluxes in the two conditions were scored and ranked in decreasing order based on their absolute difference.

2.2.3 Flux Variability Analysis

For the detailed interpretation of FBA results it is important to keep in mind that intracellular flux patterns predicted by linear optimisation are typically not unique, i.e. many different combinations of flux vectors can satisfy the given objective function by using different pathways, resulting in various flux variability. This is mainly due to inherent redundancy in metabolic networks (Mahadevan and Schilling, 2003). Investigation of alternative pathways that yield the same objective function obtained by FBA can give a detailed analysis of the flux distribution. In doing so, alternative pathways that may be ignored through FBA can be analysed. Using Flux Variability Analysis (FVA), the range of flux values for each reaction in the GEM are considered and possible minimum and maximum allowable fluxes are returned (Orth et al., 2010). Minimal and maximal possible fluxes were obtained for each reaction whilst constraining the biomass production in the model to a growth rate obtained from FBA (flux values from FVA are contained in **supplementary files 2.4** and **2.5**). For each reaction in both conditions, the minimal possible flux under mixotrophic conditions was subtracted from the maximal flux under phototrophic conditions. Conversely, the minimal flux under phototrophic conditions was subtracted from the maximal flux under mixotrophic conditions.

Reactions are classified as essential if the minimum flux is not equal to zero. Blocked reactions are those where the maximum and minimum flux are zero (i.e. all solutions result in a zero flux). Substitutable reactions are those where the range of possible solutions result in

zero and non-zero fluxes - that is there are solutions that include flux through the reaction and others that do not. This ensures that for any given condition, we can look for any possible overlapping fluxes associated to any reaction and determine if it is essential or substitutable.
For reactions where there was a clear separation between fluxes of phototrophic and mixotrophic conditions, these were classified as non-overlapping fluxes; in other words, there was always a difference in the flux between the two growth conditions. Meanwhile, overlapping fluxes were given a score of 0 and discounted. For non-overlapping fluxes, all positive fluxes were identified. FBA and FVA were performed using the COBRA toolbox within the MATLAB (R2013a) environment and used in conjunction with the Gurobi optimiser solver (version 5.6), employing a linear programming based optimisation algorithm (see **supplementary file 2.6** for flux values obtained under phototrophic and mixotrophic conditions).

2.2.4 Reaction essentiality analysis

To determine which reactions and metabolic pathways are active or dormant in a particular condition, a reaction essentiality analysis was performed for the non-overlapping reactions derived from the absolute difference values calculated from FVA (Henry et al., 2006) as described in **section 2.2.3.** For a given condition, reactions of *i*RC1080 were classified as flux essential (requiring a non-zero flux), flux substitutable (where the range of possible fluxes span zero) and flux blocked (reactions with minimum and maximum flux of zero). This method uses FVA results to determine whether a flux is always required for optimal biomass production, is potentially used for optimal biomass production, or is never used for optimal biomass production.

2.2.5 Cell cultivation and growth

Cultures of *C. reinhardtii* wild-type (137C) were used in this study. Cells were cultured in 250 ml conical flasks with 200 ml medium, which were placed in a shaker at 180 rpm and illuminated on a 16 hour light / 8 hour dark cycle with light provided by warm-white LED lamps (colour temperature 3000-3200 K), at 140 μmol m^{-2} s^{-1}, 22°/16°C day/night. Mixotrophic cultures were grown in a Tris-Acetate-Phosphate (TAP) with added potassium

phosphate (pH 7.0) and Hutner trace elements (Hutner et al., 1950), whilst phototrophic cultures were grown in light using a modified minimal medium without acetate. The pH of minimal and TAP media was adjusted to 7.8.

2.2.6 Cell growth analysis

For inoculation, 250 µl phototrophic cultures in exponential growth phase were axenically transferred to 250 ml conical flasks containing 200ml of the appropriate medium. Following introduction of algae, cell growth was monitored at intervals for 12 days, until a stationary or death phase was reached. The optical density of cultures at 680 nm (OD_{680}) was measured using an Ocean Optics USB4000 spectrophotometer (Ocean Optics, Dunedin, FL, USA). Specific growth rates (µ) were derived from cells in an exponential phase of growth, from two time points (t_1, t_2) with associated OD readings used in the equation below.

$$\mu = \frac{lnOD_2 - lnOD_1}{(t_2 - t_1)}$$

2.2.7 Chlorophyll analysis

Chlorophyll concentration was used as a variable to calculate oxygen evolution. 1.5 ml of cell suspension was centrifuged for 5 minutes at 2400 x g. The cell pellet was re-suspended in 1.5 ml of 80% v/v acetone and homogenised vigorously. The cell samples were again centrifuged before estimating the chlorophyll content, using the method of Porra *et al*. (1989).

2.2.8 Oxygen evolution

Measurements of O_2 evolution were performed under saturating light conditions using a Hansatech oxygen electrode in a DW2 liquid-phase oxygen electrode chamber (Hansatech Instruments, Norfolk, UK). Intact *C. reinhardtii* cells in culture medium were placed into the chamber, maintained at 20°C and continuously stirred. Saturating light was provided by a Led Engin LZ4 warm-white LED (LED Engin, San Jose, CA, USA.) driven by a laboratory built constant current power supply. Rates of photosynthesis were normalised to cell number for each sample. Oxygen evolution was determined every 24 hours from Day 4 until cells reached a stationary phase**,** expressed as oxygen evolution on a cellular basis.

2.3 Results

2.3.1 Simulations describe acetate assimilation into the TCA cycle

FBA was employed for the prediction of metabolic fluxes that vary as a result of acetate introduction, giving a theoretical description of pathways that are altered following addition of acetate to induce mixotrophic growth. During phototrophic growth, the cell fixed carbon dioxide by converting light into cellular energy (reducing equivalents and ATP), whilst mixotrophic growth was simulated using the phototrophic model as a base model and allowing the uptake of acetate at an experimentally defined rate (Hoober, 1989). All other constraints imposed on the system were conserved. Steady state metabolic flux distribution was mapped for both phototrophic and mixotrophic growth. Under mixotrophic conditions, the largest subset of reactions showing the greatest change in flux involved acetate assimilation and integration into the TCA cycle (**Figure 2.1**). This carried flux an order of magnitude higher than in phototrophically growing cells (**Figure 2.2**). Predictions indicate that acetate taken up into the cytoplasm was converted to acetyl-CoA by the enzyme acetyl-CoA synthase (ACS) in a single step. Acetyl-CoA then feeds into the TCA cycle, resulting in the conversion of oxaloacetate into citrate. A little over half of the citrate was converted into isocitrate. The remaining citrate was exported in exchange of malate. From isocitrate, most flux is predicted to be via isocitrate lyase (ICL), resulting in a 'half TCA cycle' being operational that closely resembles the glyoxylate cycle. ICL ensures that the CO_2 evolution steps of the TCA cycle are bypassed, resulting in retention of organic carbon by the cell. Model simulations are consistent with published experimental data, which have shown that ICL activity is essential for efficient mixotrophic growth (Plancke et al., 2014). After ICL, mixotrophic growth results in flux through succinate dehydrogenase (SUCDH(q8)m), producing reduced ubiquinol, associated with the mitochondrial electron transport chain feeding into oxidative phosphorylation. In addition to ubiquinol, the other product formed by SUCDH(q8)m is fumarate which is converted to malate by fumarase. Malate shuttles in and out of the mitochondrion, where export of malate in exchange for sodium ions is followed by a re-entry of malate in exchange for oxaloacetate. Oxaloacetate within the TCA was converted to phosphoenolpyruvate (PEP), the precursor compound of gluconeogenesis.

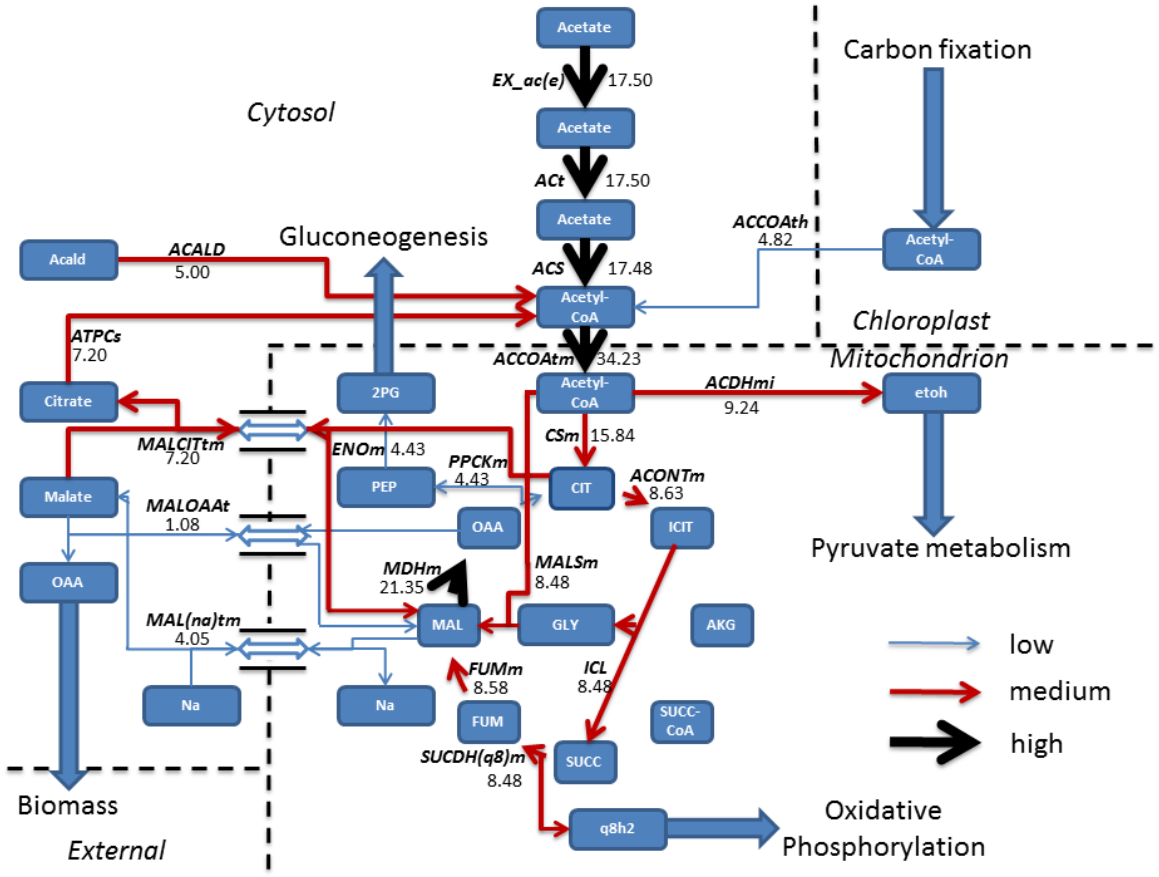

Figure 2.1 |Mixotrophic simulations following acetate assimilation

Resulting fluxes (mmol gdw-1 h-1) from mixotrophic growth reveal the incorporation of acetate into the TCA cycle, albeit a 'half TCA' cycle due to flux being carried by isocitrate lyase bypassing the CO2 evolving steps. To sustain the TCA cycle, mixotrophic cells have a constant shuttle of malate from the mitochondrion to allow sodium ions, oxaloacetate import and export of citrate, used to fuel acetyl-CoA production which is further fed back into the TCA cycle or re-allocated for pyruvate metabolism. Following export of malate from the TCA cycle, conversion into oxaloacetate ensures a gain in biomass, whilst the gluconeogenesis precursor phosphoenolpyruvate is synthesised from oxaloacetate obtained from the TCA cycle. Fluxes were categorised as low (<5 mmol gdw^{-1} h^{-1}, thin blue arrow), medium, (>5-10 mmol gdw^{-1} h^{-1}, red arrow) and high (>10 mmol gdw^{-1} h^{-1}, thickest black arrows). Antiport reactions have been denoted by a reversible arrow. **Abbreviations:** 2PG: Glycerate 2-phosphate, Acald: Acetaldehyde, ACALD: Acetaldehyde dehydrogenase (Cytosolic), ACCOAth: Acetyl-CoA/CoA antiporter, ACCOAtm: Acetyl-CoA transport, ACDHmi: Acetaldehyde-CoA dehydrogenase (mitochondrial), ACONTm: Aconitate hydratase, ACS: acetyl-CoA synthetase, ACt: acetate transport, AKG: Alpha Ketogluterate, ATPCs: ATP citrate synthase, CIT: Citrate, CSm: Citrate synthase, ENOm: Enolase, etoh: Ethanol, EX_ac(e): Acetate exchange, FUM: Fumerate, FUMm: fumarate hydratase, GLY: Glyoxylate, ICIT: Isocitrate, ICL: Isocitrate lyase, Mal: Malate, MALCITtm: Malate/citrate antiporter, MAL(na)tm: Malate/sodium antiporter, MALOAAt: Malate/Oxaloacetate antiporter, MALSm: malate synthase, MDHm: malate dehydrogenase, OAA: Oxaloacetate,

PEP: Phosphoenolpyruvate, PPCKm: Phosphoenolpyruvate Carboxykinase, q8h2: Ubiquinol, SUCC: Succinate, SUCC-COA: Succinyl-CoA, SUCDH(q8)m: Succinate Dehydrogenase.

In phototrophic simulations, pyruvate originating from carbon fixation is converted into acetyl-CoA and fed into the TCA cycle. ICL activity was redundant and the model chose to export isocitrate to the cytosol in exchange for malate. Cytosolic isocitrate was ultimately converted into biomass and the newly imported malate was converted into oxaloacetate and exported into the cytosol which fed back into pyruvate metabolism.

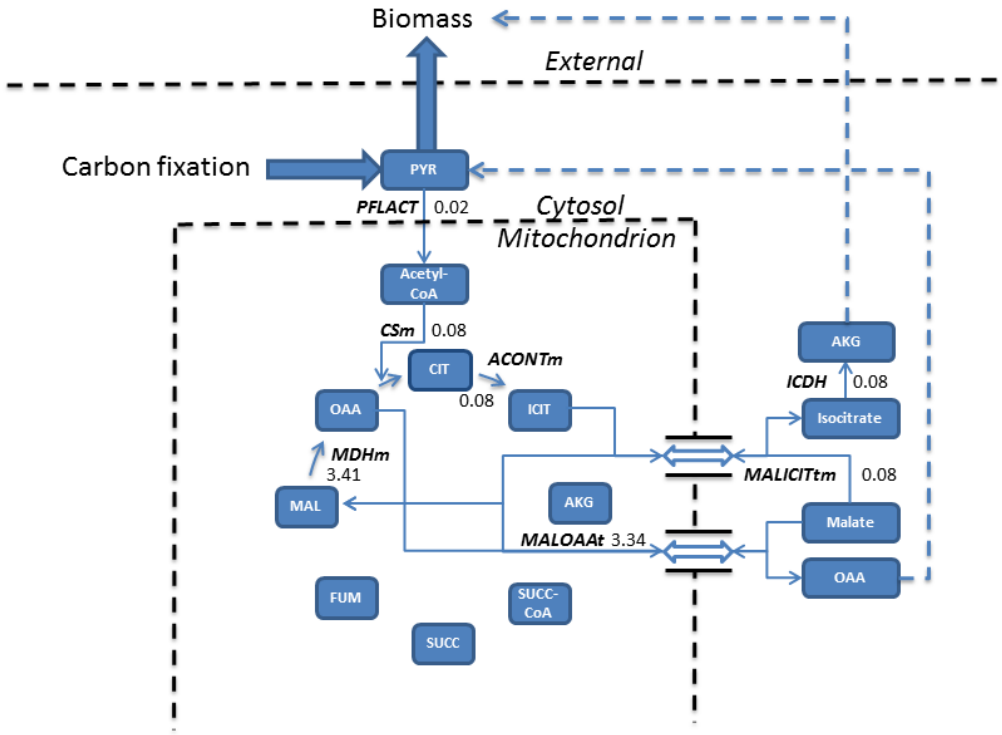

Figure 2.2 |Simulated phototrophic TCA cycle fluxes

Phototrophic simulations indicate the TCA cycle carried a much reduced flux (mmol gdw^{-1} h^{-1}) than that obtained from mixotrophic simulations, resulting from the conversion of pyruvate into acetyl-CoA into the cycle. The import of malate, exchanged for isocitrate export, forms the basis of biomass production. Meanwhile, malate re-entry into the cycle occurs to allow the export of oxaloacetate feeding back into pyruvate metabolism. Dashed lines assemble multiple steps for clarity. Double arrows represent antiporter reactions. **Abbreviations:** AKG: alpha ketogluterate, ACONTm: Aconitate hydratase, CIT: Citrate, CSm: Citrate synthase, ICDH: Isocitrate dehydrogenase, ICIT: Isocitrate, FUM: Fumarate, MAL: Malate, MALICITtm: Malate/isocitrate antiporter, MALOAAt: Malate/Oxaloacetate antiporter, MDHm: malate dehydrogenase, OAA: Oxaloacetate, PFLACT: Formate C-acetyltransferase, PYR: Pyruvate, SUCC: Succinate, SUCC-CoA: Succinyl-CoA.

2.3.2 Theoretical predictions suggest acetate increases glycolytic fluxes resulting in starch and sucrose accumulation

In addition to increasing fluxes through enzymes involved in the TCA cycle and localised in the mitochondria, acetate also increased fluxes associated with the glycolytic pathway. Oxaloacetate, generated in TCA cycle reactions is converted into glycerate 2-phosphate (2PG) and exported into the cytosol, where a flux partition occurs, resulting in the majority of flux continuing through gluconeogenesis and leading to the formation of both starch and sucrose accumulating within biomass. Both starch and sucrose are the main products of photosynthesis (Klein et al., 1983). For higher plants, sucrose is the main transport sugar yet a lack of knowledge exists for the function of sucrose in algae. Flux not channelled into the gluconeogenesis is diverted towards the production of pyruvate within the cytosol, which is transported into the mitochondrion (**Figure 2.3**).

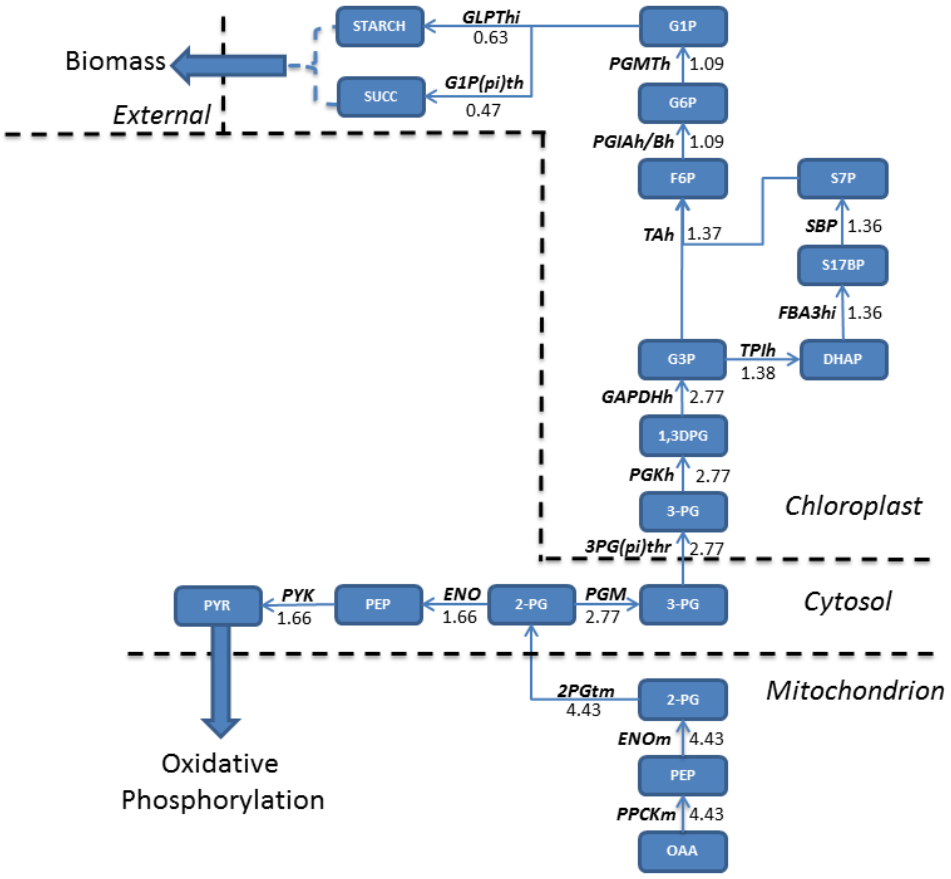

Figure 2.3 |Mixotrophic glycolytic flux

Absolute flux (mmol gdw^{-1} h^{-1}) residing within the glycolytic pathways was mapped for mixotrophic growth. Oxaloacetate produced in the mitochondrion is the precursor molecule for gluconeogenesis. A relatively large flux entering gluconeogenesis allows for a branching of fluxes within the cytosol, with one branch feeding forwards into pyruvate metabolism and eventually fuelling oxidative phosphorylation, and the other continuing the gluconeogenetic pathway. As a result, both starch and sucrose accumulate within biomass when compared to phototrophically grown cultures. **Abbreviations:** 1,3DPG: 1,3-Phospho-D-glyceroyl phosphate, 2-PG: Glycerate 2-phosphate, 2PGTm: Glycerate 2-phosphate transport, 3-PG: Glycerate 3-phosphate, 3PG(pi)thr: 3-Phospho glycerate/pi antiporter, DHAP: Dihydroxyacetone phosphate, ENO: Enolase, ENOm: Enolase (mitochondrial), F6P: Fructose 6-phosphate, FBA3hi: Sedoheptulose 1,7-bisphosphate glyceraldehyde-3-phosphate-lyase, G1P: Glucose 1-phosphate, G1P(pi)th: Glucose 1-phosphate/pi antiporter, G3P: Glyceraldehyde 3-phosphate, G6P: Glucose 6 phosphate, GLPThi: glucose-1-phosphate adenylyltransferase, OAA: Oxaloacetate, PEP: Phosphoenolpyruvate, PGIAh/Bh: Glucose-6-phosphate isomerase, PGKh: Phosphoglycerate kinase, PGM: phosphoglycerate mutase, PGMTh: phosphoglucomutase, PPCKm: Phosphophenol carboxykinase, PYK: pyruvate kinase, PYR: Pyruvate, S17BP: Sedoheptulose 1,7-bisphosphate, S7P: Sedoheptulose 7-phosphate, SBP: Sedoheptulose bisphosphatase, SUCC: Sucrose, TAh: Transaldolase, TPIh: Triosephosphate Isomerase.

Phototrophic metabolism (**Figure 2.4**) on the other hand resulted in the gluconeogenesis pathway commencing from chloroplastic glycerate 3-phosphate (3PG). 3PG originally derived from conversion of ribulose 1, 5-bisphosphate (Rb15Bp) and CO_2 by Rubisco (RBPCh), the primary reaction of photosynthetic carbon fixation. The reactions of gluconeogenesis in the mitochondrion are otherwise inactive. The predominant flux from 3PG was branched towards the Calvin–Benson cycle in the chloroplast. A further branching of flux towards erythrose 4-phosphate (E-4P) and sedoheptulose 7-phosphate (S7P) and their immediate removal from gluconeogenesis towards carbon fixation is observed. The resulting flux towards glucose 1-phosphate (G1P) production was reduced due to branching in the network, and when compared to mixotrophic simulations was reduced by a factor of 2.4. As such, only starch was accumulated within biomass.

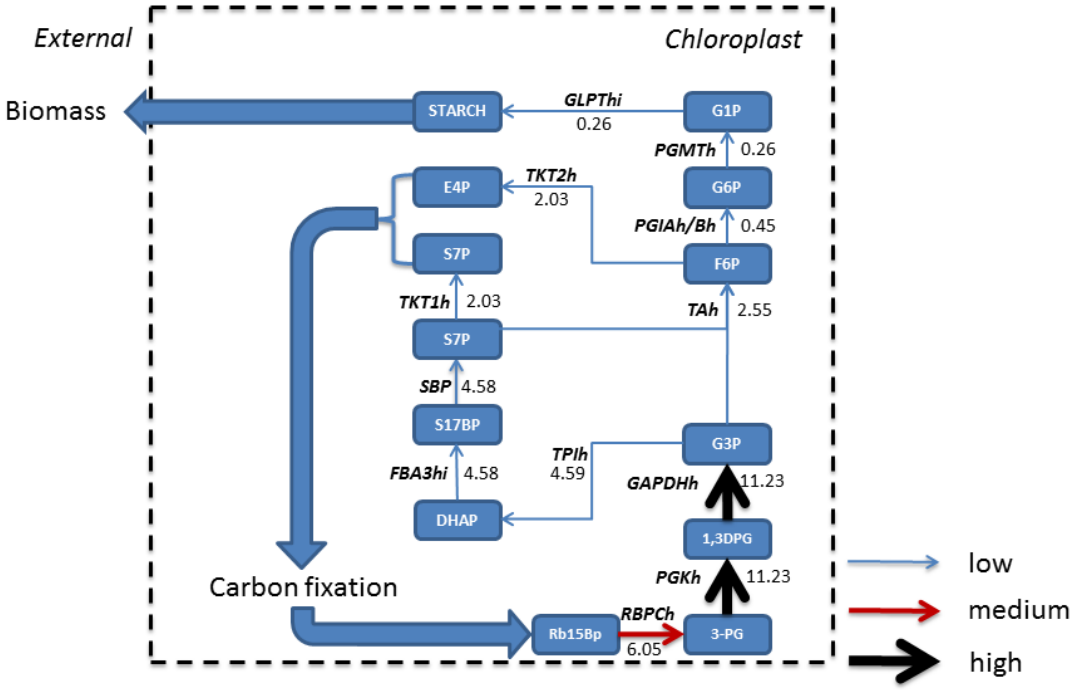

Figure 2.4 |Phototrophic glycolytic flux

Absolute fluxes (mmol gdw^{-1} h^{-1}) residing within the glycolytic pathways were mapped for phototrophic growth. Fluxes were categorised as low (<5 mmol gdw^{-1} h^{-1}, thin blue arrow), medium, (>5–10 mmol gdw^{-1} h^{-1}, red arrow) and high (>10 mmol gdw^{-1} h^{-1}, thickest black arrows). Here, in the absence of acetate, gluconeogenesis starts in the chloroplast following from the production of triose sugars from carbon fixation within the chloroplast which is otherwise inactive under mixotrophic growth. A large resulting flux of triose phosphate allows for branching, with one branch accounting for the synthesis of DHAP and the other maintaining gluconeogenesis. However, a further branch at fructose 6-phosphate forces flux back into the Calvin–Benson cycle to maintain CO_2 fixation. As a consequence, less flux is carried to glucose 1-phosphate and ultimately allows for the formation of starch only. **Abbreviations:** 1,3DPG: 3-Phospho-D-glyceroyl phosphate, 3-PG: Glycerate 3-phosphate, E4P: Erythrose 4-phosphate, F6P: Fructose 6-phosphate, FBA3hi: Sedoheptulose 1,7-bisphosphate D-glyceraldehyde-3-phosphate-lyase, G1P: Glucose 1-phosphate, G3P: Glyceraldehyde 3-phosphate, G6P: Glucose 6 phosphate, GAPDHh: glyceraldehyde 3-phosphate dehydrogenase, GLPThi: glucose-1-phosphate adenylyltransferase, PGIAh/Bh: Glucose-6-phosphate Isomerase, PGKh: Phosphoglycerate kinase, PGMTh: Phosphoglucomutase, Rb15Bp: Ribulose 1,5-bisphosphate, RBPCh: Ribulose-bisphosphate carboxylase, S17BP: Sedoheptulose 1,7-bisphosphate, S7P: Sedoheptulose 7-phosphate, SBP: Sedoheptulose-bisphosphatase, TAh: Transaldolase, TPIh: Triose-phosphate isomerase, TKT1h: transketolase 1, TKT2h: transketolase 2.

2.3.3 FBA predicts a suppression of photosynthetic CO_2 fixation with acetate metabolism

In addition to altering fluxes in central carbon metabolism, acetate is also predicted to modulate fluxes in photosynthesis and the Calvin–Benson cycle. The Calvin–Benson cycle uses the products of photosynthetic electron transport, ATP and NADPH, to convert CO_2 into organic compounds. In mixotrophic simulations (**Figure 2.5**) the Calvin–Benson cycle receives flux from the oxidative pentose phosphate pathway (OPPP), which is diverted away from CO_2 fixation but towards production of xylulose 5-phosphate (Xu5P) and fructose 6-phosphate (F6P) via the reversible action of the enzymes ribulose 5-phosphate epimerase (RPEh) and transketolase (TKT2h) respectively. It is with these reactions that the OPPP combines with the Calvin–Benson cycle and gluconeogenesis and ultimately demonstrates the interconnectivity of photosynthesis with central carbon metabolism.

Simulations in the presence of acetate predicted a decrease in oxygen evolution in line with experimental data (Heifetz et al., 2000a) relative to the phototrophic state as flux through PSII, the oxygen producing photosystem, decreased. This resulted in a reduced flux towards plastoquinone. In contrast, flux through PSI was increased, resulting from an increased flux through CEF and into cytochrome b_6f from ferredoxin. As a result, ATP production resulting from cyclic electron flow increased without production of NADPH, as described previously. The activity of CEF was otherwise non-evident with phototrophic simulations (**Figure 2.5**).

Steady-state phototrophic conditions involved a linear flow of electrons through the photosynthetic reactions, resulting in large fluxes of oxygen evolution, NAPDH and ATP as electrons are passed along the photosynthetic chain. In addition, CO_2 uptake into the chloroplast and its fixation into the Calvin–Benson cycle carried predominant flux. Following this, the cycle allows for regeneration of Ru5P and RB15BP permitting fixation of another molecule of CO_2. 3PG diverted away from the Calvin–Benson cycle was converted into pyruvate then malate. Malate entered the cytosol and transported into the mitochondrion in exchange for both oxaloacetate and isocitrate residing within the cytosol (**Figure 2.6**).

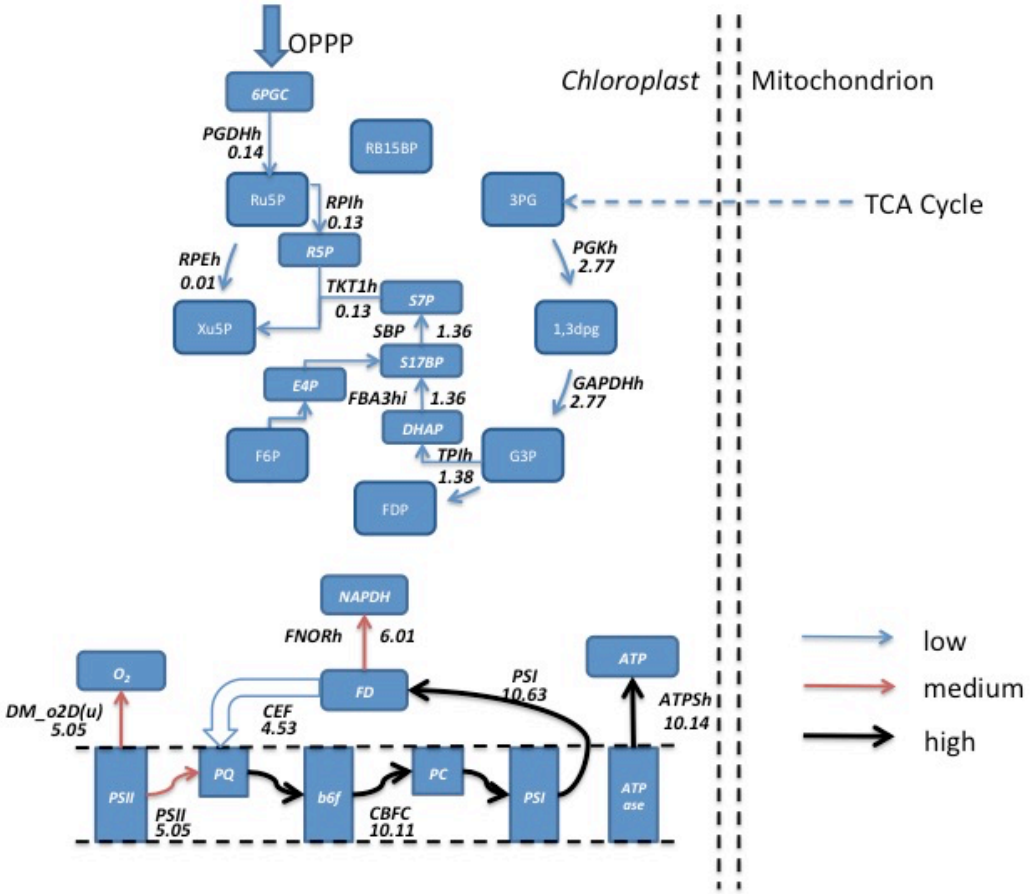

Figure 2.5 |Simulated mixotrophic photosynthetic fluxes

Simulated predictions resulting from flux balance analysis were mapped onto reactions belonging to the Calvin–Benson cycle and photosynthetic reactions for mixotrophic growth. Absolute fluxes (mmol gdw^{-1} h^{-1}) were categorised as low (<5 mmol gdw^{-1} h^{-1}, thin blue arrow), medium, (>5–10 mmol gdw^{-1} h^{-1}, red arrow) and high (>10 mmol gdw^{-1} h^{-1}, thickest black arrows). The simulations revealed an input of flux from the pentose phosphate pathway into the Calvin–Benson cycle and flux being diverted away from CO_2 and into ribulose 5-phosphate. Calvin–Benson cycle fluxes were further maintained by triose phosphate entry into the cycle, originating from within the mitochondrion. Upon inspection of photosynthetic fluxes, a cycling of electrons around photosystem I into the plastoquinone pool was active, resulting in flux diversion from the production of NAPDH back into the electron transport chain at plastoquinone. As a result of electron re-direction, ATP production is increased. **Abbreviations:** 1,3DPG: 3-Phospho-D-glyceroyl phosphate, 3PG: 3-Phospho-D-glycerate, 6PGC: 6-Phospho-Gluconate, ATPase: ATP synthase, ATPSH: ATP producing synthase, b6f: Cytochrome *b*6F, CEF: Cyclic Electron Flow, DHAP: Dihydroxyacetone phosphate, DM_o2D(u): Oxygen Demand, E4P: Erythrose 4-phosphate, F6P: Fructose 6-phosphate, FBA3hi: Sedoheptulose 1,7-bisphosphate D-glyceraldehyde-3-phosphate-lyase, FD: Feredoxin, FDP: Fructose 1,6-bisphosphate, FNORh: Ferredoxin-NADP+ Reductase, G3P: Glyceraldehyde 3-phosphate, GAPDHh: Glyceraldehyde 3-phosphate dehydrogenase, OPPP: Oxidative Pentose Phosphate Pathway, PC: Plastocyanin, PGDHh: 6-Phosphogluconate

Dehydrogenase, PGKh: Phosphoglycerate kinase, PQ: Plastoquinone, PSI: Photosystem I, PSII: Photosystem II, R5P: Ribose 5-phosphate, RB15BP: Ribulose 1,5-bisphosphate, RPEh: Ribulose-5-Phosphate, RPIh: Ribose-5-phosphate isomerase, Ru5P: Ribulose 5-phosphate, 3-Epimerase, S17BP: Sedoheptulose 1,7-bisphosphate, S7P: Sedoheptulose 7-phosphate, TKT1h: transketolase 1, TPIh: triose phosphate isomerase, Xu5P: Xylulose 5-phosphate.

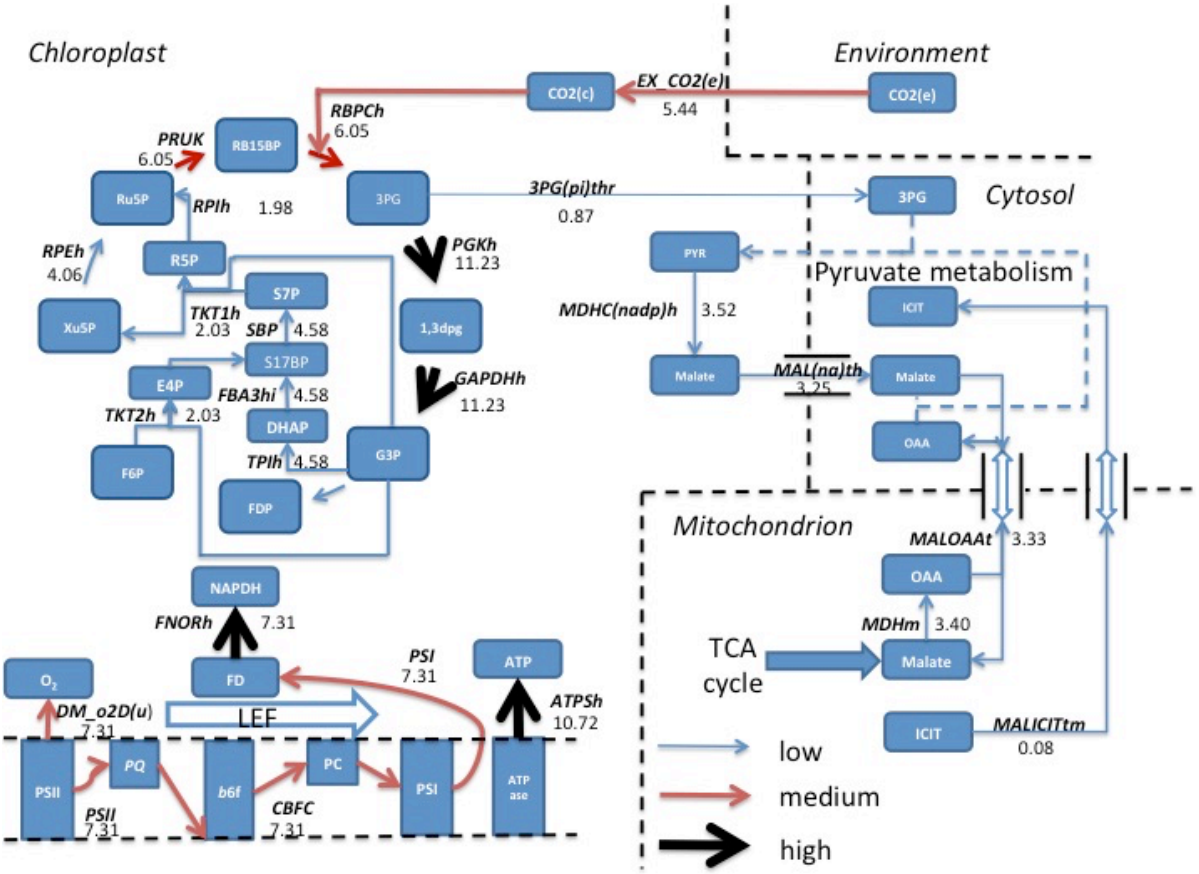

Figure 2.6 |Simulated phototrophic photosynthetic fluxes

Simulated fluxes (mmol gdw^{-1} h^{-1}) resulting from flux balance analysis were mapped onto reactions belonging to the Calvin–Benson cycle and photosynthetic reactions for phototrophic metabolism**.** Fluxes were categorised as low, (<5 mmol gdw^{-1} h^{-1}, thin blue arrow), medium, (>5–10 mmol gdw^{-1} h^{-1}, red arrow) and high (>10 mmol gdw^{-1} h^{-1}, thickest black arrows). Simulations revealed fixation of CO_2 into the Calvin–Benson cycle by the enzyme Rubisco allowing for the branching of flux at triose phosphate into pyruvate metabolism and ultimately entering the TCA cycle. Back in the chloroplast, a linear flow of eight electrons was observed resulting in production of NAPDH and ATP, and providing the reducing power and energy to fuel the Calvin–Benson cycle. **Abbreviations:** 1,3DPG: 3-Phospho-D glyceroyl phosphate, 3PG: 3-Phospho-D-glycerate, 3PG(pi)thr: 3-Phospho glycerate/pi antiporter, ATPase: ATP synthase, ATPSH: ATP producing synthase, b6f: Cytochrome *b*6F, DHAP: Dihydroxyacetone phosphate, DM_o2D(u): Oxygen Demand, E4P: Erythrose 4-phosphate, EX_CO2(e): CO_2 exchange, F6P: Fructose 6-phosphate, FBA3hi: Sedoheptulose 1,7-bisphosphate D-glyceraldehyde-3-phosphate-lyase, FD: Feredoxin, FDP: Fructose 1,6-

bisphosphate, FNORh: Ferredoxin-NADP+ Reductase, G3P: Glyceraldehyde 3-phosphate, GAPDHh: Glyceraldehyde 3-phosphate dehydrogenase, ICIT: Isocitrate, LEF: Linear Electron Flow, MALICITtm: Malate/isocitrate antiporter, Mal(na)th: Malate transport, MALOAAt: malate/oxaloacetate antiporter, MDHC(nadp)hr: malate dehydrogenase, MDHm: Malate dehydrogenase, OAA: Oxaloacetate, PC: Plastocyanin, PGKh: Phosphoglycerate kinase, PQ: Plastoquinone, PRUK: Phosphoribulokinase, PSI: Photosystem I, PSII: Photosystem II, PYR: Pyruvate, R5P: Ribose 5-phosphate, RB15BP: Ribulose 1,5-bisphosphate, RBPCh: Ribulose-bisphosphate carboxylase, RPEh: Ribulose-5-Phosphate, RPIh: Ribose-5-phosphate isomerase, Ru5P: Ribulose 5-phosphate, S17BP: Sedoheptulose 1,7-bisphosphate, S7P: Sedoheptulose 7-phosphate, TKT1h: transketolase 1, TKT2h: transketolase 2, TPIh: triose phosphate isomerase, Xu5P: Xylulose 5-phosphate. Double arrows shown represent antiport reactions.

2.3.4 Flux variability analysis determines essential reactions for phototrophic and mixotrophic growth

We have used FBA to investigate how acetate interacts with the central carbon metabolism on the global scale and in particular during the process of photosynthesis. By constraining the biomass reaction to the FBA-predicted optima for each growth condition, the entire range of feasible minimal and maximal fluxes through each reaction were calculated using FVA. A reaction essentiality analysis combined the obtained fluxes resulting from FBA and FVA and identified reactions as being either essential, substitutable or blocked for phototrophic and mixotrophic growth. We were keen to further investigate whether the highlighted reactions from the selected subsystems that FBA predicted were essential to carry the predominant flux.

The vast majority of reactions for phototrophic and mixotrophic simulations were classified as flux substitutable (1549 reactions (71%) and 1546 (70%) respectively). Flux essential reactions for phototrophic growth and mixotrophic growth comprised the lowest subset of reactions with 16 essential reactions in each condition (representing less than 1% of reactions), whilst 626 reactions (28.6%) were blocked for phototrophic simulations versus 629 (28.7%) for mixotrophic growth.

Out of the 16 essential reactions identified under mixotrophic growth, ten were also deemed essential for phototrophic growth (**Table 2.1**). These reactions all consisted of photon exchange and uptake. The remaining six reactions were classified as substitutable (O2t,

CO2tm, CSm, PPCKm), whilst acetate uptake (EX_ac(e)) and transport into the cytoplasm ACt were blocked. There were no blocked reactions observed for mixotrophic growth. However, there were seven substitutable reactions that were classed as essential for a phototrophic simulation. These included CO_2 transport into the cytosol (CO2t), the conversion of ribulose 5-phosphate and xylulose 5-phosphate via ribulose-5-Phosphate 3-Epimerase (RPEh), cytochrome b6/f complex (CBFC), ferredoxin-NADP+ reductase (FNORh) and the two photosystems (PSI and PSII). Here, it seems that the activity of CSm, allowing for the entry of acetyl-CoA into the TCA cycle, and PEP carboxykinase suggest that TCA cycle itself is fundamentally important to provide a heightened biomass for mixotrophic growth, as these reactions were all substituble for phototrophic growth. The finding that cyclic electron flow was substitutable for both growth regimes is important indicating its non-essential role in both mixotrophic and phototrophic metabolism.

Table 2.1 |Reaction essentiality for phototrophic and mixotrophic growth

Reaction	Name	Equation	Phototrophic status	Mixotrophic status
EX_ac(e)	Acetate exchange	[e] : ac <==>	Blocked	Essential
CSm	Citrate synthase, mitochondrial	[m] : accoa + h2o + oaa --> cit + coa + h	Substitutable	Essential
PPCKm	phosphoenolpyruvate carboxykinase, mitochondria	[m] : atp + oaa --> adp + co2 + pep	Substitutable	Essential
RPEh	D-Ribulose-5-Phosphate 3-Epimerase	[h] : ru5p-D <==> xu5p-D	Essential	Substitutable
CO2t	CO_2 transport, extracellular	co2[e] <==> co2[c]	Essential	Substitutable
ICL	Isocitrate Lyase	icit --> glx + succ	Substitutable	Essential
CO2tm	CO_2 transport, mitochondrial	co2[c] <==> co2[m]	Essential	Substitutable
DM_photon(h)	Photon demand	[h] : photon450 -->	Essential	Essential
EX_photonVis(e)	Photon exchange	[e] : photonVis <==>	Essential	Essential
EX_o2(e)	O_2 exchange	[e] : o2 <==>	Essential	Substitutable
DM_o2D(u)	Demand removing dummy O_2 from system	[u] : o2D -->	Essential	Substitutable
O2t	O2 transport in via diffusion	o2[e] <==> o2[c]	Essential	Substitutable
PSII	photosystem II	[u] : (2) h2o + (4) photon673 + (2) pq --> o2D + (2) pqh2	Essential	Substitutable
CBFC	cytochrome b6/f complex	(2) h[h] + (2) pccu2p[u] + pqh2[u] --> (4) h[u] + (2) pccu1p[u] + pq[u]	Essential	Substitutable

PSI	photosystem I	[u] : fdxox + (2) pccu1p + (2) photon680 + (2) h --> fdxrd + (2) pccu2p	Essential	Substitutable
FNORh	ferredoxin-NADP+ reductase	fdxrd[u] + nadp[h] --> fdxox[u] + nadph[h] + h[h]	Essential	Substitutable

2.3.5 Cell physiology matches model simulations

We used the modified *i*RC1080 to predict primary metabolism with respect to phototrophic and mixotrophic growth. To further assess the reliability of model predictions, growth rate and oxygen evolution were measured to compare predicted growth and photosynthetic oxygen evolution in order to address the initial question of the reported down-regulation of photosynthesis with mixotrophic growth.

Specific cell growth rates under phototrophic and mixotrophic conditions were quantified for comparison with model predictions (**Figure 2.7**). *C. reinhardtii* cell growth occurred following a logistic curve for both phototrophic and mixotrophic cultures (**Figure 2.7, top**). Cell culture growth increased rapidly for mixotrophic cultures with cultures entering a stationary phase after 5-6 days. For phototrophically grown cells, the stationary phase was not reached until day 11. Specific growth rates for phototrophic and mixotrophic cultures were calculated using data points obtained from a logarithmic phase of growth for both conditions. For mixotrophic cultures, the growth rate was calculated between days 3 and 4, and 9 to 11 for phototrophic cultures. Mixotrophic growth supported a growth rate 2.8 times greater than that of phototrophically grown cultures. FBA predicted growth rates in which acetate supported an *in silico* growth rate 2.38 times greater than phototrophic cultures, closely matching experimental data (**Table 2.2**).

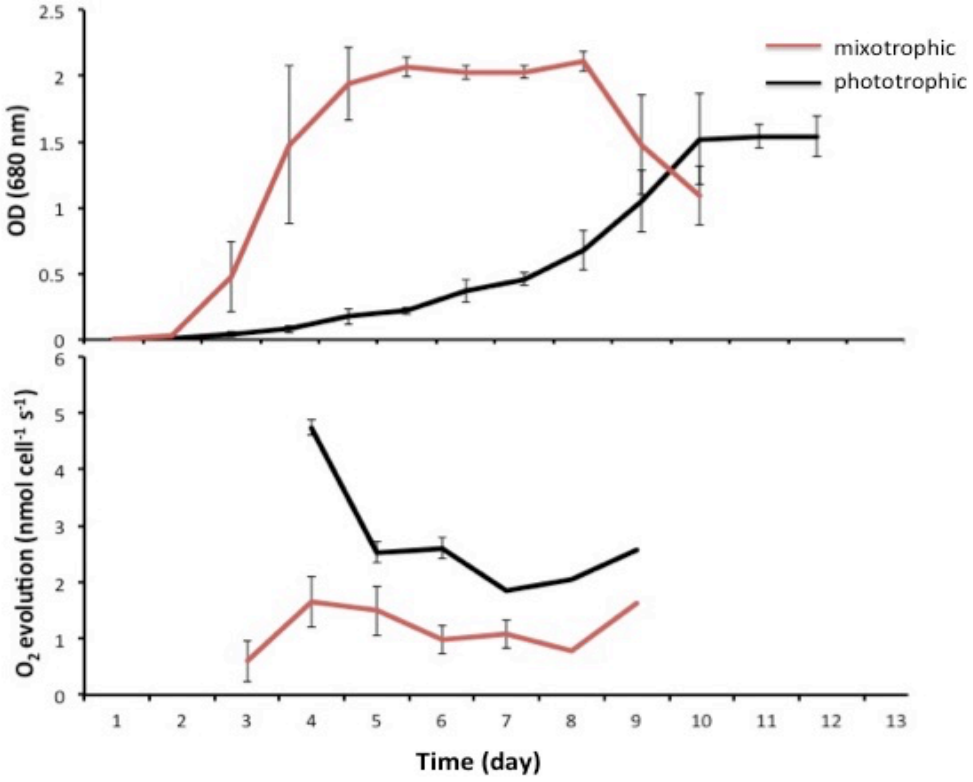

Figure 2.7 |Acetate increases the growth rate but deceases photosynthesis

Cell density measurements (top) and oxygen evolution as a measure of photosynthesis (bottom) under phototrophic and mixotrophic growth. Despite supporting a higher growth capacity, acetate has the effect of decreasing oxygen evolution. Error bars represent +/- standard deviation of triplicate biological replications.

It has been widely documented that despite promoting an enhanced growth rate, acetate results in inhibition of photosynthesis. We were able to quantify this effect and to compare results with the predictions of the modified version of *i*RC1080. The capacity for photosynthetic O_2 evolution was estimated on a per-cell basis for both conditions during the exponential phase of growth, at time points when the cell density was sufficient to give measureable photosynthetic rates (**Figure 2.7, bottom**). *C. reinhardtii* grown under mixotrophic conditions exhibited a reduced capacity for photosynthesis, consistent with reported findings (Roach et al., 2013). The biggest comparable reduction in O_2 evolution was observed at four days of growth. The oxygen evolution capacity of cultures was higher in phototrophic cultures than in mixotrophic on all days except at the final measuring day. Average oxygen evolution for phototrophic cultures was measured as 2.5 x 10^{-7} mMol O_2

cell^{-1} s^{-1}, whilst cells grown mixotrophically had an average capacity of 1.5 x 10^{-7} mMol O_2 cell^{-1} s^{-1}; a 0.6 fold decrease as a result of acetate addition. For simulations of phototrophic growth, a flux of 7.31 mMol gDw h^{-1} was estimated through the oxygen-evolving reactions. Under mixotrophic constrains, a flux of 5.05 mMol gDw h^{-1} was associated with the oxygen evolution reaction of photosynthesis representing a 0.70 fold decrease (**Table 2.2**).

Table 2.2 |*in silico* predictions closely match experimental data comparing phototrophic and mixotrophic specific growth and oxygen evolution rates.

Condition	**Phototrophic growth rate**	**Mixotrophic growth rate**	**Fold change**
***i*RC1080 prediction (mMol gDw h^{-1})**	0.135	0.321	2.38
Experimental result (OD day^{-1})	0.406 ± 0.04	1.130 ± 0.02	2.79
Condition	**Phototrophic O_2 evolution**	**Mixotrophic O_2 evolution**	**Fold change**
***i*RC1080 prediction (mMol gDw h^{-1})**	7.31	5.05	0.70
Experimental result (nMol cell^{-1} s^{-1})	2.51 ± 0.19	1.51 ± 0.04	0.60

Acetate had the effect of increasing the growth rate of cultures by a factor of 2.79 and decreasing oxygen evolution with a factor of 0.53 when compared to phototrophically grown cells. These factors are close to those predicted by the model. Experimental results were derived from triplicate biological replications. Error measurements represent that of the observed standard error.

We thus conclude that our model, revised from the original *i*RC1080 model, is able to provide a realistic simulation of the response of *C. reinhardtii* to acetate, showing correlative trends between acetate metabolism, cell growth and oxygen evolution as markers of model validation. This model is able to predict and explain emergent physiological and metabolic changes that occur as a result of acetate addition.

2.4 Discussion

It is widely accepted that growth in the presence of acetate induces a down-regulation of photosynthesis in the model organism *C. reinhardtii* (Johnson et al., 2014b). Here, we used a GEM (*i*RC1080) to evaluate the down-regulation of photosynthesis associated with a mixotrophic growth regime in the presence of acetate. Furthermore, model predictions have been validated using experimental results presented here and can be compared to results in the literature (Merchant et al., 2007, Roach et al., 2013). To the best of our knowledge this is the first time this phenomenon of photosynthetic down-regulation in response to acetate has been addressed using predictive modelling. In addition, we combined this with a reaction essentiality analysis to gain more detailed understanding of the importance of specific reactions in this process.

Mixotrophic simulations included the uptake of acetate set at an experimentally determined level and allowed for the free exchange of gasses. It has been previously reported that the incorporation of acetate into acetyl CoA might occur via two possible pathways. The first pathway involves a two-step reaction involving acetate kinase prior to phosphate-acetyltransferase, whilst the second pathway involves a single-step conversion catalysed by acetyl-CoA synthase (Johnson and Alric, 2013). Furthermore, acetate is thought to enter one of two cycles, either the glyoxylate or TCA cycle (Heifetz et al., 2000a, Johnson and Alric, 2013). Boyle and Morgan (Boyle and Morgan, 2009), using a FBA model with 484 reactions, which partially represented the compartmentalisation of the cell and specifically did not take into account the presence of a glyoxylate cycle, predicted acetate entry into a complete TCA cycle under a heterotrophic growth condition. In the light however, they suggested a switch towards a modified TCA cycle using the enzyme isocitrate lyase (ICL).

Different models contain different structures, constraints and different optimisation criteria, and are hence used to address different questions. Based on the annotated genome and metabolic reconstruction *i*RC1080 has the capacity to metabolise acetate to acetyl-CoA in a number of different compartments; either directly in the cytosol, the mitochondria, the glyoxysome housing the glyoxylate cycle, or in the chloroplast; due to localisation of the enzyme ACS in each of these organelles. Our analysis resulting from FBA suggests that acetate taken up into the cytoplasm is converted to acetyl-CoA by the enzyme acetyl-CoA synthase. However, the essentiality analysis did show this reaction to be substitutable for both

conditions. Therefore we are not able to conclusively say which reaction is responsible for acetate assimilation.

Regardless of the primary acetate assimilatory reaction, we predict that acetyl-CoA feeds directly into a simplified TCA cycle within the mitochondria using ICL, with reducing power being consumed through oxidative phosphorylation. Operation of mitochondrial ICL was deemed essential for mixotrophic growth yet substitutable for phototrophic growth according to the reaction essentiality analysis. This remains in slight contrast to an experimental study in which ICL was deemed non-essential for mixotrophic cultures of *C. reinhardtii* (Plancke et al., 2014). Essentiality aside, the model simulations are thus consistent with the experimental observation that acetate induces the expression of ICL and that ICL is required for growth on acetate.

Acetyl-CoA was then fed into the mitochondria with the export of succinate towards mitochondrial respiration and increasing flux towards ubiquinol. In addition, acetate increased fluxes along the pathway of gluconeogenesis whilst suppressing CO_2 fixation, yet still exhibiting a greater biomass than phototrophically growing cells. With regards to Rubisco activity, *C. reinhardtii* mutants devoid of active Rubisco are still able to grow in the presence of acetate, albeit sub-optimally, compared to wild type (Pinto et al., 2013).

Quantitative experimental evidence exists to describe that acetate addition decreases both carbon fixation and oxygen evolution by up to 50% (Heifetz et al., 2000). We have observed a similar trend in oxygen evolution because the model was predicting a photosynthetic decrease of 40% in mixotrophic conditions (**Figure 2.5**); however, the model predicted a complete inhibition of CO_2 fixation indicating an overestimation of the inhibitory effect of acetate. The suppression of CO_2 fixation by acetate has been previously predicted under a mixotrophic growth regime at low light, however it still remains a contrast to experimental data. These studies show that metabolically active cells growing in mixotrophic environments are capable of fixing CO_2 in addition to acetate.

As reported here, the prediction of a complete inhibition of CO_2 fixation is simply an incorrect prediction result, possibly resulting from the choice of objective function placed upon the network. There are an infinite number of possible flux distributions that could arise from FBA given the constraints imposed upon the model. We aimed to achieve a flux distribution that closely resembles *in vivo* metabolism, one that accounts for the dynamic and

flexible nature of biology. The onset of night time after a sunny day, or depletion of acetate from a growth medium, are examples in which external conditions change. For an organism to be successful, the evolution of flexible metabolic mechanisms to cope with changing conditions is an essential requirement. To achieve this, microorganisms have retained genes that have previously ensured successful growth, following adaptive evolution. It is metabolically expensive to express every pathway simultaneously, in anticipation for an environmental change, and far more efficient to express the required genes as and when needed; on the other hand, if rapid changes are expected, maintaining at least a basal level of enzyme activity avoids costly delays in adaptation. The maintenance of such residual non-essential activities ensures that cells are not fully committed to favour one environmental state, but capable of making a metabolic shift that will favour another environmental condition, ensuring survival. As the flux distribution resulting from FBA only gives one optimal state, the distribution observed here is one in which the model favours acetate uptake, as opposed to CO_2 fixation as a source of carbon. Realistically, we would expect the flux in this pathway to be low, as observed by Heifetz *et al.* (2010), but not to equal zero. The function of the Calvin–Benson cycle is to produce triose phosphate used for starch and sucrose biosynthesis. A repression of CO_2 fixation, as qualitatively predicted by the model, would therefore result in reduced production of these carbon storage metabolites, unless alternative pathways to allow for their production are active. This qualitative misprediction does affect the reliability of other predictions, such as the low starch and sucrose production entering biomass in addition to the false prediction of zero acetate transport into the model (unless the model was forced to do so). In this case, the observation that CO_2 fixation is suppressed by acetate is seen in experiments and is also predicted by the model, albeit to an exaggerated extent relative to the experimental result. Nevertheless, we specifically investigated the response of photosynthesis with active acetate metabolism in the light, and the model was able to make correct predictions with respect to the reactions of photosynthesis.

By looking at the fluxes associated to the reactions of photosynthesis in closer detail, we can see that the resulting fluxes from the model suggest known physiology that accounts for the down regulation of photosynthesis with active acetate metabolism. We observe an increased flux through the CEF reactions, consistent with the suggestion that CEF around PSI explains the down-regulation of photosynthesis (Johnson and Alric, 2012). Cyclic electron flow involves the transfer of electrons from photosystem I to the plastoquinone pool via unknown

electron carriers, then back to photosystem I via the cytochrome b_6f complex. Previously, Dal'Mollin et al (2011) reported that CEF suppresses H_2 production and suggested that hydrogen production and CEF are competing valves for the prevention of excess reducing equivalents (Dal'Molin et al., 2011). Consistent with this, our results indicate that CEF is the primary reaction rebalancing ATP and NADPH under mixotrophic conditions and that enhancing CEF optimises biomass production. At least two distinct pathways have been proposed to account for CEF, these being the PGR5 and NDH dependent pathways (Johnson, 2011). The general purpose of CEF is generally understood to be that of a protection against photo damage of PSI at high light intensities (Johnson et al., 2014b). The way in which CEF elicits this protective role is generally accepted to be by sustaining an increased pH gradient across the thylakoid lumen to regulate photon absorption (Johnson, 2011). CEF also functions to regulate the balance of ATP/NAPDH production resulting from the photosynthetic reactions. ATP can be regenerated when NADPH (at high concentrations) is consumed in an NDH cyclic electric flow, in the absence of linear electric flow, promoting proton translocation and generating a trans-thylakoid pH gradient (Peng et al., 2009). However, regarding algae, the formation of tightly associated super complexes involving PSI, cytochrome b_6f complex and feredoxin NADPH oxidoreductase has been characterised (Iwai et al., 2010). It is believed that switching between cyclic and non-cyclic pathways provides a degree of flexibility in ATP and NAPDH production and hence plants and algae can adjust the ATP:NAPDH ratio to meet the demands of metabolism (Foyer et al., 2012). One hypothesis explaining how acetate decreases photosynthesis can be presented. Acetate provides an alternative reduced source of carbon to CO_2. As such, our mixotrophic simulations suggest *C. reinhardtii* prefers to assimilate acetate into a mitochondrial TCA cycle facilitated by ACS. Acetate assimilation via ACS, however, still requires ATP (Morales-Sanchez et al., 2015). The ratio for ATP: NAPDH would therefore change resulting from acetate metabolism. To facilitate this change, a shift in electron flow from a linear to a cyclic flow is one way in which the cell can meet this demand. As explained previously, CEF results in an injection of electrons to compensate for the oxygen-evolving photosystem of photosynthesis, explaining a decrease in oxygen evolution. The non-essentiality of CEF as suggested by the model has been supported experimentally as mutants devoid of PGR mediated CEF still grow, however sub-optimally (Johnson et al., 2014b). There is other circumstantial experimental evidence to suggest that CEF activity is likely to be greater in the presence of acetate, even though this evidence is indirect since CEF cannot be directly

measured, only inferred from spectral data. The results of the model therefore support and strengthen the conclusions from existing literature.

Here we have presented a GEM that is able to predict and explain the role of CEF in acetate metabolism while demonstrating the non-essentiality of CEF. It is well known that acetate metabolism leads to an increased growth rate and biomass. Model simulations are able to reproduce this and suggest that an enhanced biomass is achieved in mixotrophic cells relative to phototropic cultures by increasing flux into starch and sucrose metabolism resulting from increased gluconeogenesis. In addition, the oxidative pentose phosphate pathway was active, resulting in the incorporation of 6PGC into R5P. R5P is used in the synthesis of nucleotides and nucleic acids, supporting greater cell proliferation and increased biomass (Bar-Peled and O'Neill, 2011). Despite the fact that acetate metabolism and photosynthesis are deeply connected, the idea of a complete inhibition of carbon fixation does however remain too simplistic.

As a tool, flux balance models are becoming increasingly popular for explaining biological phenomena. As we have shown here, FBA is a powerful tool for qualifying experimental data. Of course, assumptions are made in constraint-based modelling approaches and as such the questions investigated need to be applicable to the methodology being used. To accurately predict the fate of acetate using constraint-based modelling techniques presents a challenge due to the presence of isozymes. To fully constrain the solution space requires integration of targeted omics data to account for metabolic regulation and careful use of an appropriate objective function.

We have modelled acetate metabolism in the light and have chosen to ignore photosynthetic pathways that are specifically active in the night. For example, starch degradation was constrained to zero to reflect the suppression of this reaction in the light. Although starch contributed to the biomass, its accumulation was not specifically optimised to account for low synthesis of starch. Experimental studies have shown that phototrophic growth favours starch accumulation when compared to mixotrophic cultures (Singh et al., 2014). This is a problem that it may in the future be possible to address by using advanced techniques of flux modelling such as dynamic flux balance analysis.

Just as the ratio of ATP and NADPH has been shown to modulate the reactions of photosynthesis, elemental ratios of carbon and nitrogen have also been shown to affect cellular metabolism of photosynthetic microalgae (Talmy et al., 2014). Nitrogen and carbon rich molecules such as amino acids are stoichiometrically constrained with the biomass reaction. As previously described, there was an overall increase in biomass production with acetate metabolism; however there was no evidence for a specific up-regulation of reactions involved with nitrogen metabolism. Nitrogen assimilation reactions increased in response to acetate in line with increase in biomass. This reflects one limitation of the modelling approach used, which might be addressed using an elemental analysis of cells grown in both conditions to adjust the biomass composition for each case.

In conclusion, we have produced a curated version of a GEM of *C. reinhardtii* with an accurate representation of CEF, which is now able to explain the down-regulation of photosynthesis observed under mixotrophic growth conditions in the presence of acetate. The predictive capabilities of the model were used to highlight changes in metabolism that were essential for this trait. We can conclude that acetate incorporation into metabolism is achieved via reactions of the TCA cycle before entering central metabolism requiring CEF. Cyclic electron flow serves to support the production of a proton motive force that allows ATP generation without the net formation of NADPH, serving as a balance to meet metabolic demands imposed on the system. The functioning of CEF is, however, non-essential. In this report, we have demonstrated how the reactions of photosynthesis interconnect with carbon metabolism on a global scale, and how systems approaches play a viable tool in understanding complex relationships at the cell-wide scale.

Conflict of interest statement:
The authors declare that the research was conducted in the absence of any commercial or financial relationships that could be construed as a potential source of conflict.

Acknowledgements
We thank Roger L. Chang for providing advice and support in using the *i*RC1080 model, and Cristiana Gomes de Oliveira Dal'Molin and Lake-Ee Quek for useful discussions. This work was fully supported by the Biotechnology and Biological Sciences Research Council in association with the Doctoral Training Centre for Integrative Systems Biology (BB/G530225/1).

2.5 References

Alric, J. (2014). Redox and ATP control of photosynthetic cyclic electron flow in *Chlamydomonas reinhardtii*: (II) involvement of the PGR5-PGRL1 pathway under anaerobic conditions. *Biochim Biophys Acta* 6, 825-834.

Bar-Peled, M., and O'Neill, M.A. (2011). Plant nucleotide sugar formation, interconversion, and salvage by sugar recycling. *Annu Rev Plant Biol* 62, 127-155.

Boyle, N.R., and Morgan, J.A. (2009). Flux balance analysis of primary metabolism in *Chlamydomonas reinhardtii*. *BMC Systems Biology* 3, 4-4.

Cahoon, A.B., and Timko, M.P. (2000). yellow-in-the-dark mutants of *Chlamydomonas* lack the CHLL subunit of light-independent protochlorophyllide reductase. *The Plant Cell* 12, 559-569.

Chang, R.L., Ghamsari, L., Manichaikul, A., Hom, E.F., Balaji, S., Fu, W., Shen, Y., Hao, T., Palsson, B.O., Salehi-Ashtiani, K., and Papin, J.A. (2011). Metabolic network reconstruction of *Chlamydomonas* offers insight into light-driven algal metabolism. *Mol Syst Biol* 7, 52.

Colijn, C., Brandes, A., Zucker, J., Lun, D. S., Weiner, B., Farhat, M. R., ... & Galagan, J. E. (2009). Interpreting expression data with metabolic flux models: predicting *Mycobacterium tuberculosis* mycolic acid production. *PLoS Comput Biol*, *5*(8), e1000489.

Dal'molin, C.G., Quek, L.E., Palfreyman, R.W., and Nielsen, L.K. (2011). AlgaGEM-a genome-scale metabolic reconstruction of algae based on the *Chlamydomonas* reinhardtii genome. *BMC Genomics* 22, 1471-2164.

Dal'molin, C.G., Quek, L.E., Palfreyman, R.W., Brumbley, S.M., and Nielsen, L.K. (2010). AraGEM, a genome-scale reconstruction of the primary metabolic network in *Arabidopsis*. *Plant Physiol* 152, 579-589.

Feist, A. M., & Palsson, B. O. (2010). The biomass objective function. *Current opinion in microbiology*, *13*(3), 344-349.

Foyer, C.H., Neukermans, J., Queval, G., Noctor, G., and Harbinson, J. (2012). Photosynthetic control of electron transport and the regulation of gene expression. *J Exp Bot* 63, 1637-1661.

Hannon, M., Gimpel, J., Tran, M., Rasala, B., and Mayfield, S. (2010). Biofuels from algae: challenges and potential. *Biofuels.* 2010 Sep;1(5):763-84.

Harris, E.H. (2001). *Chlamydomonas* as a Model Organism. *Annu Rev Plant Physiol Plant Mol Biol* 52, 363-406.

Heifetz, P.B., Forster, B., Osmond, C.B., Giles, L.J., and Boynton, J.E. (2000). Effects of acetate on facultative autotrophy in *Chlamydomonas reinhardtii* assessed by photosynthetic measurements and stable isotope analyses. *Plant Physiol* 122, 1439-1445.

Henry, C.S., Jankowski, M.D., Broadbelt, L.J., and Hatzimanikatis, V. (2006). Genome-scale thermodynamic analysis of *Escherichia coli* metabolism. *Biophys J* 90, 1453-1461.

Hoober, J.K. (1989). The *Chlamydomonas* Sourcebook. A Comprehensive Guide to Biology and Laboratory Use. Elizabeth H. Harris. Academic Press, San Diego, CA, 1989. xiv, 780 pp., illus. *Science* 246, 1503-1504.

Hutner, S.H., Provasoli, L., Schatz, A., and Haskins, C.P. (1950). Some Approaches to the study of the role of metals in the metabolism of microorganisms. *Proceedings of the American Philosophical Society* 94, 152-170.

Iwai, M., Takizawa, K., Tokutsu, R., Okamuro, A., Takahashi, Y., and Minagawa, J. (2010). Isolation of the elusive supercomplex that drives cyclic electron flow in photosynthesis. *Nature* 464, 1210-1213.

Johnson, G.N. (2011). Physiology of PSI cyclic electron transport in higher plants. *Biochim Biophys Acta* 3, 384-389.

Johnson, X., and Alric, J. (2012). Interaction between starch breakdown, acetate assimilation, and photosynthetic cyclic electron flow in *Chlamydomonas reinhardtii*. *J Biol Chem* 287, 26445-26452.

Johnson, X., and Alric, J. (2013). Central carbon metabolism and electron transport in *Chlamydomonas reinhardtii*: metabolic constraints for carbon partitioning between oil and starch. *Eukaryot Cell* 12, 776-793.

Johnson, X., Steinbeck, J., Dent, R.M., Takahashi, H., Richaud, P., Ozawa, S., Houille-Vernes, L., Petroutsos, D., Rappaport, F., Grossman, A.R., Niyogi, K.K., Hippler, M., and Alric, J. (2014). Proton gradient regulation 5-mediated cyclic electron flow under ATP- or redox-limited conditions: a study of DeltaATpase pgr5 and DeltarbcL pgr5 mutants in the green alga *Chlamydomonas reinhardtii*. *Plant Physiol* 165, 438-452.

Klein, U., Chen, C., and Gibbs, M. (1983). Photosynthetic properties of chloroplasts from *Chlamydomonas reinhardii*. *Plant Physiology* 72, 488-491.

Levi, C., and Gibbs, M. (1984). Starch degradation in synchronously grown *Chlamydomonas reinhardtii* and characterization of the amylase. *Plant Physiology* 74, 459-463.

Mahadevan, R., and Schilling, C.H. (2003). The effects of alternate optimal solutions in constraint-based genome-scale metabolic models. *Metab Eng* 5, 264-276.

Merchant, S.S., Prochnik, S.E., Vallon, O., et al. (2007). The *Chlamydomonas* genome reveals the evolution of key animal and plant functions. *Science* 318, 245-250.

Mitchell, S.F., Trainor, F.R., Rich, P.H., and Goulden, C.E. (1992). Growth of *Daphnia-Magna* in the laboratory in relation to the nutritional state of its food species, *Chlamydomonas reinhardtii*. *Journal of Plankton Research* 14, 379-391.

Morales-Sanchez, D., Martinez-Rodriguez, O.A., Kyndt, J., and Martinez, A. (2015). Heterotrophic growth of microalgae: metabolic aspects. *World J Microbiol Biotechnol* 31, 1-9.

Munekage, Y.N., Genty, B., and Peltier, G. (2008). Effect of PGR5 impairment on photosynthesis and growth in *Arabidopsis thaliana*. *Plant Cell Physiol* 49, 1688-1698.

Murakami, S., Kuehnle, K., and Stern, D.B. (2005). A spontaneous tRNA suppressor of a mutation in the *Chlamydomonas reinhardtii* nuclear MCD1 gene required for stability of the chloroplast petD mRNA. *Nucleic Acids Research* 33, 3372-3380.

Mustroph, A., Stock, J., Hess, N., Aldous, S., Dreilich, A., and Grimm, B. (2013). Characterization of the phosphofructokinase gene family in rice and Its expression under oxygen deficiency stress. *Frontiers in Plant Science* 4, 125.

Orth, J.D., Thiele, I., and Palsson, B.O. (2010). What is flux balance analysis? *Nat Biotech* 28, 245-248.

Peng, L., Fukao, Y., Fujiwara, M., Takami, T., and Shikanai, T. (2009). Efficient operation of NAD(P)H dehydrogenase requires supercomplex formation with photosystem I via minor LHCI in *Arabidopsis. Plant Cell* 21, 3623-3640.

Pinto, T.S., Malcata, F.X., Arrabaça, J.D., Silva, J.M., Spreitzer, R.J., and Esquível, M.G. (2013). Rubisco mutants of *Chlamydomonas reinhardtii* enhance photosynthetic hydrogen production. *Applied Microbiology and Biotechnology* 97, 5635-5643.

Plancke, C., Vigeolas, H., Hohner, R., Roberty, S., Emonds-Alt, B., Larosa, V., Willamme, R., Duby, F., Onga Dhali, D., Thonart, P., Hiligsmann, S., Franck, F., Eppe, G., Cardol, P., Hippler, M., and Remacle, C. (2014). Lack of isocitrate lyase in *Chlamydomonas* leads to changes in carbon metabolism and in the response to oxidative stress under mixotrophic growth. *Plant J* 77, 404-417.

Porra, R.J., Thompson, W.A., and Kriedemann, P.E. (1989). Determination of accurate extinction coefficients and simultaneous equations for assaying chlorophylls a and b extracted with four different solvents: verification of the concentration of chlorophyll standards by atomic absorption spectroscopy. *Biochimica et Biophysica Acta (BBA) - Bioenergetics* 975, 384-394.

Roach, T., Sedoud, A., and Krieger-Liszkay, A. (2013). Acetate in mixotrophic growth medium affects photosystem II in *Chlamydomonas reinhardtii* and protects against photoinhibition. *Biochim Biophys Acta* 10, 17.

Schilling, C.H., Edwards, J.S., and Palsson, B.O. (1999). Toward metabolic phenomics: analysis of genomic data using flux balances. *Biotechnol Prog* 15, 288-295.

Schuetz, R., Kuepfer, L., & Sauer, U. (2007). Systematic evaluation of objective functions for predicting intracellular fluxes in Escherichia coli. *Molecular systems biology*, *3*(1), 119.

Singh, H., Shukla, M.R., Chary, K.V.R., and Rao, B.J. (2014). Acetate and Bicarbonate Assimilation and Metabolite Formation in *Chlamydomonas reinhardtii*: A (13)C-NMR Study. *PLoS ONE* 9, e106457.

Talmy, D., Blackford, J., Hardman-Mountford, N.J., Polimene, L., Follows, M.J., and Geider, R.J. (2014). Flexible C : N ratio enhances metabolism of large phytoplankton when resource supply is intermittent. *Biogeosciences* 11, 4881-4895.

3. Cyclic flux distribution reveals novel hypothesis explaining a photosynthetic down-regulation for the model organism *Chlamydomonas reinhardtii*

Stephen Chapman[1], Marcelo Trindade dos Santos[2], Giles N. Johnson[1], Jean-Marc Schwartz[1]*, and Mauricio Kritz[2]

[1] The University of Manchester, Faculty of Life Sciences, Michael Smith Building, Oxford Road, Manchester, M13 9PT, UK

[2] Laboratório Nacional de Computação Científica (LNCC), Petrópolis, RJ

*** Correspondence:** Dr Jean-Marc Schwartz, University of Manchester, Faculty of Life Sciences, Michael Smith Building, Oxford Road, Manchester, M13 9PT, UK

jean-marc.schwartz@.manchester.ac.uk

Keywords: glycolysis, mixotrophic growth, metabolic model, photosynthesis, green algae, flux balance analysis, acetate metabolism, cyclic electron flow

Author contributions: All work presented in this chapter was conducted by the lead author supervised by Dr. Trindade dos Santos and Prof. Kritz in the use of PEARL and MySQL. Dr. Johnson and Dr. Schwartz provided additional supervision and review of written work.

Abstract

Regulation of metabolic networks has previously been shown to be distributed and shared through the action of metabolic cycles. Cycles play important roles in maintaining flux availability for multiple pathways to supply cellular energy and contribute to dynamic stability.

By understanding the cyclic and acyclic flows of matter through a network, we are closer to understanding how complex dynamic systems distribute flux along interconnected pathways. In this work, we have applied a cycle decomposition algorithm to a GEM of *Chlamydomonas reinhardtii* to test whether cyclic decomposition can reveal how environmental changes affect cyclic flux distributions.

We were able to examine the role of cycles that can explain the down-regulation of photosynthesis observed when cells are grown in the presence of acetate. Our results suggest that acetate modulates changes in the pentose phosphate pathway and increases mitochondrial respiration activity. Here, we show the importance of understanding how metabolic cycles affect organism behaviour on the genome scale.

3.1 Introduction

GEnome-scale Models (GEMs) aim to compile all known biochemical knowledge associated with an organism, derived from the genome sequence annotation and literature, to provide an accurate representation of all known metabolic reactions (Orth et al., 2010). Their popularity has resulted in an increasing number of publications that use GEMs to explain observed physiological traits (Baart and Martens, 2012). At present however, GEMs ignore genetic and metabolic regulation assumptions involving mass-balance. One inherent property of metabolic networks is the importance of cycles in regulating metabolic flux distribution (Marinari et al., 2007).

It has been widely documented that substrate cyclic structures play a central role in the homeostasis of biological systems. For example, the Tricarboxylic Acid (TCA) cycle, also known as the Krebs cycle, is one of the most fundamental cycles in nature. The TCA cycle

can be thought of as starting with the reaction of acetyl-CoA with oxaloacetate (OAA), producing citrate. With every turn of the cycle the substrate OAA, a 4-carbon compound, is recycled and can therefore be used again for subsequent cycles. As with the TCA cycle, cycles play a pivotal role of retaining substrate matter and maintaining flux availability for multiple pathways to supply the cell with energy. In addition, cycles help maintain the organisational characteristics of a system, contributing to dynamic stability (Ma'ayan et al., 2008).

Substrate cycles however, do not give a complete description of the cycling that occurs at the molecular level. In order to gain a better understanding of living phenomena, a better understanding of the role of cycles and their involvement of regulation within metabolic networks must be sought. One way of achieving this is to use cycle decomposition in metabolic networks (Kritz et al., 2010). Kritz et al. (2010) introduced a way of addressing and analysing the cycling of matter in metabolic networks by adapting a pre-existing algorithm used to inspect cycles in ecological food webs. The novelty of their work rests with the fact that unlike previous approaches they were able to describe cycles involving fragments of molecules, which are transferred between chemical compounds. This cyclic decomposition methodology allowed the possibility to distinguish between cyclic and acyclic flows of molecular fragments using a probabilistic assignment. Using representative GEMs the authors were able to observe the metabolic changes that occur with gene knockout experiments, unveiling novel hypotheses on how organismal growth can be optimised (Kritz et al., 2010).

C. reinhardtii is a unicellular green algae that has been a model organism for the study of photosynthesis and cellular function for the past 50 years (Harris, 2001). Recent concerns over fossil fuel depletion have led to research into the use of micro-algae such as *C. reinhardtii* to produce sustainable biofuels (Hannon et al., 2010). The cells of this alga fix carbon from the atmosphere via the Calvin–Benson cycle, the products of which can be channelled into tri-acyl glyceride lipid bodies providing the building blocks of biofuel (Merchant et al., 2012). The high-energy requirement of this process is met by light capture in the photosynthetic reactions. Photosynthesis is a highly tuned system and is one of the most regulated processes in nature. To improve biofuel yields from micro-algae we need to fully understand the connections between photosynthesis and metabolism.

Here we use this cycle decomposition methodology to investigate the cyclic flux distribution in the model organism, *Chlamydomonas reinhardtii*, using a published and validated GEM (Chang et al., 2011) in an attempt to present a comprehensive description of cyclic and acyclic metabolic fluxes for the organism. Using this methodology we identify novel hypotheses that explain the down-regulation of photosynthesis that has been widely observed when cells experience a change from phototrophic to mixotrophic growth (Johnson et al., 2014b). By applying the decomposition algorithm to these two conditions we have identified biologically relevant cycles in addition to major changes between the growth conditions. In this work we have shown through cyclic decomposition analysis that acetate addition results in modulation of key glycolytic and mitochondrial reactions, tipping the requirement of reducing power and ATP that feeds back on the photosynthetic reactions. We show that this innovative metabolic network analysis leads to a scenario that explains the down-regulation of photosynthesis induced by growth on acetate.

3.2 Methods and protocols

The procedure used for full-cycle decomposition consists of two distinct steps. The first is the production of a mass-consistent version of the *i*RC1080 model and an adequate representation of it, whilst the latter describes the procedure for cycle enumeration and decomposition. The metabolic network is represented by a directed bipartite graph, in which metabolites and reactions are represented by distinct nodes, from two disjoint sets, connected by arcs. An arc from a metabolite node to a reaction node indicates that the metabolite is a substrate for that reaction. In contrast, an arc from a reaction node to a metabolite node indicates that the metabolite is a product of that reaction. Each reaction may therefore have one or multiple associated substrates and products, and each metabolite may be associated with multiple reactions. A mass flux can then be associated to each arc of the bipartite graph. Mass flux here takes into account the mass, stoichiometric coefficient and molar flux (e.g. obtained from Flux Balance Analysis) for each species involved in the reaction.

The main reason for using mass flux rather than molar flux is that we are aiming at enumerating all possible cycles of matter in the metabolic network, including those that involve fragments of molecules, and not only stoichiometric cycles composed of entire molecules. Accurate mass representation is an essential precondition of this study. Molar

conservation only applies to whole molecules, whereas mass conservation is a fundamental law that applies to any exchange of matter in biological systems. It is possible to find mass inconsistencies in stoichiometric models, for example when generic molecular types are used as entities in the model (e.g. an 'alcohol' entity may refer to ethanol in some reactions and butanol in others) (Gevorgyan et al., 2008; Ponce-de-Leon et al., 2015). The use of mass fluxes instead of molar fluxes makes it possible to extend our analysis to all potential cycles of matter, including those that involve exchanges of molecular fragments between different molecules, not just entire molecules.

The process of enforcing mass consistency is explained below.

Mass inconsistencies arise through a number of factors including but not limited to incorrect descriptions of biochemical reactions, inconsistent chemical formulas, missing cofactors and use of incorrect protonation states of metabolites. The presence of generic compounds such as glycogen and starch can also induce mass inconsistency; these are composed of a core structure associated to a varying number of branched repeats, hence it is impossible to attribute a single mass value for such generic compounds. They can have distinct masses in distinct reactions. In addition to generic compounds, proteins and protein complexes described in biochemical reactions can also contribute to mass imbalance despite not being part of the metabolic network. Similarly, transfer RNA (tRNA)-amino acids present in GEMs represent an additional mass inconsistency as the tRNA molecule itself remains unchanged and does not take immediate part in metabolism.

With regards to reactions there are instances where the description of a reaction naturally leads to a mass-inconsistency. One example is the use of exchange reactions, used to allow uptake of constituents from the medium into the cell. Typically, these reactions only contain substrates so the mass inconsistency is directly attributed to the missing product. Reactions involving cofactors also need special attention. By default, the topological representation of a GEM enables a cofactor to be available for multiple reaction pathways simultaneously and, as such, to have the ability to create network connections that are biologically meaningless. The problem lies in that the participating reactions are mass inconsistent, therefore imposing a mass imbalance on the system.

By definition, a model achieves mass consistency when, for each and every reaction within the network, the mass sum of all substrates is equal to the mass sum of products. If this is not the case for a reaction, a manual curation is required involving application of a gateway (a reaction node associated with an open arc). A gateway is a conceptual approach that represents mass exchange with the environment. The mass of a gateway is equal to the mass imbalance of the reaction, hence each mass-imbalanced reaction will need a specific gateway. The use of gateways to correct for mass imbalance circumnavigates the risk of involuntarily changing the mass of a species that was previously mass-balanced in other reactions (otherwise we could introduce new mass inconsistencies while trying to correct others).

3.2.1 Application of gateways to achieve global mass balance

Gateways are introduced to easily correct mass imbalances in metabolic reactions for theoretical analysis. The reason why this solution is preferable to adjusting the mass of metabolites themselves is because it prevents the risk of involuntarily introducing new imbalances in other reactions; there are cases where the same metabolite is balanced in some reactions but imbalanced in others. In addition, some compounds do not need to be explicitly represented in the model, for example transfer RNAs. These compounds were also replaced by gateways, which represent matter exchanges between the network and its environment as previously described (Kritz et al., 2010). Typically, mass-imbalanced reactions were corrected by application of a gateway, composed of a reaction node associated to a specific type of open arc. The various gateway types described below were used to balance mass-inconsistent reactions.

Cofactor gateways: Cofactors are ubiquitous molecules associated with the storage and transfer of energy. The presence of cofactors has the potential to create spurious connections as cofactors are assumed to be available to several reactions at any one time. This relationship of cofactors and their involvement in multiple reactions indicates a biochemical relationship that is often not representable in living conditions as many reactions are separated in space and time. Cofactor replacement by gateways therefore separates each cofactor's involvement into specific reactions, breaking any spurious network connections.

Proteins and protein complex gateways: these are additional elements replaced by gateways as their involvement in biochemical pathways is often minimal, usually involving the catalysis of substrate to product without themselves taking part in the reaction.

Transfer RNA-amino acids gateways: These represent complexes formed when a tRNA molecule is transporting an amino-acid to be polymerised into a peptide. Like proteins, their mass remains unchanged.

Demand gateways: Demand reactions are present to draw excess metabolites from compartments and complete metabolic pathways. As such, demand reactions only include substrates; the absence of products therefore is directly responsible for a mass imbalance.

Exchange gateways: Similar to demand reactions, exchange reactions typically only involve substrates. Gateways were added as products for exchange reactions to balance the equation.

Generic compound gateways: Generic compounds may require replacement with a gateway if they induce mass imbalances. The number of repeating units associated with a generic compound cannot be specified, so each use of the same generic compound can have a different mass that is distinct from the mass of the same generic species present elsewhere in the network. Identification of a generic compound is facilitated by the presence of a 'R' in the formula of the species, representing an unspecified radical chain.

Small gateways: A metabolite can exist in distinct protonation states depending on the pH of the immediate environment. Hence a compound occurring in two compartments of distinct pH can have distinct formulas resulting from different protonation states. Small gateways were introduced for each reaction exhibiting a mass imbalance due to hydrogen ion (proton) discrepancies.

Large gateways: Reactions involving a mass difference greater than can be accounted for by small gateways require the addition of large gateways. Such examples include missing substrates or products from a reaction.

Reactions involving multiple gateways were ultimately merged into a single gateway.

3.2.2 Bipartite graph representation

A general mathematical description of a metabolic network can be achieved by means of hypergraphs, where several metabolites (hypergraph nodes) can be associated by a reaction

(hypergraph arc). Hypergraphs can also be depicted as bipartite graphs having the following two sets of nodes: metabolite nodes connected to reactions nodes. As an input model, a validated GEM for *C. reinhardtii, i*RC1080 (Chang et al., 2011), was used. This model consists of 2191 reactions encoded by 1080 genes, with a total metabolite complement of 1061 species (compounds). All reactions and species were assigned to one of ten cellular compartments; therefore each species exists with unique compartment identification. The introduction of a *species_type* for every species ensured that a species could be sought, independent of its location, whilst species is attributed to a specific compartment. Therefore unique species in different compartments can be associated to the same *species_type* facilitating addition of gateways for specific species in the model. Data representation and manipulation was facilitated using MySQL in conjunction with Perl.

3.2.3 Cycle decomposition procedure

The cycle decomposition procedure requires the use of four distinct steps. Firstly, as a pre-requisite for the decomposition algorithm, molar fluxes are obtained from Flux Balance Analysis. Secondly, molar fluxes are converted to mass fluxes. Thirdly, cycles are enumerated, followed by the final cycle decomposition step.

3.2.4 Flux Balance Analysis

The cycle decomposition algorithm requires the conservation of mass fluxes along each reaction of the bipartite graph. This requirement of mass flux conservation comes from the method itself (internal distribution of probabilities), since, for the decomposition to be meaningful, the flux through each network node should be conserved. FBA was used to provide a molar flux for each reaction, which was then converted into a mass flux. FBA was performed using the COBRA toolbox (Becker et al., 2007) using conditions that resemble phototrophic growth of the organism (growth using only light as an energy source) and mixotrophic growth (growth using both light and acetate, an organic carbon source). To ensure the set of fluxes for each condition were representative of physiological traits further constraints were applied to mimic experimental conditions with regards to biomass, known carbon metabolism pathways, and experimentally determined photosynthetic rates.

3.2.5 Conversion of molar flux to mass flux

Following FBA, the molar fluxes obtained for each condition were converted to a mass flux. Mass flux takes into account the mass of a species, its stoichiometric coefficient, and the molar flux for the associated reaction. The mass flux is given by mass_flux = molar_flux * stoich_coefficient * metabolite_mass. The mass flux associated with each pair (reaction, metabolite) was projected onto the bipartite graph representation prior to cyclic decomposition.

3.2.6 Cycle enumeration using Tarjan's algorithm

Tarjan's algorithm (Tarjan, 1973) was used to enumerate all cycles in the bipartite graph representation of the mass consistent version of *i*RC1080. The algorithm seeks to enumerate cycles by traversing the network along an elementary path. An elementary path can be described as a path in which there is no repetition of any node. Following identification, the cycle is enumerated and the algorithm continues by backtracking one previous node, following another arc to traverse. The process is repeated until all cycles have been enumerated. Tarjan's algorithm provides the most suitable method for cycle enumeration with regards to computational efficiency, due to pruning methods that avoid searching in already traversed paths that would return no new cycles, reducing the search space and increasing algorithm efficiency.

3.2.7 Cycle decomposition

The final phase is cyclic decomposition of the network, achieved by removing enumerated cycles from the network based on the mass flux values up to a point where there are no more cycles to be removed. The algorithm first identifies a critical arc in the network, defined as the arc(s) bearing a minimal mass flux among all cycles. It then proceeds to find all cycles sharing the critical arc, identifying its nexus, a collection of simple cycles sharing the same critical arc. Cycle decomposition proceeds to calculate the probability of mass flux entering any of the nexus cycles via any adjacent node to the critical arc. The decomposition algorithm further distributes the mass flux shared among the nexus cycles based on the circuit probability of each cycle. Circuit probability is defined as the probability that a number of starting mass at any point in the cycle will follow its elementary path until reaching the initial starting point again. The flux of the critical arc is divided among all cycles of the nexus in which it appears in proportion to their respective circuit probabilities. Then each cycle sharing the nexus is removed from the model by subtracting its flux from the critical arc. The

algorithm then re-searches the set of cycles for the next critical arc and repeats critical arc removal until the resulting network is void of cycles (Kritz et al., 2010).

3.2.8 Cycle uniqueness and ranking

After applying the decomposition algorithm for mixotrophic and phototrophic conditions, unique and non-unique cycles for each growth condition were identified and ordered based on the mass flux carried by the critical arc of each cycle as computed by the decomposition algorithm. The relative change of flux was calculated between the two conditions and listed in decreasing order.

3.3 Results

The metabolic model, *i*RC1080, representing the model organism *C. reinhardtii* was used for the production of a mass consistent model, mSC2191 (**supplementary file 3.1**). Fluxes obtained from FBA with *i*RC1080 were then used to compute mass fluxes for the decomposition of mSC2191.

3.3.1 *C. reinhardtii* model mass inconsistencies

From the original 2191 reactions present in the model, a total of 81 reactions were mass-inconsistent. All mass-inconsistent reactions were identified and resolved using gateways (**Table 3.1**). Some specific examples of mass-inconsistency and correction methodology are described below.

Example 1) Application of a large gateway

R_CEF: This reaction is an important photosynthetic regulatory mechanism in which electrons are re-directed about photosystem I, resulting in increased ATP production. This reaction was imbalanced by 412.56 g/mol attributed to a substrate. Upon closer inspection of the reaction, it was realised that one of the substrates, plastocyanin (a protein present in the reactions of photosynthesis), was without a formula and without a mass. A large gateway was introduced into the reaction, containing the mass of the imbalance.

Example 2) Application of a tRNA gateway

R_GLUTRS: This reaction is a glutamyl-tRNA synthetase reaction occurring in the chloroplast. This reaction catalyses the attachment of glutamyl to its cognate tRNA molecule. Since the function of this tRNA-amino acid is to facilitate the traffic of the tRNA molecule, its mass should remain constant as it does not take immediate part in metabolism. An imbalance owing to the mass of a proton bought this reaction to our attention. We could not change the mass of the metabolite being directly attributed to the mass imbalance (M_glutrna_h) as this species was involved in another reaction, R_GLUTRR, which was mass-balanced. A tRNA gateway was therefore introduced for this inconsistent reaction.

Example 3) Application of an exchange gateway

To allow for the uptake of acetate, for example, the model requires an exchange reaction representing the uptake of acetate from an external to an internal compartment. Following the example given, this reaction was identified as R_EX_ac(e). The equation for this reaction is as follows: 'ac <==>'. This reaction is unbalanced by 59.04 mass units; achieved due to the missing product of the reaction. A gateway was added for this reaction with the mass of 59.04 to balance the reaction.

Table 3.1 |Total number of gateway additions to produce mSC2191, a mass consistent version of *i*RC1080

Number of gateways	Gateway type
3813	Cofactor gateways
422	Proteins and protein complex gateways
31	tRNA-amino acid gateways
26	Demand gateways
46	Exchange gateways
61	Generic gateways

We applied the cycle decomposition algorithm to mSC2191, a mass consistent bipartite representation of *i*RC1080, to reveal cycles resulting from two distinct growth conditions. Cycles from the mitochondrion, thylakoid lumen and chloroplast compartments were analysed both independently and together due to their importance in housing reactions belonging to central carbon metabolism. Inspections of cycles resulting from the whole network required an unusually high computational power due to the high number of cycles and were not necessary in our study since we were able to analyse cycles in selected key compartments.

Table 3.2 |Cycles resulting from cyclic decomposition for key compartments for phototrophic and mixotrophic growth, showing common and unique cycles to both conditions

Compartment (s)	#Total phototrophic cycles	#Total mixotrophic cycles	#Common cycles to both conditions	#Unique phototrophic cycles	#Unique mixotrophic cycles
Mitochondrion	13	11	9	4	2
Thylakoid lumen	20	4	4	16	0
Chloroplast	587	1885	51	536	1834
Mitochondrion, thylakoid lumen and chloroplast	5228	1900	64	5164	1836

3.3.2 Cycle decomposition reveals acetate modulates changes in TCA flux and mitochondrial respiration

Out of the compartments chosen for cycle decomposition, we initially started with the mitochondrion due to its importance in metabolism. The mitochondrion is the location of the TCA cycle and the respiratory electron transport chain providing a major source of ATP to fuel metabolism.

Following cyclic decomposition of the mitochondrion, we observe nine cycles being common to both conditions, leaving four cycles unique to phototrophic growth and two unique mixotrophic cycles. The most interesting unique cycle is attributable to phototrophic metabolism, carrying the largest mass flux involving pyruvate and lactate metabolism

(mass_flux = 239) (**Figure 3.1a**), and flux through the TCA cycle intermediates: citrate, malate and oxaloacetate (mass_flux = 10) (**Figure 3.1b**).

Mixotrophic decomposition revealed the unique cycle carrying the greatest mass flux involves the mitochondrial respiratory electron transport chain (mass_flux = 1244). This cycle involved the continued recycling of ubiquinone (M_q8) and ubiquinol (M_q8h2), the two key components involved in facilitating the electron transport chain to generate ATP (**Figure 3.2**). Associated to this cycle are the reactions of ubiquinone oxidoreductase Complex I (R_NADHOR) and ubiquinol-cytochrome c oxidoreductase Complex III (R_CYOR(q8)). This quinone pool accepts and donates electrons and protons (H^+) to appropriate acceptor molecules. Coupled to the flux of electrons, protons are pumped out of the mitochondrion resulting in the generation of a proton-motive force to drive ATP synthesis (Chaban et al., 2014). The other unique cycle present for mixotrophic metabolism carried much less mass flux (0.47 mass_flux) and was associated with the metabolism of propanoate.

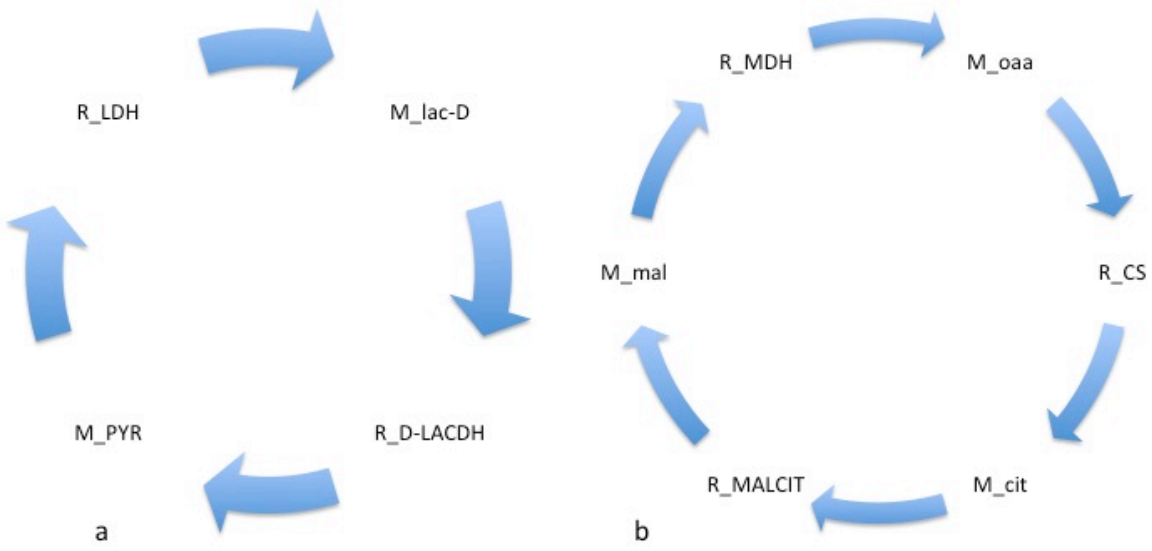

Figure 3.1 |Phototrophic cycles of the mitochondrion

(a) Pyruvate regeneration and (b) increased mass flux associated with TCA cycle intermediates. Species starting with 'R_' indicate reactions whilst 'M_' indicate metabolites. **Abbreviations:** CS: Citrate synthase, cit: Citrate, lac-D: Lactate, LDH: Lactate dehydrogenase, D-LACDH: D-lactate dehydrogenase (cytochrome), mal: malate, MALCIT: Malate/citrate antiport, MDH: Malate dehydrogenase, oaa: Oxaloacetate, pyr: Pyruvate.

Inspections of the residual acyclic graphs in mixotrophic growth suggest that acetate is directly transported into the mitochondrion, and ultimately branched towards the reactions of gluconeogenesis replacing the need of pyruvate. In this scenario therefore, pyruvate was channelled into other pathways such as valine, formate and fatty acid metabolism (**supplementary file 3.2**).

These unveiled cycles in the mass-consistent model have shown how their presence can feed-forward to enhance other cycles downstream in metabolism. Phototrophic cycles have shown that increased flux through pyruvate metabolism and its entry into the TCA allows for the production of TCA cycle intermediates in excess, which was otherwise redundant in the mixotrophic case. Instead, cycling of components of the mitochondrial electron transport chain, which is active under mixotrophic growth, is otherwise redundant in phototrophic metabolism and it is only with cyclic decomposition that these perturbations can be analysed. It is important to note here this is a purely mathematical exercise and these results may not reflect true *in vitro* metabolism.

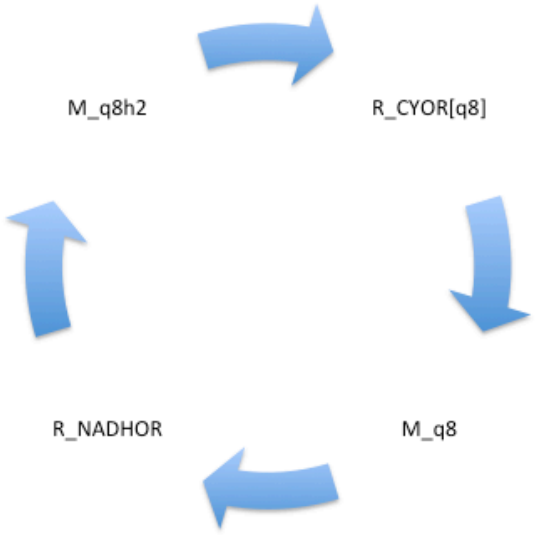

Figure 3.2 |Mixotrophic cycle carrying the greatest mass flux within the mitochondrion

Species starting with 'R_' indicate reactions whilst 'M_' indicate metabolites. **Abbreviations:** q8: Ubiquinone, q8h2; Ubiquinol, NADHOR: Ubiquinone oxidoreductase Complex I , CYOR(q8): Ubiquinol-cytochrome c oxidoreductase Complex III

3.3.3 Cycles within the thylakoid lumen reveal an increased cycling of ascorbate and increased flux carried through photosystem II reaction associated to phototrophic growth

Our next analysis considered the cycles within the compartment representing the thylakoid lumen. This sub-compartment of the chloroplast houses the light-driven electron transport reactions of photosynthesis. Following cycle decomposition, there was no unique cycle associated with the mixotrophic condition but 16 cycles were unique to phototrophic growth and four cycles were common to both conditions (**supplementary file 3.3**). The highest scoring unique phototrophic cycle (0.019 mass_flux) involved ascorbate metabolism, consisting of the cycling of ascorbate (M_ascb) by the ascorbate reductase reaction (R_VIOXANOR), resulting in the re-oxidation of ascorbate (M_dhdascb) (**Figure 3.3a**). This cycle describes the xanthophyll cycle, a well-known photo-protective cycle for plants and green algae to adapt and maintain efficient photosynthesis under fluctuating light conditions (Jahns and Holzwarth, 2012). In addition, ascorbate was involved in nine other cycles; however carrying a much-reduced mass flux of 0.002. The remaining six cycles all involved components of the photosynthetic electron transport chain all associated to carotenoid biosynthesis with the highest mass flux being 0.0002, as seen in **Figure 3.3b**.

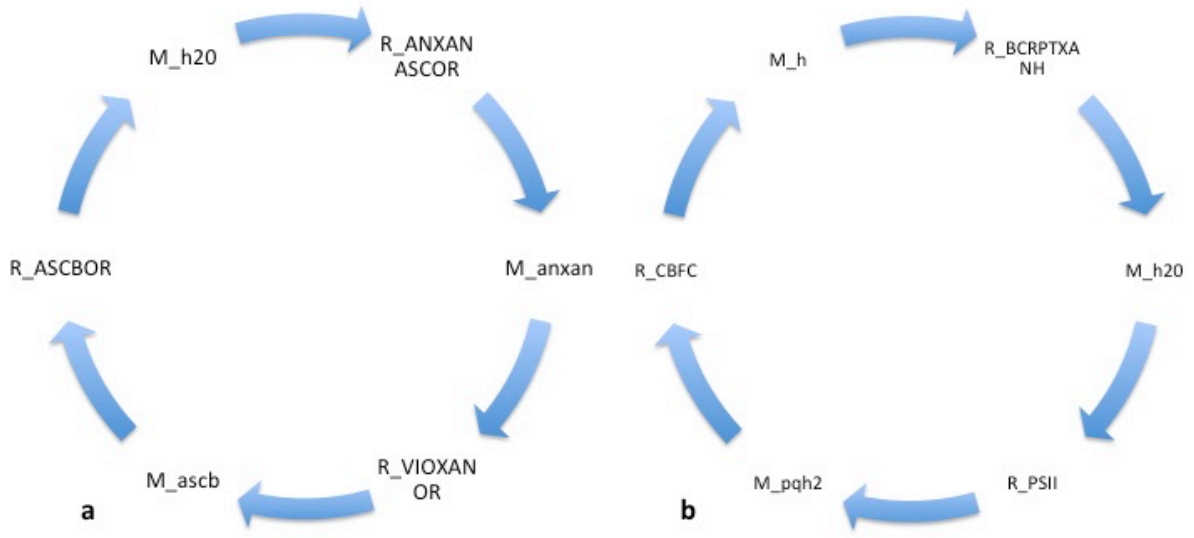

Figure 3.3 |Phototrophic cycle decomposition revealed two prominent cycles taking place within the thylakoid lumen

(a) Ascorbate metabolism and (b) recycling of plastoquinone associated with proton production (M_h) and activation of photosystem II (R_PSII), accountable for oxygen

evolution. Species starting with 'R_' indicate reactions whilst 'M_' indicate metabolites. **Abbreviations:** anxan: Antheraxanthin, ANXANASCOR: Ascorbate oxidoreductase, ascb: Ascorbate, ASCBOR: Ascorbate-oxygen oxidoreductase, BCRPTXANH: beta-Cryptoxanthin hydroxylase, CBFC: Cytochrome b6/f complex, h: Proton, h20: Water molecule, pqh2: Reduced plastoquinone, VIOXANOR: Violaxanthin.

The four cycles common to both conditions all involved cycling of matter through the reactions of photosynthetic electron transport involving both photosystems I and II. This suggests the importance of both photosystems to support a phototrophic and mixotrophic biomass. Furthermore, the finding that flux through the xanthophyll cycle was observed with phototrophic simulations is a proof of principle that cyclic decomposition can be used to unveil realistically important biological cycles otherwise ignored by FBA alone.

3.3.4 Acetate metabolism results in activation of the oxidative pentose phosphate pathway rather than glycolysis

To gain a further understanding of cycles between compartments, we expanded the cycle decomposition analysis to include the mitochondria, thylakoid lumen and chloroplast compartments. The addition of the chloroplast, the largest organelle in *C. reinhardtii,* resulted in a vast increase in the number of unique cycles for both phototrophic and mixotrophic cultures (5164 and 1836 cycles respectively) (**supplementary file 3.4**). Analysis of the theoretical cycles unique to each condition revealed a large percentage of similar sequences of reaction and metabolite nodes. 64 theoretical cycles were found common to both growth regimes.

For both conditions, the cycle carrying the greatest mass flux included the Calvin–Benson cycle (**Figure 3.4,** blue arrows) associated with different glycolytic reactions. Out of the 5164 unique phototrophic cycles, 5143 cycles (99.6%) contained the classic Calvin–Benson cycle intermediates D-Ribulose 1,5-bisphosphate (M_rb15bp) and ribulose 5-phosphate (M_ru5p-D). In addition to this finding, the cycle with the highest mass flux (322) was associated with the Calvin–Benson cycle associated with reactions of gluconeogenesis (**Figure 3.4a**).

Cycles unique to mixotrophic growth revealed that the same Calvin–Benson cycle intermediates were present in 1174, or 64% of decomposed cycles (**Table 3.3**), suggesting a

reduced importance of a fully operational Calvin–Benson cycle. In addition to this cycle, mixotrophic analysis suggested a prominent occurrence of the Oxidative Pentose Phosphate (OPPP) cycle in carbon metabolism. An OPPP results in the synthesis of carbon skeletons for nucleotide synthesis and to provide a source of reductant in the form of NAPDH for fatty-acid synthesis**.** Sedoheptulose 7-phosphate (S7P) (M_s7p, Fig. 4b) is the key metabolite used for nucleotide biosynthesis by the reductive steps of the PPP and sugar re-entry into the Calvin–Benson cycle (20) (**Figure 3.4b**). As seen in **Table 3.3**, the presence of S7P-containing cycles was greater for mixotrophic growth; 58.3% (1071 cycles) as opposed to 36.9% (1910 cycles) observed for phototrophic growth, thus representing an increase of 57.9%.

When **Figures 3.4 (a**) and **(b)** are compared, the presence of metabolites resulting from glycolysis (as represented by red arrows) only appears in the cycle carrying the highest mass flux for phototrophic growth. To further investigate the functioning of glycolysis associated with each growth condition we looked at the species R_GAPDH(nadp), which occurs in the reaction responsible for the production of triose phosphate and NADP from 3-Phospho-D-glyceroyl in the chloroplast. This reaction resembles one of the final committed steps of 'upper half' glycolysis in *C. reinhardtii*, with the 'lower half' (triose phosphate to pyruvate) occurring in the cytosol (Johnson and Alric, 2013). Occurrence of this key glycolytic node shows a 43.1% increase associated to phototrophic metabolism (**Table 3.3**). These predictions suggest that acetate has the effect of increasing OPPP activity, whilst decreasing reactions associated to the glycolytic pathway but again this is a purely mathematical exercise to find theoretical cycles only.

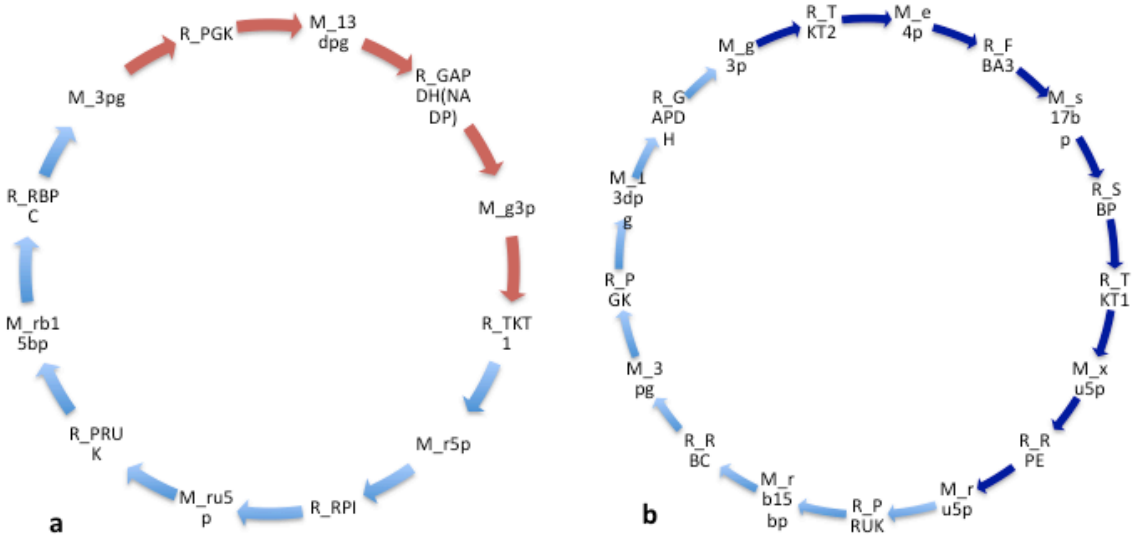

Figure 3.4 |Unique cycles resulting from the mitochondrion, thylakoid lumen and chloroplast

(a) Phototrophic cycles included reactions of the Calvin–Benson cycle (blue arrows) and glycolysis (red arrows), whilst (b) mixotrophic growth resulted in the same Calvin–Benson cycle reactions (blue arrows) associated to the reactions of the pentose phosphate pathway (purple arrows). Species starting with 'R_' indicate reactions whilst 'M_' denotes metabolites. **Abbreviations:** 13dpg: 3-Phospho-D-glyceroyl phosphate, 3pg: 3-Phospho glycerate, e4p: Erythrose 4-phosphate, FBA3: Sedoheptulose 1,7-bisphosphate D-glyceraldehyde-3 phosphate lyase, g3p: Glyceraldehyde 3-phosphate, GAPDH: Glyceraldehyde 3 phosphate dehydrogenase, GAPDH(NADP): Glyceraldehyde 3 phosphate dehydrogenase (NADP+), PGK: Phosphoglycerate kinase, PRUK: Phosphoribulokinase, r5p: Ribose 5-phosphate, RBC: Ribulose-bisphosphate carboxylase, rb15bp: Ribulose 1,5-bisphosphate, RPE: Ribulose-5-Phosphate 3-epimerase, RPI: ribose-5-phosphate isomerase, ru5p: Ribulose 5-phosphate, s7p: Sedoheptulose 1,7-bisphosphate, s17bp: Sedoheptulose 1,7-bisphosphate, TKT1: Transketolase 1, TKT2: Transketolase 2, xu5p: Xylulose 5-phosphate.

Table 3.3 |Percentage of cycles containing key metabolites of the pentose phosphate pathway and glycolysis for phototrophic and mixotrophic growth

Carbon metabolism pathway	Phototrophic (% unique cycles)	Mixotrophic (% unique cycles)
Oxidative pentose phosphate pathway	36.9	58.3
Glycolysis	49.8	34.8

Out of the 64 cycles common to both growth conditions, there were four cycles associated to large mass flux differences between the two conditions (two for each condition). **Figure 3.5 (a), (b)** displays cycles that increase as a result of mixotrophic growth, whilst **Figure 3.5 (c)** and **(d)** display cycles that increase with phototrophic growth. Cycles with the largest absolute difference with respect to mixotrophic metabolism involve glutamate (M_glu) and galactose (m_GAL) synthesis (>1500% increase) (**Figure 3.5a**) and carbon assimilation into the OPPP to produce the intermediate sugars E4P (M_e4p), S7P (M_s7p) and Sedoheptulose 1, 7-bisphosphate (M_s17bp) (132% increase).

Phototrophic metabolism resulted in increasing matter being cycled through reactions involving pyruvate metabolism within the mitochondrion (**Figure 3.5c**) and an increased shuttling of malate out of the mitochondria antiporter (R_MALOAATm) synchronised with the import of oxaloacetate, representing a 445% increase and 22% increase respectively. These results collectively suggest that both phototrophic and mixotrophic growth are able to channel photosynthate towards the OPPP and to metabolise pyruvate into alternative pathways as and when needed.

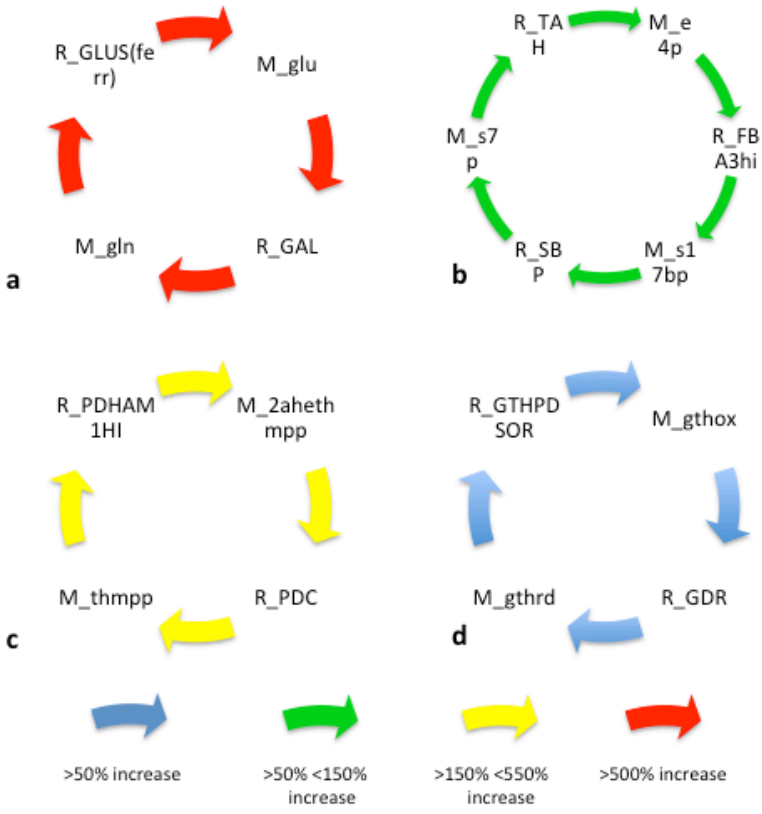

Figure 3.5 |Common cycles within the mitochondrion, thylakoid lumen and chloroplast carrying the largest mass flux

Theoretical cycles observed in both conditions, with the largest % increase of matter being passed through each cycle. (a) Our predictions suggest mixotrophic growth results in increased cycling of glutamine and galactose and (b) increased pentose phosphate pathway activity (c) Phototrophic growth resulted in an increase of pyruvate metabolism within the mitochondrion and (d) increased cycling of glutathione. **Abbreviations:** 2ahethmpp: 2-(alpha-Hydroxyethyl)thiamine diphosphate, e4p: Erythrose 4-phosphate, FBA3hi: Sedoheptulose 1,7-bisphosphate D-glyceraldehyde-3-phosphate-lyase, GAL: Glutamate-ammonia ligase, GDR: Glutathione-disulfide reductase, gln: Glutamine, gthox: Oxidized glutathione, gthrd: Reduced glutathione, GTHPDSOR: Glutathione:protein-disulfide oxidoreductase, glu: Glutamate, GLUS(ferr): Glutamate synthase (ferredoxin dependent), PDC: Pyruvate decarboxylase, PDHAM1HI: Pyruvate dehydrogenase, s17bp: Sedoheptulose 1,7-bisphosphate, s7p: Sedoheptulose 7-phosphate, SBP: Sedoheptulose-bisphosphatase, TAH: Transaldolase, thmpp: Thiamine diphosphate.

3.4 Discussion

The original intent of this research was to investigate theoretical metabolic cycles occurring as a result of altering the growth conditions of the model organism, *C. reinhardtii*. Substrate cycles are fundamental to maintaining organisation within living systems. Cycle decomposition of a model of metabolism of an organism can give detailed descriptions of processes unique to certain physiological conditions. It is well established that cells grown mixotrophically with acetate produce a greater biomass, while exhibiting a lower capacity to perform photosynthesis. Cycle decomposition of a metabolic network of *C. reinhardtii* can provide a description of metabolic cycles that are fundamental to living systems. A prerequisite of the cycle decomposition algorithm is the conservation of mass between substrates and products of all reactions in the metabolic network, a feature frequently ignored in current GEMs. For the model used here, *i*RC1080, a total of 81 reactions were found to be mass inconsistent, showing the need of manual curation. These inconsistencies violate the law of mass-conservation, a fundamental physical principle that cannot be ignored if we want to model complex biological systems with accuracy.

Following cycle decomposition we are able to describe the interlocking of unveiled cycles and how these inhibit or enhance other cycles. Additionally, we are able to observe how changes in the environment can induce changes in cycle fluxes. Here we show that the presence of acetate in the growth medium results in a fundamental change in the primary routes of carbon metabolism, which feeds back into the reactions of photosynthesis. To understand the effect of acetate assimilation on overall metabolism it is first important to consider the cycles unveiled with phototrophic metabolism.

Phototrophic cultures fix CO_2 into triose phosphate. Triose phosphate is incorporated into metabolism by the reactions of gluconeogenesis to generate hexose sugars, which can be stored as starch reserves. In times of need, these reserves can be degraded by glycolytic pathways to release ATP. Glycolysis is compartmentalised in *C. reinhardtii* with the upper half in the chloroplast and the lower half in the cytosol (Kruger and von Schaewen, 2003). Cyclic decomposition analysis reveals a positive feedback loop commencing with the fixation of CO_2, culminating with an increased pyruvate cycling and TCA cycle activity.

The increased cycling of reduced and oxidised plastoquinone as observed in **Figure 3.3(b)** ensures a constant traffic of electrons through the photosynthetic transport chain, specifically though PSII, the photosystem responsible for oxygen evolution. This cycle is therefore closely associated to the cycle observed in **Figure 3.4a**. The products of photosynthesis, ATP and NADPH, are utilised by the Calvin–Benson cycle for the fixing of CO_2 and incorporation of photosynthate into gluconeogenesis. An increased flux of glycolysis would ensure a constant production of pyruvate, as observed in **Figure 3.1a**, maintaining substrate material required for continued TCA activity. As a result, flux is seen to enhance further cycling of TCA intermediates, malate, citrate and oxaloacetate, finally resulting in an increased flux of malate out of the mitochondria associated with an import of oxaloacetate to continue the TCA cycle (**Figure 3.5d**) allowing the model to utilise malate elsewhere.

For mixotrophic cultures, perturbations in the environmental conditions by the addition of acetate have a profound effect on metabolism, as unveiled by cyclic decomposition. Here we are able to show that mixotrophic growth results in an increased number of cycles involving the OPPP intermediates, ultimately enhancing further cycles involving mitochondrial respiration whilst reducing the flux associated with carbon fixation, reducing the requirement of NAPDH.

The OPPP can be thought of as a carbon sink, channelling photosynthate into nucleotide synthesis. This explains associated increases in both the growth rate and biomass observed with a mixotrophic growth regime.

The OPPP occurs in two steps; a reductive and an oxidative step. The oxidative PPP results in the production of NAPDH, without any net gain of ATP (Kruger and von Schaewen, 2003). NAPDH is a well-known electron donor that provides a source of electrons in the mitochondrion to sustain electron transfer during respiration. As we have observed in **Figure 3.2**, the continual cycling of reduced and oxidised ubiquinone could ensure a faster rate of electron acceptance and proton migration to prevent any toxic accumulation of NADPH. Here we see that activation of the OPPP occurs as carbon fixation into the Calvin–Benson cycle is reduced, explaining a down-regulation of photosynthesis and, furthermore, initiates a tight link with the mitochondrial respiratory electron chain. **Figure 3.5b** suggests the OPPP is not a unique attribute associated with mixotrophic growth, as phototrophic simulations also reveal the channelling of material into these pathways, albeit at reduced rates.

By way of cycle decomposition we have unveiled many theoretical cycles that play fundamental roles in adapting to changes in environmental conditions to explain previously observed physiology. By complementing FBA with cyclic decomposition methodology we are presented with a more detailed map of metabolism that would otherwise be ignored. By way of example our previous FBA simulations gave qualification of physiological observations yet failed to predict differences in fluxes through the mitochondrial respiration reactions and a detailed reasoning behind an active OPPP (Chapman et al., 2015). Ultimately, using cyclic decomposition, we have been able to improve our understanding of the network behaviour.

In conclusion, we were able to show a feedback loop existing with the presence of acetate, resulting in a decrease of glycolysis and an increase or activation of the OPPP. These changes in the carbon metabolism pathway all have implications on the ATP: NAPDH budget of the model that ultimately feed deeper into the photosynthetic and respiratory pathways. It is clear that the reactions of photosynthesis are deeply rooted within global metabolism. We have used a completely theoretical approach to gain an insight into the connections between carbon metabolism, photosynthesis and respiration.

Acknowledgements

This work was fully supported by the Biotechnology and Biological Sciences Research Council in association with the Doctoral Training Centre for Integrative Systems Biology (BB/G530225/1) and Fundação de Amparo à Pesquisa do Estado do Rio de Janeiro (101.261/2014).

3.5 References

Baart, G.E., and Martens, D. (2012). "Genome-Scale Metabolic Models: Reconstruction and Analysis," in *Neisseria meningitidis,* ed. M. Christodoulides. Humana Press), 107-126.

Becker, S.A., Feist, A.M., Mo, M.L., Hannum, G., Palsson, B.O., and Herrgard, M.J. (2007). Quantitative prediction of cellular metabolism with constraint-based models: the COBRA Toolbox. *Nat Protoc* 2**,** 727-738.

Chaban, Y., Boekema, E.J., and Dudkina, N.V. (2014). Structures of mitochondrial oxidative phosphorylation supercomplexes and mechanisms for their stabilisation. *Biochimica et Biophysica Acta (BBA) - Bioenergetics* 1837**,** 418-426.

Chapman, S.P., Paget, C.M., Johnson, G.N., and Schwartz, J.-M. (2015). Flux balance analysis reveals acetate metabolism modulates cyclic electron flow and alternative glycolytic pathways in *Chlamydomonas reinhardtii*. *Frontiers in Plant Science* 6.

Chang, R.L., Ghamsari, L., Manichaikul, A., Hom, E.F., Balaji, S., Fu, W., Shen, Y., Hao, T., Palsson, B.O., Salehi-Ashtiani, K., and Papin, J.A. (2011). Metabolic network reconstruction of *Chlamydomonas* offers insight into light-driven algal metabolism. *Mol Syst Biol* 7**,** 52.

Gevorgyan, A., Poolman, M. G., & Fell, D. A. (2008). Detection of stoichiometric inconsistencies in biomolecular models. *Bioinformatics*, *24*(19), 2245-2251.

Hannon, M., Gimpel, J., Tran, M., Rasala, B., and Mayfield, S. (2010). Biofuels from algae: challenges and potential. *Biofuels*. 2010 Sep;1(5):763-84.

Harris, E.H. (2001). *Chlamydomonas* as a Model Organism. *Annu Rev Plant Physiol Plant Mol Biol* 52**,** 363-406.

Jahns, P., and Holzwarth, A.R. (2012). The role of the xanthophyll cycle and of lutein in photoprotection of photosystem II. *Biochim Biophys Acta* 1**,** 182-193.

Johnson, X., and Alric, J. (2013). Central carbon metabolism and electron transport in *Chlamydomonas reinhardtii*: metabolic constraints for carbon partitioning between oil and starch. *Eukaryot Cell* 12**,** 776-793.

Johnson, X., Steinbeck, J., Dent, R.M., Takahashi, H., Richaud, P., Ozawa, S., Houille-Vernes, L., Petroutsos, D., Rappaport, F., Grossman, A.R., Niyogi, K.K., Hippler, M., and Alric, J. (2014). Proton gradient regulation 5-mediated cyclic electron flow under ATP- or redox-limited conditions: a study of DeltaATpase pgr5 and DeltarbcL pgr5 mutants in the green alga *Chlamydomonas reinhardtii*. *Plant Physiol* 165**,** 438-452.

Kritz, M.V., Trindade Dos Santos, M., Urrutia, S., and Schwartz, J.M. (2010). Organising metabolic networks: Cycles in flux distributions. *J Theor Biol* 265**,** 250-260.

Kruger, N.J., and Von Schaewen, A. (2003). The oxidative pentose phosphate pathway: structure and organisation. *Curr Opin Plant Biol* 6**,** 236-246.

Ma'ayan, A., Cecchi, G.A., Wagner, J., Rao, A.R., Iyengar, R., and Stolovitzky, G. (2008). Ordered cyclic motifs contribute to dynamic stability in biological and engineered networks. *Proceedings of the National Academy of Sciences* 105**,** 19235-19240.

Marinari, E., Semerjian, G., and Van Kerrebroeck, V. (2007). Finding long cycles in graphs. *Phys Rev E Stat Nonlin Soft Matter Phys* 75**,** 29.

Merchant, S.S., Kropat, J., Liu, B., Shaw, J., and Warakanont, J. (2012). TAG, You're it! *Chlamydomonas* as a reference organism for understanding algal triacylglycerol accumulation. *Current Opinion in Biotechnology* 23**,** 352-363.

Orth, J.D., Thiele, I., and Palsson, B. Ø.. (2010). What is flux balance analysis? *Nat Biotech* 28**,** 245-248.

Ponce-de-Leon, M., Calle-Espinosa, J., Peretó, J., & Montero, F. (2015). Consistency Analysis of Genome-Scale Models of Bacterial Metabolism: A Metamodel Approach. *PloS one*, *10*(12), e0143626.

Schellenberger, J., Lewis, N. E., & Palsson, B. Ø. (2011). Elimination of thermodynamically infeasible loops in steady-state metabolic models. *Biophysical journal*, *100*(3), 544-553.

Tarjan, R. (1973). Enumeration of the Elementary Circuits of a Directed Graph. *SIAM Journal on Computing* 2**,** 211-216.

4. Global proteomic analysis reveals that acetate alters global metabolism

Stephen Chapman[1], Jean-Marc Schwartz[1] and Giles N. Johnson[1]*

[1] The University of Manchester, Faculty of Life Sciences, Michael Smith Building, Oxford Road, Manchester, M13 9PT, UK

*** Correspondence:** Dr Giles Johnson, University of Manchester, Faculty of Life Sciences, Michael Smith Building, Oxford Road, Manchester, M13 9PT, UK

giles.Johnson@.manchester.ac.uk

Keywords: *Chlamydomonas*, mixotrophic growth, photosynthesis, proteome, flux balance analysis, cyclic electron flow

Author contributions: All work in this chapter was conducted by the lead author except the quantitative proteomic analysis, which was conducted by the Faculty of Life Sciences Bio-Mass spectroscopy core facility. Protein extraction and data analysis was conducted by the lead author.

Abstract
Cultures of *Chlamydomonas reinhardtii* grown in the presence of acetate experience a down-regulation of photosynthesis when compared to their phototrophic counterparts. In an attempt to understand this photosynthetic regulation, label-free proteomics was used to quantify, in relative terms, almost 3000 polypeptides from the organism, to determine their response to growth in acetate.

We obtained a good coverage of proteins involved in the assimilation route of acetate, photosynthesis, the Calvin–Benson cycle, central carbon metabolism and oxidative phosphorylation. Employing a systems biology analysis, we integrated this information into a validated genome scale metabolic model to yield further predictions that highlight what reactions may limit biomass.

We show how acetate assimilation induces a shift in central carbon metabolism to activate the oxidative pentose phosphate pathway, resulting in the cycling of electrons around photosystem I, which accounts for the down-regulation of photosynthesis. We go on to show that isocitrate lyase may be limiting optimal biomass.

In this chapter we show how experimental and computational methodologies can be combined to explain emergent biological phenomena such as the intricate interplay between photosynthesis and carbon metabolism.

4.1 Introduction

Recent efforts to improve the viability of algae for the production of biofuels such as biodiesel (Merchant et al., 2012) or hydrogen (Ghirardi et al., 2000b), have led to increased in interest in understanding the regulation of photosynthesis and metabolism. As a result, the unicellular microalga *Chlamydomonas reinhardtii* has emerged as a model organism to study many cellular processes (Merchant et al., 2007). The sequencing of the genome for this species (Merchant et al., 2007) combined with the development of publicly available genome databases, such as Phytozome (Goodstein et al., 2012), is giving rise to a uniform set of tools and automated analyses which can be applied to the organism. To complement the genome, knowledge of the metabolome, transcriptome and proteome are beginning to allow a true systems biology approach to be applied in understanding cellular phenomena.

Several studies have previously concentrated on analysing the proteome, metabolome and transcriptome of cells grown in nitrogen depleted conditions (Valledor et al., 2014, Park et al., 2015, Wienkoop et al., 2010). However, few studies in the literature have attempted to address the proteomic changes able to explain the down-regulation of photosynthesis that occurs when cells are grown in acetate supplemented media (Heifetz et al., 2000a). This analysis would provide new potential bioengineering strategies that exploit the dynamic behaviour of cellular metabolism in response to acetate availability for increased carbon fixation into biomass.

The primary reactions of photosynthesis are heavily integrated into wider metabolism (Johnson and Alric, 2013). Photosynthesis produces ATP and reducing power to fuel metabolism; hence metabolic changes will feedback into the reactions of photosynthesis (Johnson and Alric, 2012). Proteome changes that alter metabolism are the result of altered gene expression and can give detailed information on acclimatory responses and on the inhibitory role of acetate for photosynthesis. We previously investigated the effect of acetate on metabolism using a range of constraint-based modelling techniques and came to the conclusion that acetate decreased carbon fixation into the Calvin–Benson cycle in addition to the reactions of primary carbon metabolism. We predicted the assimilatory route of acetate into a modified TCA cycle following its conversion to acetyl-CoA using acetyl-CoA synthase (Chapman et al., 2015). Acetate was also predicted to induce a change from a Linear Electron Flow (LEF) between the two photosystems to a Cyclic Electron Flow (CEF) involving only photosystem I (PSI), accounting for the down-regulation of photosynthesis and validated by comparison with published experimental evidence (Johnson et al., 2014b).

Constraint-based modelling techniques are very effective at addressing complex biological behaviour, however one limitation of these approaches is that they ignore other biological processes such as genetic and metabolic regulation (Machado and Herrgård, 2014). With this in mind integration of proteomic data, which follows downstream from such regulation, can more closely resemble living systems.

In the present study, we have examined changes in the proteome of *C. reinhardtii* in response to acetate. Results are analysed in comparison with previous predictions (Chapman et al., 2015) using a genome-scale metabolic model of *C. reinhardtii* (Chang et al., 2011). We performed relative quantitation of the proteome of cells grown either phototrophically and mixotrophically in the presence of acetate. Data on changes in protein content were then used

to refine our previous model to gain a more detailed understanding of how this alga metabolises acetate.

4.2 Method

4.2.1 Cell cultivation and growth

Cultures of *C. reinhardtii* wild-type (137C) were grown in 250 ml conical flasks with 200 ml medium, which were placed in a shaker at 180 rpm and illuminated on a 16-hour light/8-hour dark cycle with light provided by warm-white LED lamps (colour temperature 3000-3200 K) at 140 µMol photons m^{-2} s^{-1}, 22°/16°C day/night.

Mixotrophic cultures were cultivated using 1 mMol Tris-Acetate-Phosphate (TAP), with added potassium phosphate (pH 7.0) and Hutner trace elements (Hutner et al., 1950). Phototrophic cultures were grown in light using a modified minimal medium, which is TAP medium without addition of acetate. The pH of minimal and TAP media was adjusted to a final pH of 7.8.

For inoculation, 250 µl phototrophic cultures in exponential growth phase were axenically transferred to 250 ml conical flasks containing 200 ml of the appropriate medium. Following inoculation of algae, cell growth was monitored at regular intervals until an early logarithmic phase of growth was reached for both cultures, Day 3 for mixotrophic cultures and Day 7 for phototrophic cultures. Growth was assayed as the optical density of cultures at 680 nm (OD680), measured using an Ocean Optics USB4000 spectrophotometer (Ocean Optics, Dunedin, FL, USA). Five replicate cultures were grown for each condition.

4.2.2 Protein extraction

Prior to protein extraction, wet biomass for each sample of each condition was calculated to ensure a sufficient number of cells were maintained for adequate proteomic analysis via centrifugation. Volumes of cell cultures giving cell counts of 3.44 x 10^7 cells +/- 1.50 x 10^6 cells ml^{-1} were calculated for normalisation. Cells were flash-frozen using liquid nitrogen and stored at -20°C prior to extraction. For total protein concentration measurements, proteins were extracted in a buffered solution containing 20 µl of 1 mMol DTT, 780 µl of 25 mMol ammonium bicarbonate, 3% sodium deoxycholate solution, 100 µl of 11% sodium laurate

solution and 1 mMol calcium chloride. 100 µl of working buffer was added to every 10 µg of wet biomass. Each sample was sonicated at 30% for five seconds, and then centrifuged at 500 g for 15 seconds. Another round of sonication and centrifuged was performed to ensure a complete cell disruption. Cells were observed using a light microscope and examined for complete lysis. The whole procedure was performed on ice.

4.2.3 Quantitative proteomic analysis (LC-MS/MS)

Liquid chromatography coupled with tandem mass spectrometry (LC-MS/MS) was used in this study. Total protein concentrations for each sample were quantified using a Direct Detect Spectrometer (Merck Millipore, Germany). 2 µl of sample was spotted onto the reader of the spectrometer and blanked with the extraction buffer for quantification.

For LC-MS/MS analysis, five replicates were used per condition, and 50µg of protein extract was added to 200µl of 25 mM ammonium bicarbonate solution. Samples were denatured at 60°C for 10 minutes, followed by reduction with 3 mM DTT for 10 minutes at 60°C, and alkylation with 9 mM iodoacetamide for 30 minutes at room temperature in the dark. Samples were then digested overnight using proteomics-grade trypsin (Sigma-Aldrich) at 37°C at a protein: enzyme ratio of 50: 1. The sodium laurate and sodium deoxycholate detergent was removed by the addition of trifluoroacetic acid pH 3, and removed using a phase transfer method with two cycles of ethyl acetate. Peptides were desalted with reversed phase R3 beads.

Digested samples were analysed by LC-MS/MS using an UltiMate 3000 Rapid Separation LC (RSLC, Dionex Corporation, Sunnyvale, CA) coupled to an Orbitrap Elite mass spectrometer (Thermo Fisher Scientific, MA, USA). Peptide mixtures were separated using a mixture of two solutions, the first consisting of 92% of 0.1% Formic acid (FA) in water and the second involving a gradient between 8% to 33% of acetonitrile in water, with a constant 0.1% FA. Run time was a total of 120 min at a flow rate of 300 nL min^{-1}. A 75 mm x 250µm i.d. 1.7 µM BEH C18 analytical column (Waters) was used for separation. Peptides were selected for fragmentation automatically by data-dependent analysis.

The acquired MS data were analysed using Progenesis LC-MS (v4.1, Nonlinear Dynamics). The retention times in each sample were aligned using one LC-MS run as a reference, then the 'Automatic Alignment' algorithm was used to create maximal overlay of the two-dimensional feature maps. Features with charges ≥ +5 were masked and excluded from

further analyses, as were features with fewer than three isotope peaks. The resulting peak lists were searched against the *Chlamydomonas reinhardtii* database (V5.5) (Goodstein et al., 2012) using Mascot v2.4 (Matrix Science). Search parameters included a precursor tolerance of 5 ppm and a fragment tolerance of 0.5 Da. Enzyme specificity was set to trypsin and one missed cleavage was allowed. Carbamidomethyl modification of cysteine was set as a fixed modification while methionine oxidation was set to variable. The Mascot results were imported into Progenesis LC-MS for annotation of peptide peaks.

All data were normalised to the median sample using default Progenesis normalisation

4.2.4 Statistics

The standard deviation for protein abundance was calculated from the normalised abundance values. For significance testing, a Bonferroni multiple testing corrected *P*-value was obtained for all proteins resulting from ANOVA, calculated by multiplying the initial *P*-value by the number of quantified proteins and significance was based on corrected *P* values that were less than 0.05.

4.2.5 Protein ontology analysis

To identify enriched functional groups resulting from acetate metabolism, a gene ontology (GO) enrichment analysis was conducted using the singular enrichment analysis tool from AgriGO (http://bioinfo.cau.edu.cn/agriGO/). The statistical test used was Fisher (exact test) and the (Benjamini-) Hochberg correction with a significance level of 0.05 was applied. Functional GO classifications for *Chlamydomonas* proteins were first obtained from the *Chlamydomonas reinhardtii* database (V5.5). Proteomic data resulting from LC-MS/MS was ranked according to fold change and all quantified proteins were categorised using GO terms. This set of proteins was imported as the reference population and the significantly up-regulated and down-regulated proteins from LC-MS/MS were imported for ontological enrichment analysis separately.

4.2.6 Integration of proteomic data into *i*RC1080

Proteomic data from this study were compared to the predictions made in a previous study (Chapman et al., 2015). Discrepancies between model simulations and experimental data were introduced as constraints of the model to further constrain the solution space.

Flux Balance Analysis (FBA) was performed using a pre-existing model of *C. reinhardtii* metabolism, *i*RC1080 (Chang et al., 2011). Maximisation of biomass (μ) was used as the

objective function for FBA. To simulate a mixotrophic growth on acetate, the model inputs were represented as experimental nutrients, light uptake and acetate (constraints found in **Supplementary file 4.1**). Additional constraints imposed on the system included constraining the dry weight of an actively metabolising algal cell (Mitchell et al., 1992), known starch degradation rates in the light (Levi and Gibbs, 1984), and the light-induced inhibition of the enzymes protochlorophyllide reductase (Cahoon and Timko, 2000), phosphofructokinase, glucose-6-phosphate-1-dehydrogenase, glucose 6-phosphate dehydrogenase (Mustroph et al., 2013) and fructose-bisphosphate aldolase (Murakami et al., 2005).

4.3 Results

4.3.1 Acetate increases protein content of cultures and results in a modification of the proteome

Chlamydomonas cell cultures were grown until Day 3 for mixotrophic cultures and Day 7 for phototrophic cultures. At these time points, cultures of cells were entering an early logarithmic growth phase, hence were metabolically active. Cells grown phototrophically had a greater photosynthetic capacity (1.84 nMol O_2 $cell^{-1}s^{-1}$) than cells grown mixotrophically (0.46 nMol O_2 $cell^{-1}$ s^{-1}) (**Chapter 2**). Cells grown phototrophically had significantly greater protein per cell (**Figure 4.1**).

Amongst the ten samples (five replicates for each condition) a total of 2954 proteins were quantified. We applied a filter to the dataset to identify proteins that were significantly up- or down-regulated in the presence of acetate; proteins were only considered when a minimum of three unique peptides could be identified, and were considered to have changed when the relative abundance differed by >1.4 fold (uncorrected P-value <0.05). All replicates in each condition were normalised to total protein content per cell. Following normalisation, 509 proteins were deemed to be significantly up-regulated with acetate, whilst 797 proteins were significantly down-regulated with acetate (for full proteomic dataset, see **Supplementary data file 4.1**).

A principal component analysis was conducted for the proteomic LC – MS/MS data obtained. The first two principal components accounted for 73% of the total variation within the dataset

with the first principle component accounting for the largest separation of data. This analysis indicates that acetate had indeed caused a change in the proteome (**Figure 4.4**).

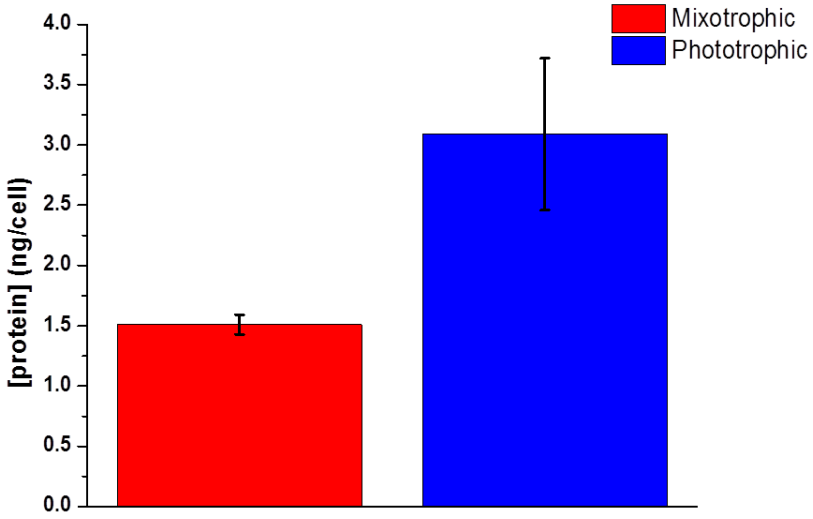

Figure 4.1 |Protein content of mixotrophic and phototrophic cells

Taken from cells entering an early logarithmic phase of growth, Day 3 for mixotrophic cultures and Day 7 for phototrophic cultures. Error bars represent the standard deviation from five biological replicates. Cells grown phototrophically had significantly higher protein content per cell ($P<0.05$; T-test)

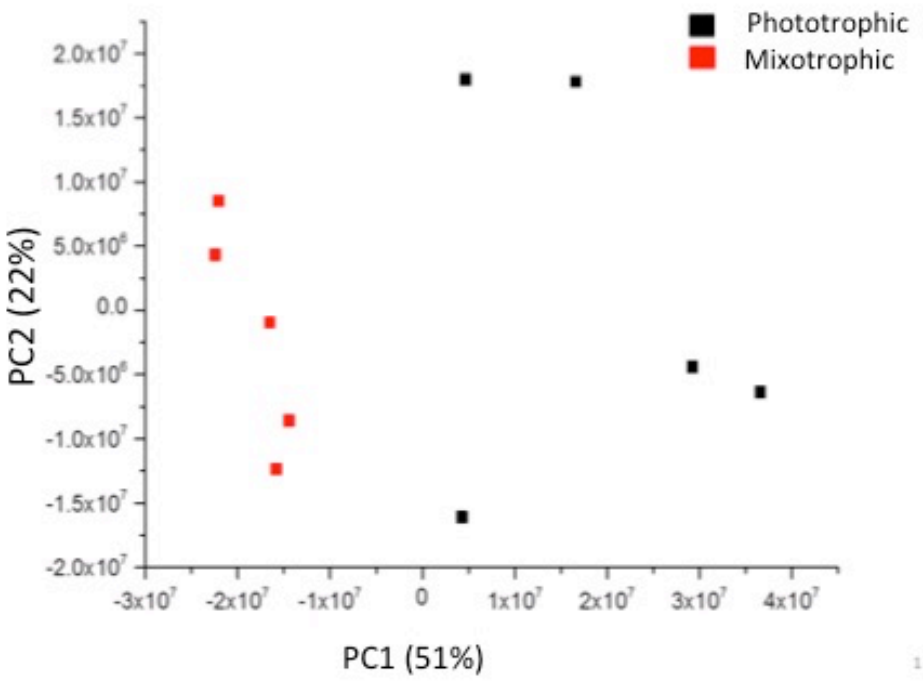

Figure 4.2 |PCA analysis from proteomic analysis from biological replicates of *Chlamydomonas* grown phototrophically and mixotrophically
A principle component analysis was conducted for the entire complement of quantified proteins for phototrophic and mixotrophically grown cultures. Each point represents one biological sample, with phototrophic replicates represented by black squares and mixotrophic replicates by red squares.

4.3.2 Protein ontology analysis to investigate the major biological processes affected by acetate metabolism

Out of the 1711 quantified proteins with GO annotations, 273 up-regulated proteins and 560 down-regulated proteins were considered for protein ontological analysis, based on the ANOVA *P* value. Following protein ontological analysis with AgriGO, there were seven GO terms that were significantly enriched among the up-regulated proteins **(Table 4.1),** and four among the down-regulated proteins whose corrected *P* value was less than 0.05 **(Table 4.2)**. **Figure 4.3** presents the enriched up-regulated GO terms. The top panel shows enriched GO terms related to biological processes and the bottom panel depicts enriched GO terms describing molecular functions, in the context of the Gene Ontology Directed Acyclic Graph for enriched GO terms that are up-regulated with acetate. Significantly enriched down-regulated GO terms relating to biological processes are shown in **Figure 4.4, (top**) whilst the bottom panel displays enriched GO terms describing molecular functions, in the context of the Gene Ontology Directed Acyclic Graph for enriched GO terms that are down-regulated with acetate.

Significantly enriched GO terms up-regulated with acetate include 'translation' (GO:0006412, FDR = 2.0E-03), 'cellular biosynthetic process' (GO:0044249, FDR = 8.6E-4) and 'structural constituent of ribosome' (GO:005198, FDR = 1.4E-04). The observed increase in abundance of proteins associated with the GO terms 'translation', 'ribosome' and 'cellular biosynthesis process' are indicative that acetate induces a switch in metabolism, and increases the translation of metabolic enzymes to facilitate the assimilation of acetate into metabolism, hence cells fed with acetate are more metabolically active which may support a heightened growth rate as we have seen in **Figure 2.7**.

Enriched proteins that were significantly down-regulated with acetate include 'proteolysis' (GO:0006508, FDR =4.2E-04), 'peptidase activity' (GO:0008233, FDR = 1.3E-3' and 'endopeptidase activity' (GO:0004175, FDR = 3.3E-02). Photosynthetic GO terms were not

significantly enriched with acetate as otherwise expected, despite 'photosynthesis' (GO:0015979) occurring nine times in the list of identified down regulated GO terms, however this number was deemed insufficient for statistically significant enrichment.

Table 4.1 Significantly enriched up-regulated GO terms. GO terms are displayed with their description, the number of significantly up-regulated proteins annotated with the GO term, the total number of quantified proteins annotated with the GO term and corrected p-value.

GO term	Description	Number in upregulated list	Number in reference list	p-value	FDR
GO:0044249	cellular biosynthetic process	86	313	2.0E-06	8.6E-04
GO:0006412	translation	46	144	4.6E-06	2.0E-3
GO:0009058	biosynthetic process	90	341	6.5E-06	2.8E-03
GO:0009059	macromolecule biosynthetic process	53	182	1.9E-05	8.2E-03
GO:0034645	cellular macromolecule biosynthetic process	53	182	1.9E-05	8.2E-03
GO:0003735	structural constituent of ribosome	36	95	5.1E-07	1.4E-04
GO:005198	structural molecule activity	36	105	7.2E-06	1.9E-03

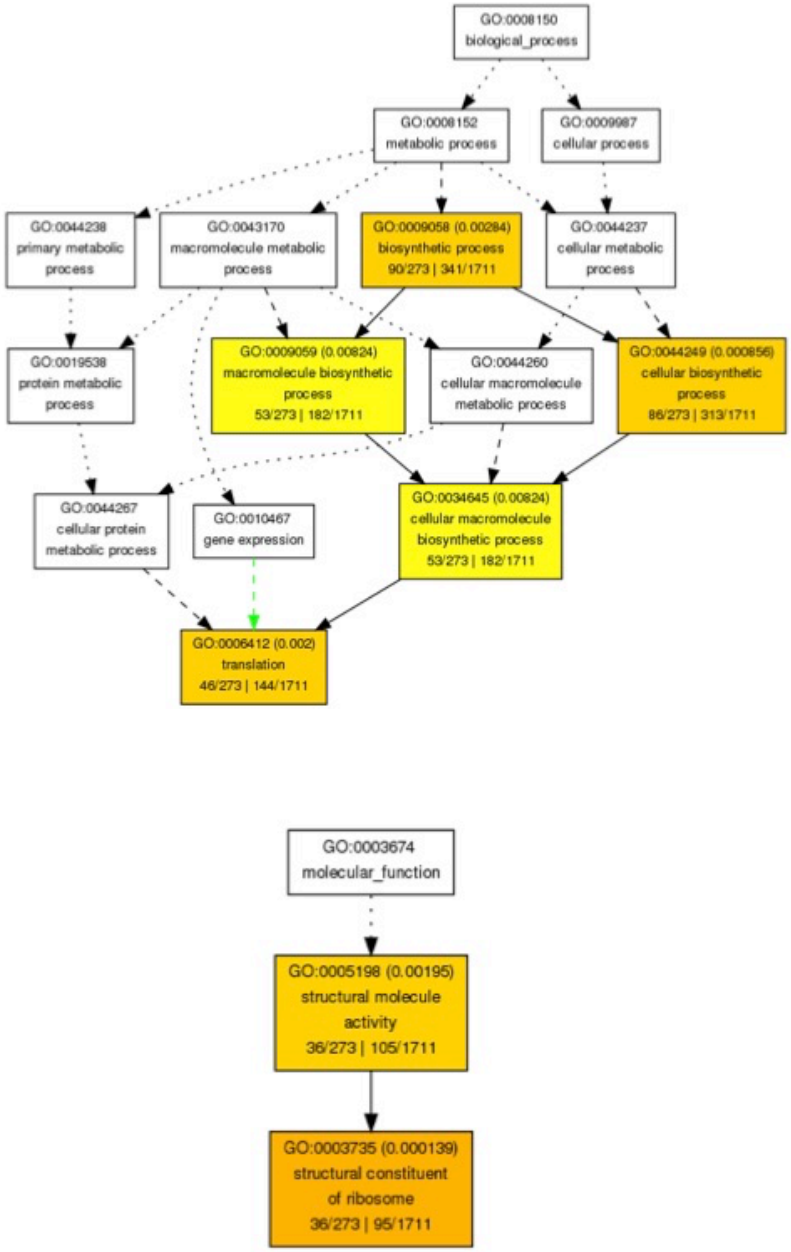

Figure 4.3 | Significantly enriched proteins that are up-regulated with acetate

The top panel shows enriched GO terms related to biological processes and the bottom panel enriched GO terms describing molecular functions, in the context of the Gene Ontology Directed Acyclic Graph. Colouration indicates significance, with yellow representing a lower significance, orange representing a higher significance and white reflecting non significance following Benjamini-Hochberg correction (FDR <0.05, displayed within parenthesis next to the GO term. The description of the GO term is also displayed. Statistical information is displayed for each significantly enriched GO term that refers to the number of times that particular GO term is identified in the up-regulated list and the number of instances it appears

in the reference or background list. ‘Translation’, ‘biosynthetic process’ and ‘cellular biosynthetic process’ are amongst the most significantly enriched GO biological processes, along with ‘structural constituent of ribosome’ being the most significantly enriched molecular function.

Table 4.2 Significantly enriched down-regulated GO terms. GO terms are displayed with their description, the number of significantly up-regulated proteins annotated with the GO term, the total number of quantified proteins annotated with the GO term and corrected p value.

GO term	Description	Number in upregulated list	Number in reference list	p-value	FDR
GO:0006508	proteolysis	43	69	7.9E-07	4.2E-04
GO:0070011	peptidase activity, acting in L-amino acid peptides	39	61	9.6E-07	3.9E-04
GO:0008223	peptidase activity	39	63	3.1E-06	1.3E-03
GO:0004175	endopeptidase activity	22	33	8.1E-05	3.3E-02

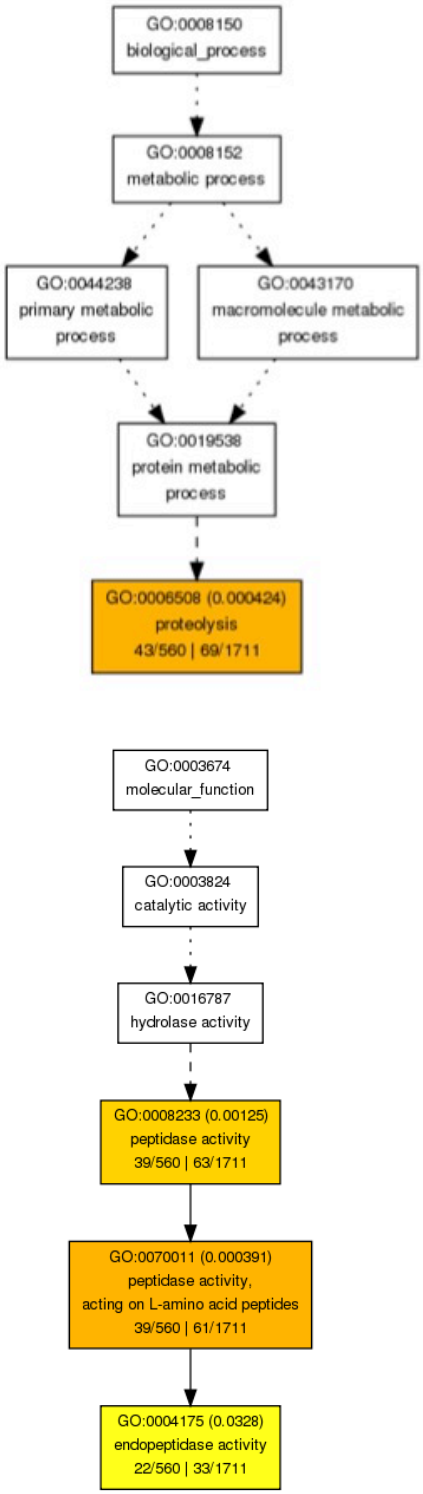

Figure 4.4 | Significantly enriched proteins that are down-regulated with acetate

The top panel shows enriched GO terms related to biological processes and the bottom panel enriched GO terms describing molecular functions, in the context of the Gene Ontology Directed Acyclic Graph. Colouration indicates significance, with yellow representing a lower significance, orange representing a higher significance and white reflecting non significance following Benjamini-Hochberg correction (FDR <0.05, displayed within parenthesis next to

the GO term. The description of the GO term is also displayed. Statistical information is displayed for each significantly enriched GO term that refers to the number of times that particular GO term is identified in the up-regulated list and the number of instances it appears in the reference or background list. 'Proteolysis' and 'peptidase activity acting on L-amino acid peptides' are the most significantly enriched GO terms that are down-regulated with acetate metabolism.

Amongst the other quantified proteins either up- or down-regulated with acetate, we found a good coverage of proteins involved in the light reactions of photosynthesis, the Calvin–Benson cycle, enzymes in gluconeogenesis/glycolysis including the synthesis of starch and enzymes of the pentose phosphate pathway. Furthermore, enzymes belonging to the TCA cycle and oxidative phosphorylation of respiration were quantified. Many other proteins involved in key metabolic pathways were also detected, including antioxidant metabolism, amino acid and lipid synthesis. From the protein ontological analysis, we can conclude that acetate does induce a shift in global metabolism, as cells fed with acetate adjust their metabolism to meet the imposing demands placed by acetate for its assimilation. The benefits of acetate assimilation can be directly observed in terms of enhanced growth rate as is observed with mixotrophic cultures. A higher growth rate, supported by acetate ensures a more successful population of cells.

4.3.3 Proteomic analysis supports the assimilation of acetate via ACS into the mitochondria

The assimilatory route of acetate might occur via different pathways that have implications for respiration and wider metabolism. The primary incorporation of acetate into metabolism has been suggested to occur through one of two steps (Johnson and Alric, 2013). The first is a direct conversion to acetyl-CoA, catalysed by the enzyme Acetyl-CoA Synthase (ACS), whilst the second is a two-step reaction, involving Acetate Kinase (AK) and Phosphate Acetyl-Transferase (PAT). The fate of acetate is also debated, with acetyl-CoA entering either the TCA cycle within the mitochondria, or entering into the glyoxylate cycle within a micro-body.

We previously predicted that acetate is converted to acetyl-CoA by the enzyme ACS and further assimilated into the TCA cycle within the mitochondria, albeit in a cycle that is

similar to the glyoxylate cycle, since isocitrate lyase (ICL) was predicted to be active. The model suggested that succinate dehydrogenase was actively feeding into oxidative phosphorylation.

As seen in **Figure 4.7**, acetate induced a relative increase in the concentration of the enzyme ACS and a decrease in the concentration of ACK. Due to a large variation within the biological samples for both enzymes, these results were not deemed significant. These results suggest acetate assimilation occurs through ACS. The next enzyme in sequence, PAT, was quantified but not significantly altered in the presence of acetate.

Consistent with the entry of acetyl-CoA into the TCA cycle within the mitochondrion, mitochondrial citrate synthase concentration was significantly increased with acetate. We also observed that the TCA cycle enzyme succinate dehydrogenase (succinate ubiquinone oxidoreductase) was also down-regulated by acetate. Inconsistent with the model's prediction, the concentration of the enzyme ICL was significantly decreased by a factor of 3.5 when cells were fed with acetate, as compared to phototrophic cultures. ICL has previously been found in isolated mitochondria from *C. reinhardtii* (Atteia et al., 2009), and despite significant decreases of the enzyme with acetate, we still see the enzyme present in both conditions. Isocitrate dehydrogenase was quantified; however its concentration was not significantly changed between the two conditions. From the detected proteins, the enzymes to be down-regulated within the modified TCA cycle were malate dehydrogenase (MDH) and isocitrate lyase; however, we were unable to obtain 100% coverage of proteins in this subsystem. Given the up-regulation of CS, these results suggest that acetate is more likely to enter the TCA cycle.

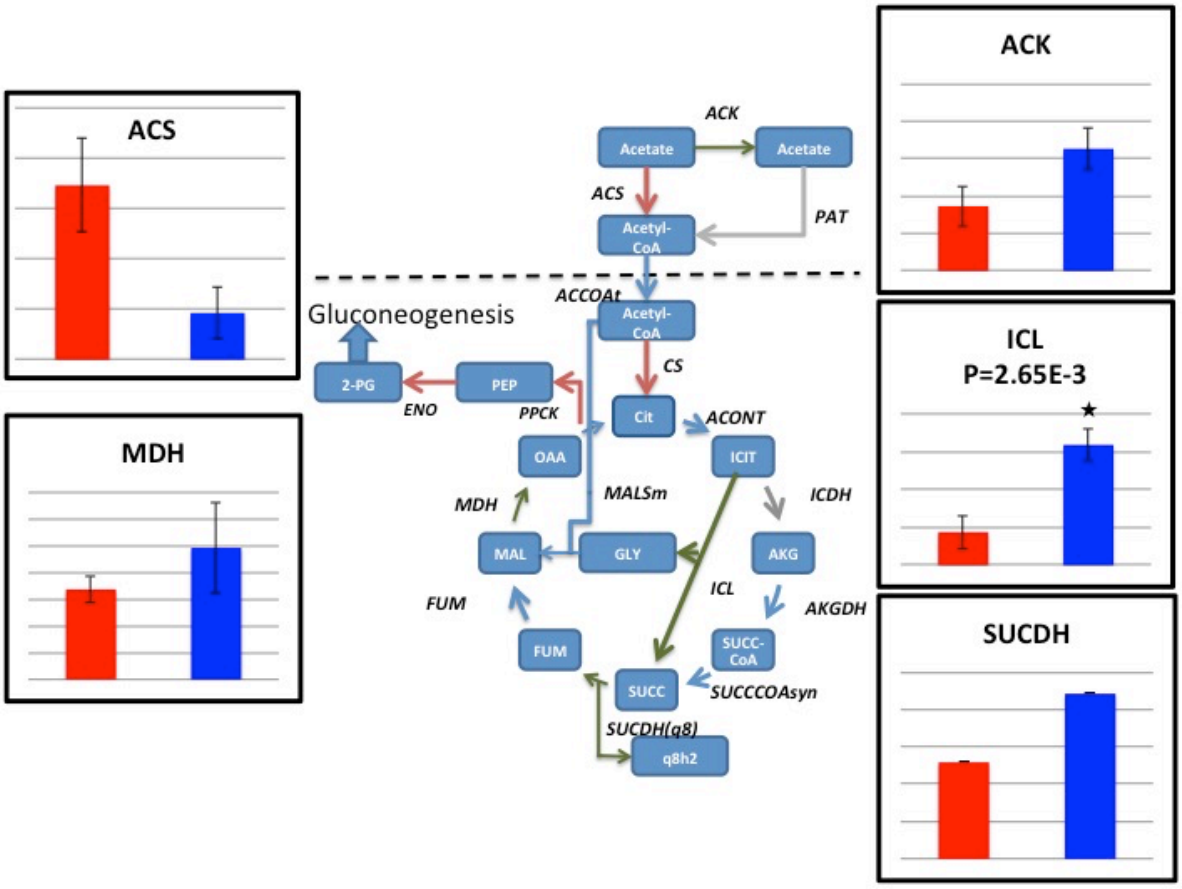

Figure 4.5 |Proteomic analysis accounts for the assimilation of acetate into the mitochondria

Up-regulated proteins with acetate are represented by red connections, down-regulated proteins with acetate are green, non-quantified proteins are blue, and identified proteins that are not significantly regulated between the growth regimes are coloured grey. The column charts surrounding the map show the relative protein concentration of selected proteins. Red bars resemble the relative protein concentration (arbitrary units) of mixotrophic cultures and blue columns are that of phototrophic cells. Starred columns represent significantly up-regulated proteins (Bonferroni-corrected *P*-values have been marked), while absence of a star means that the difference is not statistically significant following correction. Error bars represent the standard deviation of five biological replicates. **Abbreviations:** 2PG: Glycerate 2-phosphate, ACCOAt: Acetyl-CoA/CoA antiporter, ACK: Acetate kinase, ACONT: Aconitate hydratase, ACS: acetyl-CoA synthetase, AKGDH: Alpha Ketogluterate, CIT: Citrate, CS: Citrate synthase, ENO: Enolase, FUM: Fumerate, FUM: fumarate hydratase, GLY: Glyoxylate, ICIT: Isocitrate, ICL: Isocitrate lyase, Mal: Malate, MALSm: malate synthase, MDH: Malate dehydrogenase, OAA: Oxaloacetate, PAT: phosphate acetyltransferase, PEP: Phosphoenolpyruvate, PPCK: Phosphoenolpyruvate Carboxykinase, q8h2: Ubiquinol, SUCC: Succinate, SUCC-CoA: Succinyl CoA, SUCDH: Succinate Dehydrogenase.

4.3.4 Acetate up-regulated cytochrome b6f and PSI whilst down-regulating PSII

In our previous modelling work we predicted that photosynthetic electron transport switches from a linear to a cyclic flow in the presence of acetate, reducing the demand for flux through PSII (Chapman et al., 2015).

We obtained a good coverage of the protein complexes belonging to the light reactions of photosynthesis (**Figure 4.6**). The majority of the subunits belonging to both photosystems were quantified in addition to cytochrome b_6f, ferredoxin NADP reductase and peptides belonging to the ATPase.

The majority of detected PSII proteins decreased significantly in response to acetate, including PSBA and PSBB components of the reaction core of PSII. In addition, subunits of the water-splitting complex, PSBP and PSBQ, also decreased with acetate treatment. PSBO, another subunit of the water-splitting complex, increased with acetate. Variation within the complement of LHC proteins was also observed with respect to acetate metabolism. LHCb3 was identified as being down-regulated with acetate. Out of the remaining light-harvesting complex subunits, we were able to identify LHCb2, LHCb4 and LHCb5. However, these subunits were not significantly altered in response to acetate. We were unable to quantify the remaining LHC subunits or other subunits of the photosystem core. Overall, we conclude that PSII is down-regulated in the presence of acetate.

In contrast to PSII, the majority of subunits belonging to PSI were up-regulated with acetate, including all subunits from the reaction centre, and the vast majority of light-harvesting proteins. Three subunits not quantified were LHCa6, PSAP and PSAQ.

Of the four cytochrome b_6f complex subunits quantified, three increased along with three subunits of the ATP synthase complex with acetate, with the remainder not being quantified. Ferredoxin NADP reductase is the only protein, other than PSII, that is down-regulated with acetate.

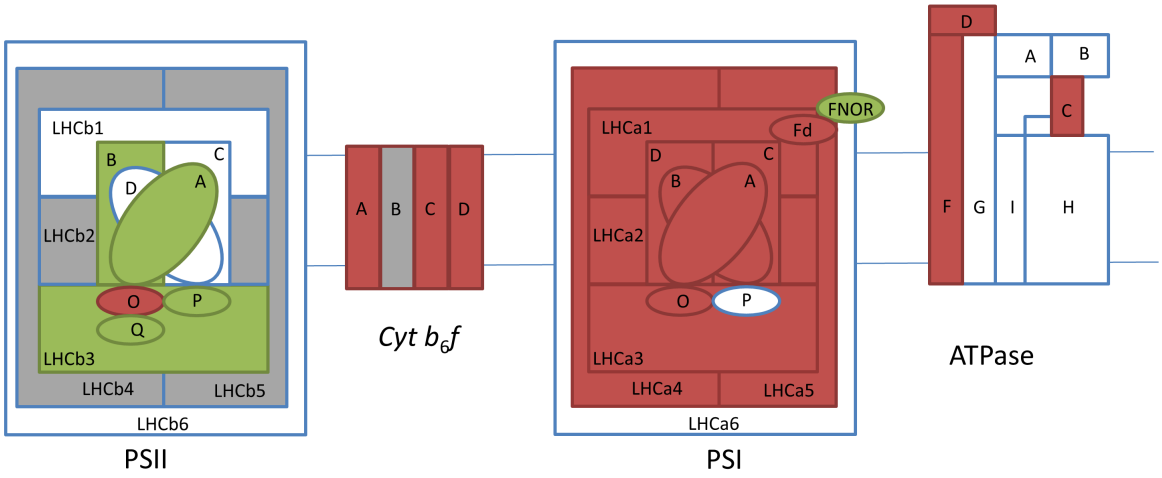

Figure 4.6 |The response of the light reactions of photosynthesis to acetate

A schematic diagram to show the significantly regulated proteins involved in the ETC for phototrophic and mixotrophic cultures. Proteins not quantified are coloured white with a blue outline, Proteins up-regulated with acetate are coloured red, and down-regulated proteins green. Detected proteins exhibiting no significant fold change are coloured grey. Proteins were considered to have significantly changed in abundance when a minimum threshold of 1.4-fold change, with a Bonferroni-corrected *P*-value of <0.05 was achieved.

4.3.5 Acetate decreases Calvin–Benson cycle protein concentrations

The majority of the detected Calvin–Benson cycle enzymes were down-regulated with acetate, however not significantly (**Figure 4.7**). We were able to quantify three Rubisco peptides, two isoforms of the large subunit of the protein, and a small subunit. We were also able to quantify Rubisco activase, an important enzyme required to form the active site of Rubisco. Out of the three Rubisco proteins, only the large β subunit isoform of Rubisco was significantly down-regulated with growth on acetate exhibiting a 46% decrease in the concentration of the subunit. Large overlapping error bars that surround the small subunit indicate non-robust data.

The concentration of other Calvin–Benson cycle enzymes were identified and quantified. We were able to quantify phosphoglycerate kinase, glyceraldehyde-3-phosphate dehydrogenase, triose phosphate isomerase, sedoheptulose-bisphosphatase and the two isoforms of transketolase. However, it was only PGK that exhibited any significantly changed in abundance. We were also able to quantify Phosphoribulokinase (PRUK), which was not significantly altered in abundance with acetate. We were unable to quantify Ribulose-5-

Phosphate 3-Epimerase and Sedoheptulose 1,7-bisphosphate D-glyceraldehyde-3-phosphate-lyase.

These data suggest that acetate does not significantly regulate expression of enzymes of the Calvin–Benson cycle, which is a contrast to previous modelling work where we predicted a loss of Rubisco activity with acetate.

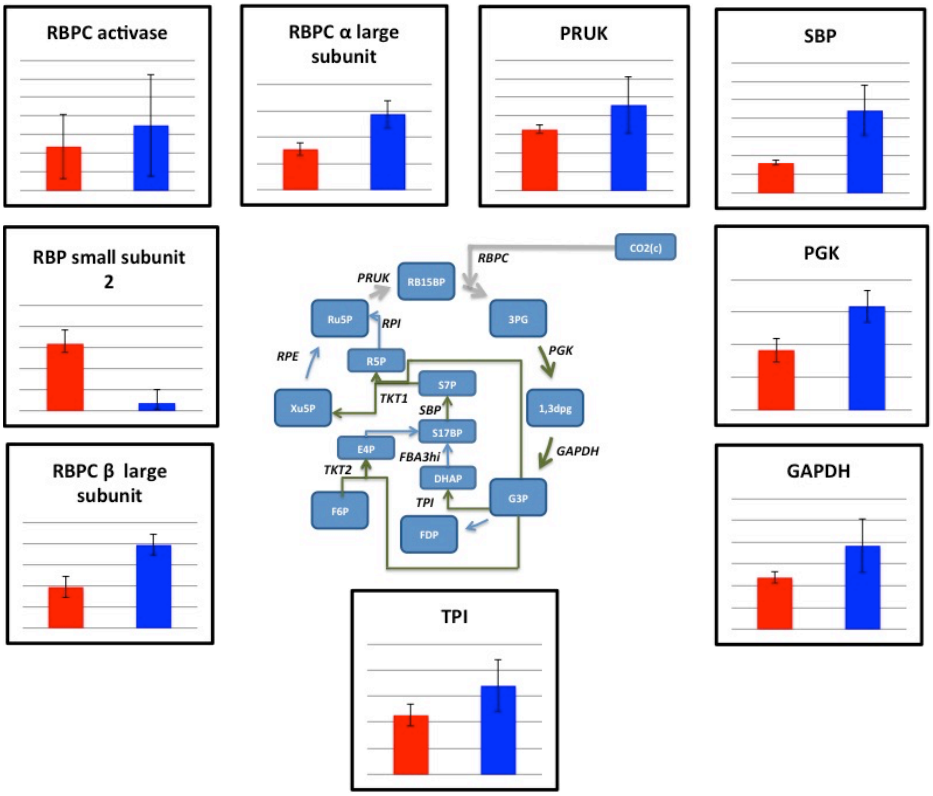

Figure 4.7 |Proteomic analysis of the Calvin–Benson cycle

Quantified proteins of the Calvin–Benson cycle are diagrammatically represented in the centre of the Figure. Up-regulated proteins with acetate are represented by red connections, down-regulated proteins with acetate are green, non-quantified proteins are blue, and identified proteins that are not significantly regulated between the growth regimes are coloured grey. The column charts surrounding the map show the relative protein concentration of select proteins. Red bars resemble the relative protein concentration (arbitrary units) of mixotrophic cultures and blue columns are that of phototrophic cells. Starred columns represent significantly up-regulated proteins. Absence of a star means that the difference is not statistically significant which was the case for all proteins shown here. Error bars represent the standard deviation of five biological replicates. **Abbreviations:** 1,3DPG: 3-Phospho-D-glyceroyl phosphate, 3PG: 3-Phospho-D-glycerate, DHAP: Dihydroxyacetone phosphate, F6P: Fructose 6-phosphate, FBA3hi: Sedoheptulose 1,7-bisphosphate D-glyceraldehyde-3-phosphate-lyase, G3P: Glyceraldehyde 3-phosphate, GAPDH: Glyceraldehyde 3-phosphate dehydrogenase, PGK: Phosphoglycerate kinase, PRUK: Phosphoribulokinase, R5P: Ribose 5-phosphate, RB15BP: Ribulose 1,5-bisphosphate, RPE: Ribulose-5-Phosphate, 3-Epimerase, RPI: Ribose-5-phosphate isomerase,

Ru5P: Ribulose 5-phosphate, SBP: Sedoheptulose 1,7-bisphosphate, S7P: Sedoheptulose 7-phosphate, TKT1: transketolase 1, TKT2: transketolase 2, TPI: triose phosphate isomerase.

4.3.6 Acetate inhibits starch synthesis and activates the oxidative pentose phosphate pathway

We were able to quantify the majority of enzymes involved in the synthesis of starch. The enzymes of glycolysis were well covered in this analysis, with at least three proteins quantified for every enzymatic step of the pathway. For cells fed with acetate, nearly all enzymes of glycolysis and starch metabolism were down-regulated, suggesting a down-regulation of glycolysis that is consistent with model predictions. What did increase with acetate, however, were two key enzymes involved in the Oxidative Pentose Phosphate Pathway (OPPP): 6-phosphogluconolactonase (6PGL) and 6-phosphogluconate dehydrogenase (6PGDH)(**Figure 4.8)**. The OPPP branches flux away from starch metabolism by converting glucose 6-phosphate (G6P) to 6-phosphoglucolactone using glucose 6-dehydrogenase. The enzyme 6PGL converts 6-phosphoglucolactone into 6-Phospho-gluconate (6PG), which is metabolised to Ribulose 5-Phosphate (Ru5P) via 6PGDH. This oxidative pathway results in two molecules of NADPH and one CO_2 molecule for every molecule of G6P that enters the OPPP. The reductive PPP continues from Ru5P to produce fructose 6-Phosphate and triose phosphate in a reversal of the Calvin–Benson cycle (Johnson and Alric, 2013).

Increased traffic of metabolites through the OPPP will increase the NADPH content within the chloroplast. As we see in **Figure 4.7**, the enzymes used for carbon fixation into the Calvin–Benson cycle tend to be down-regulated. For correct functioning the cycle requires nine molecules of ATP and six molecules of NAPDH for the net synthesis of one molecule of triose phosphate. For a cell that is actively producing NAPDH, one way to produce additional ATP is via CEF. One way in which NADPH can be obtained during CEF is through activation of the OPPP.

These experimental results regarding the OPPP are consistent with our previous predictions. However, the finding that there is no significant difference with the levels of Rubisco and PRUK contradicts previous predictions; we therefore need to integrate these new data into the model and investigate how this affects its predictions.

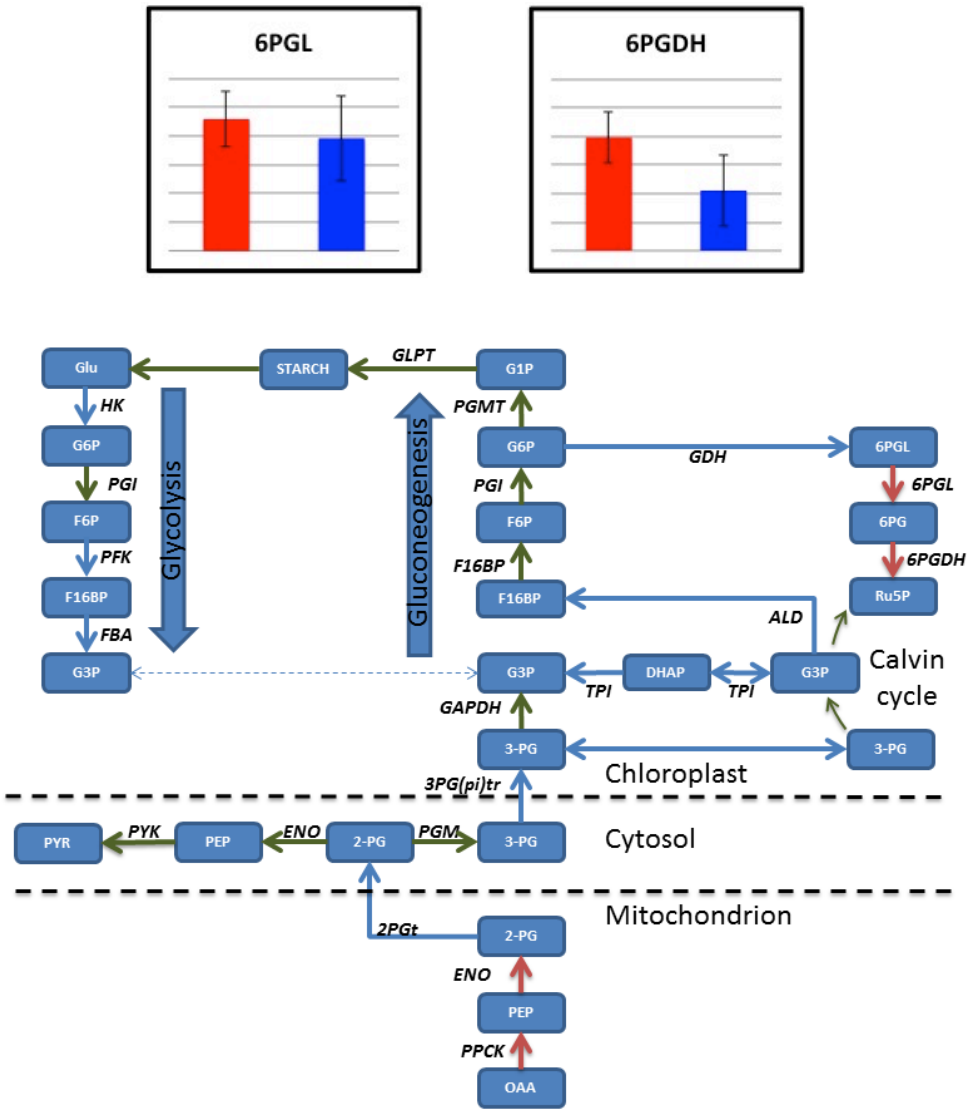

Figure 4.8 |Relative quantification of the enzymes involved with the glycolytic pathways

Quantified proteins of the glycolytic and oxidative pentose phosphate pathway (OPPP) are diagrammatically represented along with relative quantification of 6-phosphogluconolactonase (6PGL) and 6-phosphogluconate dehydrogenase (6PGDH). Up-regulated proteins with acetate are coloured red, down-regulated proteins with acetate are green, and non-quantified proteins are blue. The column charts surrounding the map show the relative protein concentration of selected proteins. Red bars resemble the relative protein concentration (arbitrary units) of mixotrophic cultures and blue columns are that of phototrophic cells. Error bars represent the standard deviation of five biological replicates. Here we show that acetate down-regulates the majority of enzymes used for starch synthesis, however up-regulates enzymes of the OPPP, feeding reductant into the chloroplast. However

these results were all non-significant. **Abbreviations:** 2-PG: Glycerate 2-phosphate, 2PGT: Glycerate 2-phosphate transport, 3-PG: Glycerate 3-phosphate, 3PG(pi)tr: 3-Phospho glycerate/pi antiporter, 6PG: 6-Phospho-gluconate, 6PGL: 6-Phosphoglucolactone, ALD: Aldose, DHAP: Dihydroxyacetone phosphate, ENO: Enolase, F6P: Fructose 6-phosphate, FBA: Sedoheptulose 1,7-bisphosphate D-glyceraldehyde-3-phosphate-lyase, G1P: Glucose 1-phosphate, G3P: Glyceraldehyde 3-phosphate, G6P: Glucose 6 phosphate, GAPDH: glyceraldehyde-3-phosphate dehydrogenase, GDH: Glucose dehydrogenase, HK: Hexokinase, OAA: Oxaloacetate, PEP: Phosphoenolpyruvate, PGI: Glucose-6-phoshate isomerase, PGM: phosphoglycerate mutase, PYK: pyruvate kinase, PYR: Pyruvate, Ru5P: Ribulose 5-Phosphate, TPI: Triose phosphate isomerase.

4.3.7 Acetate induces changes in the complexes involved with oxidative phosphorylation

In addition to the photosynthetic reactions and acetate assimilatory pathways, we analysed the complexes involved in oxidative phosphorylation. Oxidative phosphorylation provides ATP and involves electron flow between five complexes located in the inner mitochondrial membrane. Three of the five complexes act as proton pumps, in which electron migration between the complexes results in a proton gradient over the inner mitochondrial membrane that fuels the synthesis of ATP by the fifth complex, ATP synthase (Chaban et al., 2014).

We have identified peptides from all five complexes involved with oxidative phosphorylation, with four out of the five showing signs of down-regulation with acetate (**Figure 4.9**). This down-regulation of complex I is in contrast with complex II. Complex II, succinate dehydrogenase, was the only complex to contain significantly up-regulated peptides. Complexes III, IV and V remained more or less unchanged; however, the majority of the peptides from these subunits exhibited fold changes typically 50% lower than that of the subunits from complex II. We thus conclude that complex I shows signs of a down-regulation with acetate, whereas complex II is the only complex to show a clear up-regulation.

Complex II serves the function of oxidising succinate, produced in the TCA cycle, and transfers two electrons to the next complex resulting in the production of fumarate, which is converted to malate in the TCA cycle. The down-regulation of the first complex is therefore consistent with the data reported in **Section 3.3** since reductant can be shuttled out of the mitochondria into the chloroplast and channelled into the OPPP. This ensures a limiting supply of reductant in the mitochondria resulting in less protein being needed. An increase of succinate dehydrogenase protein content with acetate could be acting as a switch since succinate production is being increased concurrently as reductant is being trafficked out the

mitochondria. An increased reduction of succinate could compensate for the reduced levels of reduction at complex I to maintain mitochondrial ATP synthesis.

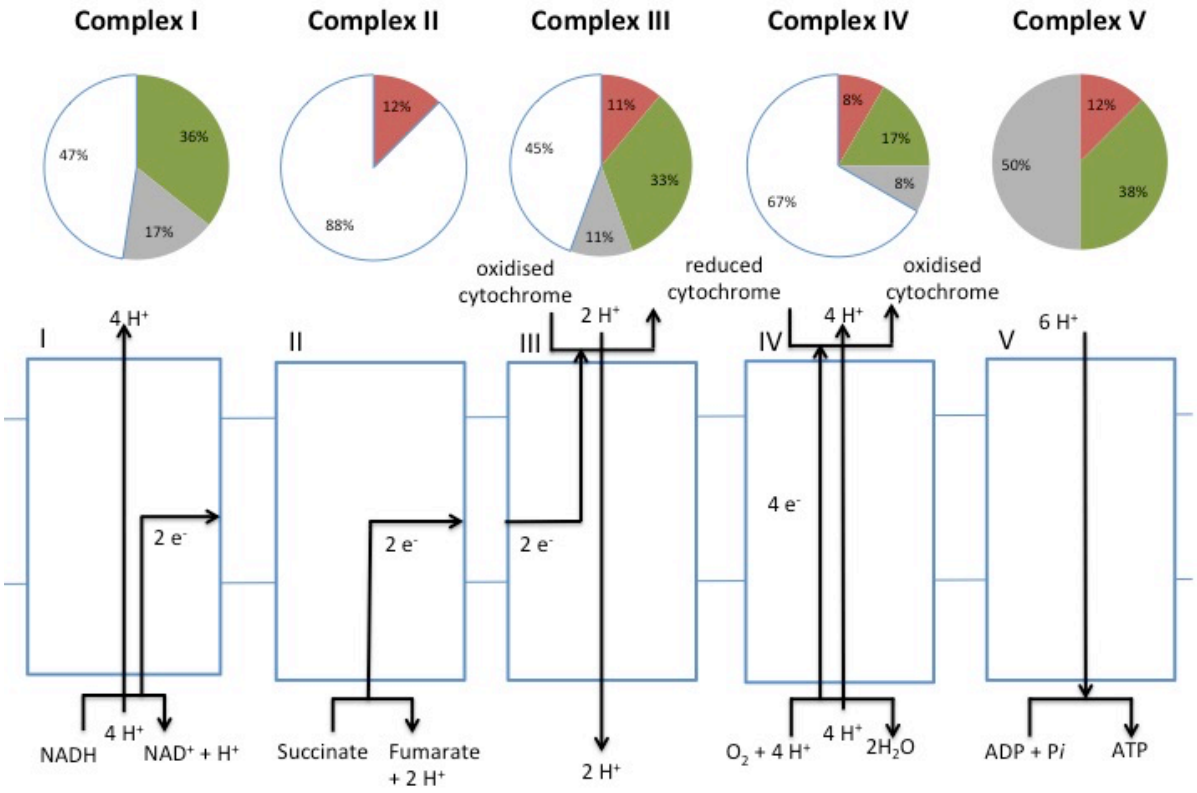

Figure 4.9 |Global proteomic analysis reveals changes to the subunits of oxidative phosphorylation

The proteome of the complexes involved with oxidative phosphorylation were analysed. The pie charts above represent the ratio of up-regulated subunits (red segments) and down-regulated subunits (green). Quantified protein subunits that are not significantly regulated between the growth regimes are represented with grey segments while the ratio of non-quantified proteins are represented by the white segments. Complexes II–V inclusive show proteins that are up- and down-regulated, whereas a large ratio of down-regulated proteins were identified in complexes I, III, IV and V. For complex II, however, we were only able to quantify subunits that are up-regulated.

4.3.8 Proteomic data integration improves the predictive scope of metabolic modelling

Contrary to previous modelling results that suggested fluxes through the reactions of PRUK and Rubisco were inhibited during mixotrophic growth, our proteomic analysis results reveal that there is no significant reduction of the concentration of PRUK, and that Rubisco is down-regulated by 46% for mixotrophically grown cells. With this in mind, constraints were set for PRUK that matched the observed phototrophic flux at 6.04 mMol gDW h^{-1}, and the new mixotrophic flux for Rubisco was constrained at 3.26 mMol gDW h^{-1} to reflect the observed proteomic data. We wanted to investigate how integration of these new data could affect the model predictions on biomass and other selected pathways. The pathways of interest included acetate uptake, the modified TCA cycle, the Calvin–Benson cycle, glycolysis and the OPPP. These pathways were monitored by modelling flux through the respective reactions of ICL, SBP PGI and 6PGL serving as indicative reactions.

As can be seen in **Figure 4.10** when fluxes through PRUK and Rubisco are constrained and the flux through acetate uptake is increased, the activity of ICL, and to a lesser extent SBP, increases. The flux associated with the reactions of PGI and PGL did not vary until acetate uptake was equal to 25 mMol gDw h^{-1}. At this point, any increments of acetate uptake increased the fluxes associated to both PGL and PGI and greatly increased the flux through SBP. As acetate increased beyond this point, the flux through ICL increased less dramatically and saturated at 15.75 mMol gDw h^{-1}, whilst the flux through the biomass reaction followed a similar trend. The capacity to increase the flux through ICL beyond its saturated value to reflect the increase of protein resulted with infeasible solutions.

It is interesting to note that under these conditions the maximum flux associated to acetate uptake was 33 mMol gDw h^{-1}; however, the predicted biomass associated with this increased acetate uptake reached a maximum of 0.173 mMol gDw h^{-1}, which is 85% lower than what was obtained when PRUK and Rubisco were not being utilised.

These results suggest that ICL could be the reaction that limits acetate uptake and biomass accumulation, as it is when flux through ICL starts to saturate that the flux through the biomass reaction also starts to saturate. From FVA (**Supplementary data 1.6**), the maximum allowable flux able to be carried with ICL is predicted to be 24.75 mMol gDw h^{-1}, therefore by relaxing the constraints on this particular reaction we can determine the maximum achievable biomass.

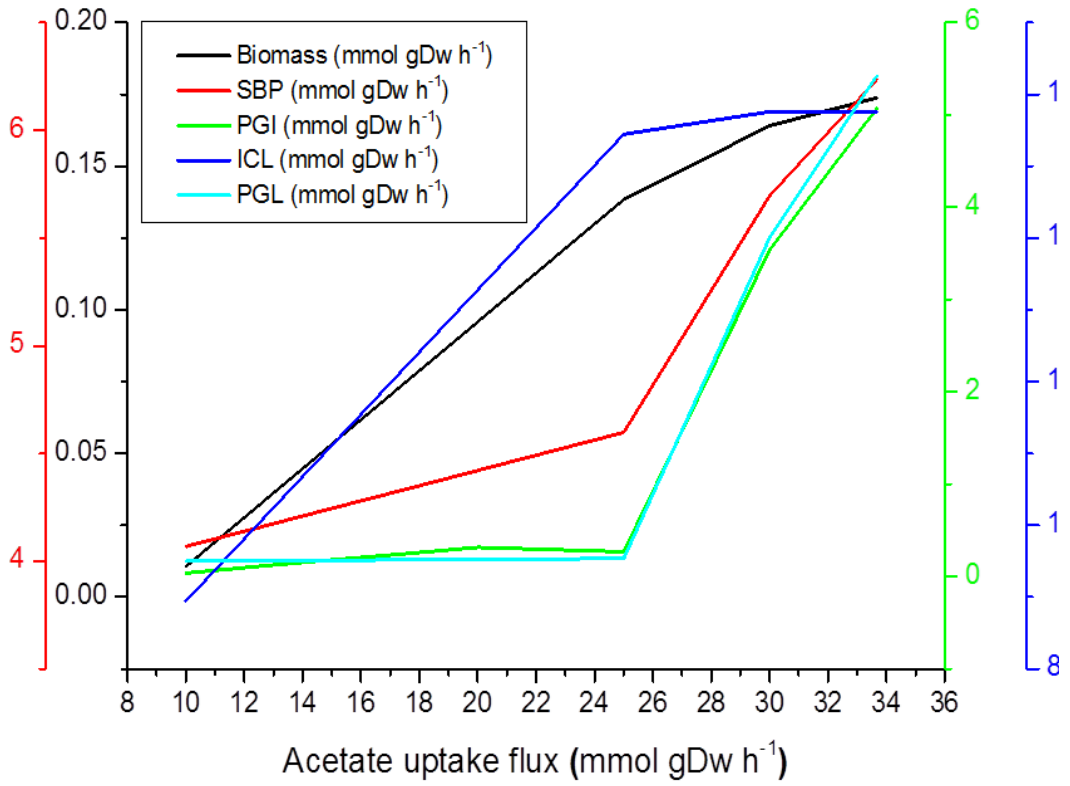

Figure 4.10 |Metabolic fluxes as a function of acetate uptake

Mixotrophic growth of *C. reinhardtii* has two distinct regions. The first region (below 25 mMol gDw h^{-1}) is characterised by increased flux through ICL (isocitrate lyase). The second region (above 25 mMol gDw h^{-1}) appears to be subject to the saturation of ICL, which, despite increasing the fluxes of SBP (sedoheptulose-bisphosphatase), PGI (glucose-6-phosphate isomerase) and PGL (6-phosphogluconolactonase), starts to limit biomass fluxes. The fluxes through Rubisco and phosphoribulokinase were constrained to match experimental data.

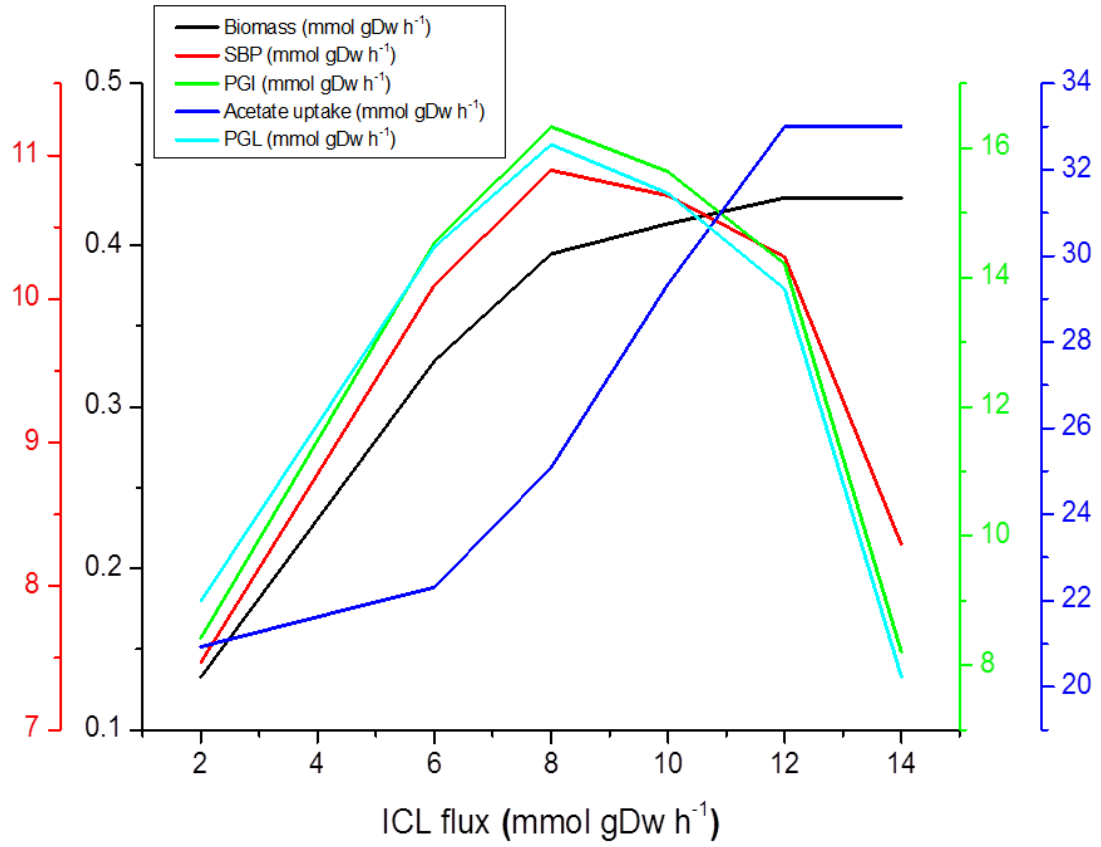

Figure 4.11| Metabolic fluxes as a function of isocitrate lyase flux

In this simulation, activity of SBP (sedoheptulose-bisphosphatase), PGI (glucose-6-phosphate isomerase) and PGL (6-phosphogluconolactonase) all exhibited the capacity to carry much greater flux, resulting in an enhanced biomass of *C. reinhardtii*, as a function of ICL (Isocitrate lyase) flux.

Whilst PRUK and Rubisco flux were still constrained to the same phototrophic values, forcing an increasing flux through ICL resulted in an increased flux through all reactions of interest; with PGI, PGL and SBP increasing drastically. An increased flux through ICL also resulted in an increased flux of acetate uptake. It was only when the flux through ICL reached 8 mMol gDw h^{-1} and above that the flux through PGI, PGL, and SBP started to decrease. Acetate uptake, on the other hand, continued to increase to its earlier measured maximum of 33 mMol gDw h^{-1}. It was only when the flux through the ICL was constrained to 12 and above that acetate uptake plateaued, whilst all other fluxes beside the biomass reaction declined rapidly (**Figure 4.11**). The biomass reaction, however, was able to carry a much

increased flux of 0.429 mMol gDw h^{-1}, displaying a 33% increase as compared to our previous validated simulations.

These simulations suggest that by increasing acetate uptake to its observable maximum and constraining the flux through ICL to 12 mMol gDw h^{-1}, whilst still conserving the activity of PRUK and Rubisco, the system sends the resulting flux through the gluconeogenetic reactions and through the OPPP, which then feeds back into the Calvin–Benson cycle. An increased flux through the OPPP ensures an increased production of NAPDH in the chloroplast, which feeds into the Calvin–Benson cycle to sustain a greater production of triose phosphate entering central metabolism to support a greater biomass production.

4.4 Discussion

In recent years, advances in mass spectrometry-based techniques for measuring metabolites and peptides, combined with the modelling approaches of systems biology, have allowed us to gain a better understanding of the functioning of organisms at a cellular level. Here we sought to analyse the proteome of metabolically active *C. reinhardtii* cells grown in acetate-replete and -deplete conditions to understand further how acetate metabolism integrates central carbon metabolism and how this process could account for an observed down-regulation of photosynthesis.

Using LC-MS/MS with in-solution protein extraction and digestion, we were able to identify and quantify a high proportion of the proteome for both cultures, with 3000 proteins being quantified based on identification of three or more non-redundant peptides. Using this approach we were able to define key metabolic unknowns that surround acetate metabolism and investigate how the metabolism of acetate can influence photosynthesis on a truly global scale. Our results provide detailed information that is consistent with our current understanding of the experimental system, thereby giving us confidence in the quantitation. Integration of the proteomic data has additionally provided insights into how cellular growth can be increased.

For any proteomic data set, there are a number of methods by which data can be normalised for relative quantification. The purpose of normalisation is to determine a global scaling factor. There are several ways to achieve this, and almost all normalisation methods used for

'omic data can be reduced to solving this problem. For example, spiking in known quantities of proteins, total protein abundance normalisation and ratiometric normalisation (with an internal standard). All techniques have to deal with technical variation that can bias the calculation of the scaling factor being used. There is no definitive normalisation strategy, but in this study we have normalised the proteomic data of both growth conditions to the total protein for each sample. Effectively we are assuming that the total protein per cell is a constant, which is not the case. As seen in **Figure 4.1**, phototrophically grown cells contain ~50% more protein per cell when compared to mixotrophically grown cells. This is an incorrect assumption and as such, we are potentially choosing to ignore other proteins specific to phototrophic cultures. The normalisation procedure used here presents the most straightforward method to normalise data. As a result all reported results herein are only correct to the extent of this normalisation procedure.

The thylakoid represents a significant compartment of a *Chlamydomonas* cell, so in spite of there generally being poor coverage of membrane proteins using the extraction procedures adopted and normalisation procedure used, we were able to gain a high level of coverage of the proteome across all compartments and functions (**Figure 4.5–4.11**). We obtained a detailed coverage of the proteins involved in the assimilation of acetate, the Calvin–Benson cycle, central carbon metabolism and mitochondrial oxidative phosphorylation, glycolysis and the pentose phosphate pathway. This aside we were unable to identify the localisation of 1254 proteins, representing 42% of the sample, and were unable to match a metabolic function to 113 proteins. This suggests an incomplete annotation of the genome and reflects the fact that different isoforms of differentially localised proteins cannot be distinguished preventing the allocation of a cellular compartment, as with the enzyme isocitrate lyase (Hayashi et al., 2015).

With the better characterised proteins that were quantified, we are able to provide a clearer description of the assimilatory route of acetate and to better explain the down-regulation of photosynthetic carbon fixation. The assimilatory route of acetate could take the form of a single-step conversion to acetyl-CoA through ACS, or a two-step pathway utilising AK and PAT. Proteomic analysis tends to support the former mode of acetate assimilation since the relative concentration of ACS was greatly increased with mixotrophic cells when compared to phototrophic cells (**Figure 4.5**). Furthermore, the finding that the relative concentration of

AK was increased in cells grown phototrophically further supports this hypothesis. In the phototrophic case, acetate must originate from the breakdown of pyruvate into acetyl-CoA resulting from glycolysis. Acetyl-CoA can then be broken down further into acetate in a mechanism in reverse to the assimilatory route, through activity of PAT and AK (Johnson and Alric, 2013). This would provide ATP to the chloroplast, which could influence a linear electron flow; again backing up the hypothesis that acetate inhibits the glycolytic pathways. Through proteomic analysis, we were able to provide further insights regarding the fate of acetate, since the feeding of acetate into the TCA cycle or glyoxylate cycle is often disputed in the literature (Heifetz et al., 2000a, Plancke et al., 2014). Our results suggest that Acetyl-CoA is fed into the TCA cycle within the mitochondria.

Following the production of Acetyl-CoA, the enzyme citrate synthase, which is responsible for converting acetyl-CoA to citrate in the TCA cycle, was more abundant in mixotrophic samples than phototrophic samples (**Figure 4.5**). Furthermore, the TCA cycle we modelled exists in a modified form that bears similarity to the glyoxylate cycle, through activity of ICL. We show in the same Figure that the concentration of ICL significantly decreased for mixotrophic samples, which remains a disagreement with previous model simulations. Reasons for this disagreement have been discussed in Chapter 2, and possibly relate to the choice of biomass production as the objective function. Furthermore, targeted experimental evidence exists to suggest that ICL is one of the limiting factors of acetate assimilation, since mutants devoid of ICL exhibited lower levels of acetate assimilation (Plancke et al., 2014). We modelled this response in **Figure 4.11** and also came to the same conclusion, i.e. that an increased ICL activity can increase acetate uptake and indeed support a higher biomass.

The finding that acetate up-regulates PSI and *Cyt b*6f whilst down-regulating PSII (**Figure 4.6**) has been previously shown on a physiological level (Roach et al., 2013) and on a targeted protein level (Johnson et al., 2014b). The cycling of electrons around PSI has previously been described to enhance ATP production at the expense of NADPH production (Alric, 2010). The exact mechanism of CEF still remains to be elucidated, as two different pathways of CEF have been described: a proton gradient regulation (PGR5)-dependent and NADPH dehydrogenase (NDH)-dependent pathway. It is believed that the potential NDH complex can associate with LHCa5 and LHCa6 subunits and form an NDH-PS1 super-complex (Peng et al., 2011). Proteomics cannot give any information about the existence of such complexes. However, our proteomic analysis of the thylakoid revealed an up-regulation

of the LHCa5 subunit, whilst LHCa6 went unquantified. This result slightly favours the NDH pathway; however, to better explain the pathway of CEF, a more targeted proteomic study is needed. Following analysis of the overall protein profile, we found no enrichment of photosynthesis although there is clear evidence that this changes from other analysis. This can be explained in terms that the relative investment in different components is changing even though the total investment in photosynthesis is not changing. The processes that do change are consistent with an increase in overall growth rate and so an increased need to invest in processes associated with cell division and growth.

Most enzymes of the Calvin–Benson cycle were significantly down-regulated with acetate (**Figure 4.7**). In the majority of cases there was a significant difference between the two conditions with protein content of mixotrophic samples being lower. The exception to this was with Rubisco and PRUK, with the relative protein content not showing any significant signs of regulation. This suggests that there is no regulation of Rubisco and PRUK with acetate. This remains in contrast to previous modelling work in which we had predicted that mixotrophic growth on acetate supresses activity of these two enzymes. Could acetate therefore reconfigure the proteome to avoid CO_2 fixation? Our results show that *C. reinhardtii* cells are still able to fix CO_2 into the Calvin–Benson cycle; however, an independent regulation of Rubisco may exist. By integrating this finding into the model we are able to increase its predictive capabilities. As seen in **Figure 4.10**, inclusion of the additional constraint imposed on Rubisco and PRUK suggests an optimal biomass can be achieved when we now consider the increasing fluxes emerging from increased acetate assimilation through the reactions of gluconeogenesis and the OPPP.

As we have seen in **Figure 4.8**, acetate decreases the relative protein content of enzymes involved in the glycolytic pathway. This has been previously investigated using labelled carbon in which phototrophic cultures were found to produce larger quantities of starch in *C. reinhardtii* (Singh et al., 2014). We were additionally able to show that acetate induces flux through the OPPP, since the relative concentrations of two key enzymes (6PGL and 6PGDH) were greatly increase (**Figure 4.8)**. The OPPP is a major source of reductant in the form of NADPH and metabolic intermediates for biosynthetic processes (Kruger and von Schaewen, 2003), therefore increased flux through the OPPP must act to supplement the chloroplast with reductant to compensate for the decrease in NAPDH production resulting from activation of CEF.

We had also previously predicted activation of the OPPP (**Chapter 3**), resulting in increased levels of chloroplastic NAPDH. Consistent with this we saw relative increases in PGL and 6PGDH (**Figure 4.8**). This excess reductant feeds back into the Calvin–Benson cycle to ensure an increased production of triose phosphate entering central carbon metabolism and into biomass. Because acetate activates the OPPP to provide excess reductant, the photosynthetic electron transport chain changes from a linear flow to a cyclic flow, thereby inhibiting the excess production of NAPDH, whilst increasing ATP production to meet the metabolic demands required to support a higher biomass. The model was able to predict a decrease in oxygen evolution since flux through the oxygen evolving centre of PSII decreased relative to cells grown without acetate. In contrast, flux through PSI was increased resulting from an increased flux through CEF with flux back into *Cyt* b_6f from feredoxin (Chapman et al., 2015). Through the cycling of electrons around PSI, electrons bypass the OEC associated to PSII, thus explaining the observed down-regulation of oxygen evolution**.** This hypothesis is consistent with other published experimental data.

Experimental evidence exists to show that the mitochondria can cooperate with photosynthesis in an attempt to re-distribute the balance of ATP:NAPDH between the cellular compartments (Dang et al., 2014). As we have reported in **Figure 4.9**, the only complex of the oxidative phosphorylation pathway showing evidence of up-regulated with acetate is succinate dehydrogenase, or complex II. Succinate dehydrogenase oxidases succinate to fumarate whilst reducing ubiquinone to ubiquinol, thereby maintaining a tight link between the TCA cycle and oxidative phosphorylation (Chaban et al., 2014). Due to ambiguous data, it is difficult to give an accurate description of the rest of the complexes since the majority of proteins belong to complex I-IV went unquantified or, as in the case of complex V, half the quantified proteins were not significantly regulated. Knockout studies using mutants of *C. reinhardtii* without the ability to perform CEF have shown that in situations where cellular ATP demand remains high (at high light, low CO_2 environments), increased mitochondrial activity is essential to maintain a similar growth rate to the wild type cells. In our study the cells were metabolically active and, as we have seen in **Figure 4.6**, are performing CEF, which increases ATP production. This ensures a level of regulation with mitochondrial respiration since the ATP demand can be met with CEF alone. These results can be exploited to enhance algal biomass yield. By forcing a flux through the OPPP an increased production of chloroplastic NAPDH might be expected. An increased flux through the OPPP ensures an

increased production of NAPDH in the chloroplast, which feeds into the Calvin–Benson cycle. Mutants unable to perform CEF in this situation would therefore utilise the reductant gained from the OPPP to fix more atmospheric CO_2 into biomass.

In conclusion, we have used LC-MS/MS analysis to quantify the global proteome of *C. reinhardtii* cells grown in the presence and absence of acetate to investigate further how acetate modulates a decrease of photosynthesis. We were able to gain a near complete coverage of the photosynthetic proteins and those of central carbon metabolism in addition to the assimilatory route of acetate. We show how acetate is assimilated into the TCA cycle using ACS which feeds into the OPPP. The ATP demands of triose incorporation into primary carbon metabolism are met through CEF, resulting in a decrease of oxygen evolution.

4.5 References

Alric J. 2010. Cyclic electron flow around photosystem I in unicellular green algae. *Photosynth Res,* 106**,** 47-56.

Atteia, A., Adrait, A., Brughiè, S., Tardif, M., Van Lis, R., Deusch, O., Dagan, T., Kuhn, L., Gonterro, B., Martin W. et al. 2009. A Proteomic Survey of *Chlamydomonas reinhardtii* mitochondria sheds new light on the metabolic plasticity of the organelle and on the nature of the α-proteobacterial mitochondrial ancestor. *Molecular Biology and Evolution,* 26**,** 1533-1548.

Cahoon A. B. & Timko, M. P. 2000. Yellow-in-the-dark mutants of *Chlamydomonas* lack the CHLL subunit of light-independent protochlorophyllide reductase. *The Plant Cell,* 12**,** 559-569.

Chaban, Y., Boekema, E. J. & Dudkina, N. V. 2014. Structures of mitochondrial oxidative phosphorylation supercomplexes and mechanisms for their stabilisation. *Biochimica et Biophysica Acta (BBA) - Bioenergetics,* 1837**,** 418-426.

Chang, R. L., Ghamsari, L., Manichaikul, A., Hom, E. F., Balaji, S., Fu, W., Shen, Y., Hao, T., Palsson, B. O., Salehi-Ashtiani, K. & Papin, J. A. 2011. Metabolic network reconstruction of *Chlamydomonas* offers insight into light-driven algal metabolism. *Mol Syst Biol,* 7**,** 52.

Chapman, S. P., Paget, C. M., Johnson, G. N. & Schwartz, J.-M. 2015. Flux balance analysis reveals acetate metabolism modulates cyclic electron flow and alternative glycolytic pathways in *Chlamydomonas reinhardtii*. *Frontiers in Plant Science,* 6.

Dang K. V., Plet, J., Tolleter, D., Jokel, M., Cuine, S., Carier, P., Auroy, P., Richaud, P., Johnson, X., Alric, J., Allahverdiveya, Y. & Peltier, G. 2014. Combined increases in mitochondrial cooperation and oxygen photoreduction compensate for deficiency in cyclic electron flow in *Chlamydomonas reinhardtii*. *Plant Cell,* 26**,** 3036-50.

Ghirardi, M. L., Zhang, L., Lee, J. W., Flynn, T., Seibert, M., Greenbaum, E. & Melis, A. 2000. Microalgae: a green source of renewable H(2). *Trends Biotechnol,* 18**,** 506-11.

Goodstein, D. M., Shu, S., Howson R., Neupane, R., Hayes, R. D., Fazo, J., Mitros, T., Dirks, W., Hellstein, U., Putnam, N. & Rokhshar, D. S. 2012. Phytozome: a comparative platform for green plant genomics. *Nucleic Acids Research,* 40**,** D1178-D1186.

Hayashi, Y., Sato, N., Shinozaki, A. & Watanabe, M. 2015. Increase in peroxisome number and the gene expression of putative glyoxysomal enzymes in *Chlamydomonas* cells supplemented with acetate. *J Plant Res,* 128**,** 177-85.

Heifetz, P. B., Forster, B., Osmond, C. B., Giles, L. J. & Boynton, J. E. 2000. Effects of acetate on facultative autotrophy in *Chlamydomonas reinhardtii* assessed by photosynthetic measurements and stable isotope analyses. *Plant Physiol,* 122**,** 1439-45.

Hutner, S. H., Provasoil, L., Schatz, A. & Haskins, C. P. 1950. Some Approaches to the Study of the Role of Metals in the Metabolism of Microorganisms. *Proceedings of the American Philosophical Society,* 94**,** 152-170.

Johnsin, X. & Alric, J. 2012. Interaction between starch breakdown, acetate assimilation, and photosynthetic cyclic electron flow in *Chlamydomonas reinhardtii*. *J Biol Chem,* 287**,** 26445-52.

Johnson, X. & Alric, J. 2013. Central carbon metabolism and electron transport in *Chlamydomonas reinhardtii*: metabolic constraints for carbon partitioning between oil and starch. *Eukaryot Cell,* 12**,** 776-93.

Johsnon, X., Steinbeck J., Dent, R. M., Takahashi, H., Richaud, P., Ozawa, S., Houille-Vernes, L., Petroutsos, D., Rappaport, F., Grossman, et al. J. 2014. Proton gradient regulation 5-mediated cyclic electron flow under ATP- or redox-limited conditions: a study of DeltaATpase pgr5 and DeltarbcL pgr5 mutants in the green alga *Chlamydomonas reinhardtii*. *Plant Physiol,* 165**,** 438-52.

Kriger, N. J. & Von Schaewen, A. 2003. The oxidative pentose phosphate pathway: structure and organisation. *Curr Opin Plant Biol,* 6**,** 236-46.

Levi, C. & Gibbs, M. 1984. Starch degradation in synchronously grown *Chlamydomonas reinhardtii* and characterization of the amylase. *Plant Physiology,* 74**,** 459-463.

Machado, D. & Herrgård, M. 2014. Systematic evaluation of methods for integration of transcriptomic data into constraint-based models of metabolism. *PLoS Comput Biol,* 10**,** e1003580.

Merchant, S. S., Kropat, J., Liu, B., Shaw, J. & Warakanont, J. 2012. TAG, You're it! *Chlamydomonas* as a reference organism for understanding algal triacylglycerol accumulation. *Current Opinion in Biotechnology,* 23**,** 352-363.

Merchant, S. S., Prochnik, S. E., Vallon, O., Harris, E. H., Karpowicz, S. J., Witman, G. B., Terry, A., Salamov, A., Fritz-Laylin, L. K., Marechal-Drourard, L., Mueller-Roeber, B., Rajamani, S., Sayre, R. T., Brokstein, P., et al. 2007. The *Chlamydomonas* genome reveals the evolution of key animal and plant functions. *Science,* 318**,** 245-50.

Mitchell, S. F., Trainor, F. R., Rich, P. H. & Goulden, C. E. 1992. Growth of *Daphnia Magna* in the laboratory in relation to the nutritional state of its food species, *Chlamydomonas reinhardtii*. *Journal of Plankton Research,* 14**,** 379-391.

Murakami S., Kuehnle, K. & Stern, D. B. 2005. A spontaneous tRNA suppressor of a mutation in the *Chlamydomonas reinhardtii* nuclear MCD1 gene required for stability of the chloroplast petD mRNA. *Nucleic Acids Research,* 33**,** 3372-3380.

Mustroph, A., Stock, J., Hess, N., Aldous, S., Dreilich, A. & Grimm, B. 2013. Characterization of the phosphofructokinase gene family in rice and its expression Under Oxygen Deficiency Stress. *Frontiers in Plant Science,* 4**,** 125.

Park J. J., Wang, H., GargouriI, M., Deshpende, R. R., Skepper, J. N., Holguin, F. O., Juergens M. T., Shachar-Hill, Y., Hicks, L. M. & Gang, D. R. 2015. The response of *Chlamydomonas reinhardtii* to nitrogen deprivation: a systems biology analysis. *Plant J,* 81**,** 611-24.

Peng, L., Yamamoto, H. & Shikanai, T. 2011. Structure and biogenesis of the chloroplast NAD(P)H dehydrogenase complex. *Biochim Biophys Acta,* 8**,** 945-53.

Plancke, C., Vigeolas, H., Hohner, R., Roberty, S., Emonds-Alt, B., Larosa, V., Willamme, R., Duby, F., Onga DhaliI, D., Thonart, P., Hiligsmann, S., Franke, F., Eppe, G., Cardol, P., Hippler, M. & Remacle, C. 2014. Lack of isocitrate lyase in *Chlamydomonas* leads to changes in carbon metabolism and in the response to oxidative stress under mixotrophic growth. *Plant J,* 77**,** 404-17.

Roach, T., Sedoud, A. & Krieger-Liszkay, A. 2013. Acetate in mixotrophic growth medium affects photosystem II in *Chlamydomonas reinhardtii* and protects against photoinhibition. *Biochim Biophys Acta,* 10**,** 17.

Singh, H., Shukla, M. R., Chary, K. V. R. & Rao B. J. 2014. Acetate and Bicarbonate Assimilation and Metabolite Formation in *Chlamydomonas reinhardtii*: A (13)C-NMR Study. *PLoS ONE,* 9**,** e106457.

Valledor, L., Furuhashi, T., Recuenco-Munoz, L., Wienkoop, S. & Weckwerth, W. 2014. System-level network analysis of nitrogen starvation and recovery in *Chlamydomonas reinhardtii* reveals potential new targets for increased lipid accumulation. *Biotechnology for Biofuels,* 7**,** 171.

Wienkoop, S., Weiβ, May, P., Kempa, S., Irgang, S., Recuenco-Munoz, L., Pietzke, M., Schwemmer, T., Rupprecht, J., Egelhofer, V. & Weckwerth, W. 2010. Targeted proteomics for *Chlamydomonas reinhardtii* combined with rapid subcellular protein fractionation, metabolomics and metabolic flux analyses. *Molecular BioSystems,* 6**,** 1018-1031.

Zhou Du, Xin Zhou, Yi Ling, Zhenhai Zhang, and Zhen Su. 2010. agriGO: a GO analysis toolkit for the agricultural community. *Nucleic Acids Research* Advance Access published on July 1, DOI 10.1093/nar/gkq310. Nucl. Acids Res. 38: W64-W70.

5. General discussion

The overriding aim of this PhD was to develop ways of combining experimental and modelling work to understand algal metabolism. The objectives were to use these approaches to investigate acetate assimilation in *C. reinhardtii* and to explain how a mixotrophic growth on acetate can lead to a repression of photosynthesis for this model organism. By using a systems biology analysis, we have indeed characterised the assimilatory route of acetate and have put forward a model that can predict the observed down-regulation of photosynthesis. Understanding the mechanism of how green microalgae regulate photosynthesis is of upmost importance and has implications for increasing the biofuel producing potential of the organism. By increasing photosynthetic activity, an enhanced partition of carbon from the atmosphere into TAG and biomass synthesis may be obtained. The initial step, however, is to understand how acetate is assimilated and how the assimilation of acetate can regulate photosynthesis at the first instance.

Photosynthesis is one of the most regulated processes in nature and is heavily integrated with metabolism on the global level. As such, methods that take global metabolism into account are most suitable for such an investigation. Following the publication of the genome sequence of *C. reinhardtii*, a number of genome-scale metabolic models (GEMs) have been built for the organism, which take primary carbon metabolism into account. Owing to the greater complexity of the photosynthetic reactions and the centrality of the chloroplast, housing the majority of metabolic reactions, *i*RC1080 was chosen as the most suitable GEM to investigate the down-regulation of photosynthesis. The original model was adapted for use for this particular investigation (**Chapter 2**), with key errors in electron transport being rectified, and the FBA predictions were compared with and validated against physiological data. The resulting metabolic fluxes were compared between the different growth regimes giving a theoretical description of acetate metabolism, and key metabolic reactions that were active or inactive as a result of acetate metabolism were identified. The next chapter (**Chapter 3**) involved cycle decomposition of the network into cyclic and acyclic flows of substances. Application of the cycle decomposition algorithm revealed how flux distributions are reorganised, following mixotrophic growth on acetate to yield further predictions. The final results chapter, **Chapter 4**, aimed to provide an enhanced level of model validation by using semi-quantitative proteomics data for comparison with the model's predictions. By

analysing the proteome of actively growing cells, we were able to quantify proteins in the majority of pathways involved with acetate assimilation, carbon fixation leading up to starch accumulation, and photosynthesis.

When the results of **Chapters 2-4** are examined together we are able to see a consistent set of results that provides a description of acetate assimilation and its effect in reducing photosynthesis. We show that when cells are fed with acetate, in addition to CO_2, the assimilatory route of acetate is into the TCA cycle, following conversion to acetyl-CoA by the enzyme acetyl synthase, requiring ATP. An increased TCA activity also increased the activity of gluconeogenic pathways; however, the OPPP is active under mixotrophic conditions, feeding carbon back into central metabolism. The OPPP results in a net production of chloroplastic reductant. As a means to regulate NADPH levels, a potentially harmful reductant, CEF is operational which increases the ATP:NAPDH ratio to satisfy the metabolic demands imposed by acetate on metabolism. As a result, electrons are cycled around PSI, which avoids the production of NAPDH and avoids the need for PSII, explaining the down-regulation of photosynthetic O_2 evolution with acetate.

As described in **Chapter 2**, we began by running simulations that optimised the biomass component of cells under phototrophic and mixotrophic growth conditions. The fluxes obtained from these simulations were compared to the growth rates of cultures of *C. reinhardtii* in acetate-replete and -deplete conditions. In addition, we measured the photosynthetic activity of the two cultures and compared this to the model's predictions. In agreement with published literature, acetate increased the growth rate at the same time as decreasing photosynthesis (**Figure 2.7**). Model predictions qualitatively matched those of experimental data, as summarised in **Table 2.2**, giving a high level of confidence in the predictive capabilities of the model. By following fluxes through carbon metabolism we concluded that the assimilation of acetate occurs via the activity of acetyl-CoA synthase (ACS), into a modified TCA cycle within the mitochondrion, as seen in **Figure 2.1**. With respect to flux being carried through ACS, allowing for the conversion of Acetyl-CoA in a single step as opposed to the double-step pathway, this could be a result of the solver being used in conjunction with the COBRA toolbox. Due to the optimality criteria of FBA and constraints imposed on the system, the pathway involving ACS reflects the most efficient pathway out of the two, hence the one most likely to be favoured by FBA, which may or may

not be reflected by nature. One can argue however, that nature must have evolved to use the most efficient pathways available. Following proteomic analysis, we were able to quantify proteins involved in acetate assimilation and these results are indicative of a change in the proteome that suggests the simpler route of acetate assimilation took place. As shown in **Figure 4.4**, the concentration of the enzyme ACS had increased, whilst ACK had decreased and PAT was not observed to significantly change between the two conditions. These data suggest that the model was correct with this prediction.

Using a reaction essentiality analysis, we theorise that ICL is an essential enzyme, induced by acetate metabolism. This prediction has been experimentally verified, since mixotrophic metabolism induced the expression of ICL. The essentiality of ICL, however, has been contested in the same study, since mutants missing ICL, and grown in the presence of acetate were still capable of sub-optimal growth supporting a non-essential role of ICL (Plancke et al. 2014). Proteomic analysis in **Chapter 4** revealed that the concentration of ICL was significantly reduced with acetate, further supporting a non-essential role of the enzyme.

The conversion of acetate into Acetyl-CoA requires ATP. Mixotrophic growth has been shown to down-regulate glycolysis, hence also decreasing ATP production that would usually derive from the glycolytic pathway. Could CEF be responsible for supplying additional ATP for the conversion of acetate into Acetyl-CoA? It is hard to say precisely what this source of ATP may be, since there are numerous ATP-producing pathways within global metabolism. To answer this question, a more directed analysis needs to be conducted. One interesting experiment could involve the use of radioactively labelled phosphate into the growth medium of phototrophic and mixotrophic cultures. By assuming that some of the labelled phosphate will end up incorporated into ATP, we would then be in a position to identify which pathways provide additional ATP, by tracking the isotope through metabolism. In this way we could assess if the ATP used for acetate assimilation is derived from CEF. If this is the case, a further interesting study could be as described above with the use of mutants devoid of CEF, such as PGR5 mutants. Cells of these mutants are unable to adjust the stoichiometry of ATP:NAPDH since cells here are only capable of performing LEF.

Our results also suggest that Acetyl-CoA is fed into the TCA cycle within the mitochondria. This was first predicted in **Chapter 2** and strengthened further by quantification of proteins

in **Chapter 3**. The alternative route of acetate assimilation that has been reported is within the glyoxylate cycle in specialised microbodies or glyoxysomes (Dal'Molin et al., 2011). In higher plants, glyoxysomes are believed to play a role in the β-oxidation of fatty acids and the glyoxylate cycle as a part of fatty acid metabolism. The glyoxylate cycle uses five enzymes that can also be found in the TCA cycle: citrate synthase, aconitase, succinate dehydrogenase, fumarase, and malate dehydrogenase. We have observed that the relative concentrations of citrate synthase increases whilst ICL decreases with acetate metabolism, despite the reduction of malate dehydrogenase for the same condition. These results are in contrast to the results obtained by Hayashi et al. (2015) who recorded an increase in the transcript levels of glyoxysomal MS, MDH, ICL and CS when cells were supplemented with acetate, suggesting that glyoxysomes are involved with acetate metabolism (Hayashi et al., 2015). Since we were unable to quantify any proteins of the glyoxylate cycle that were significantly regulated we are unable to say with confidence whether glyoxysomes or other microbodies are involved with acetate metabolism. This will require further attention through more specific targeting of glyoxysomal proteins, before we can gain a better understanding of their involvement with acetate metabolism.

Rubisco is arguably the most abundant and important protein in existence since it is responsible for the fixation of over 99% of all organic carbon on earth (Meyer and Griffiths, 2013). The finding that FBA predicted a repression of Rubisco and PRUK in **Chapter 2** came as a surprise, as this suggests acetate inhibits carbon fixation, which is not the case. In the study by Heifetz et al (2000), radioactive labelling was used to explore the effect of acetate on carbon fixation. The results of this study show that acetate metabolism did not completely supress CO_2 fixation, which is a complete contradiction to the predictions made by the model. In light of this, using proteomic analysis, we observed that the concentration of Rubisco and PRUK are not repressed, merely reduced. We concluded this chapter by integrating this information into the original model and testing the sensitivity of other key enzymes as a result of increasing acetate uptake (**Figure 4.09**) and increasing the flux through the ICL reaction (**Figure 4.10**). We were able to show how the biomass of *C. reinhardtii* can increase beyond previously validated predictions, as seen in **Table 2.2**, by increasing the flux through the gluconeogenesis pathway and diverting this flux back into the Calvin–Benson cycle facilitated by the OPPP. Activation of the OPPP ensures production of NAPDH in the chloroplast which feeds into the Calvin–Benson cycle, maintaining an enhanced efficient carbon fixation rate. It has been suggested that NADPH takes part in CEF

by reducing the plastoquinone pool (Bukhov et al., 2002). If this is correct, could the NAPDH produced from the OPPP be supporting CEF?

In this research, we wanted to investigate if computational methodologies can complement experimental techniques to address biological phenomena. As demonstrated by **Chapters 2-4**, we have indeed demonstrated that constraint-based modelling techniques can be a powerful tool in understanding metabolism for the model organism, *C. reinhardtii*. As we have discussed in **Chapter 3**, one of the main challenges remaining is to improve the predictive scope of such models by incorporating known regulatory steps. GEMs that take into account regulatory mechanisms have been developed (Herrgård et al., 2006) for relatively small-scale models. Because regulation occurs on many levels, extending to the genetic and metabolic level, integrating regulation into larger GEMs proves more of a challenge. In this study, we employed a cycle decomposition algorithm to understand how metabolic cycles affect flux distributions. Integration of transcriptomic data into the model to account for regulation might increase the predictive scope of the model. Regulation aside, GEMs can only be as accurate as their genetic annotations in the first instance. Furthermore, the solution obtained by FBA is determined by the constraints set in place for each simulation. Therefore, it is very important to invest time in gaining an appreciation for the scope of the experimental work that has been collected. One important feature that continues to be highlighted is the need for a manual curation of all models.

With regards to modelling of multi-scale systems, the choice of objective function therefore becomes more important. One of the biggest challenges of FBA in terms of user input is the definition of a biologically relevant objective function. Different objective functions will utilise different pathways. In this study we have chosen to maximise biomass as a suitable objective function. Different phenotypes may be more accurately modelled with more biologically relevant functions, especially with higher organisms. Techniques such as Minimisation of Metabolic Adjustment (MoMA) or Regulatory On-Off Minimisation (ROOM) shows potential in predicting specific phenotypes, since these techniques alter the objective for optimisation (Raman and Chandra, 2009). MoMA utilises the same stoichiometric constrains as FBA, however relaxes the optimal growth rate for mutants by seeking for sub-optimal solutions (Segrè et al., 2002). ROOM serves to minimise the overall

number of significant flux changes from wild-type organisms, therefore favouring flux distributions that only result in high growth rates following gene knockouts.
Despite FBA being able to provide descriptions of metabolism that can enhance current knowledge, FBA focuses on enzymes involved in metabolic reactions. Due to incomplete annotations and optimality assumptions, many reactions do not carry a flux. Such reactions, either upstream or downstream of flux carrying metabolic reactions, have not been characterised. These gaps in our knowledge require further attention for current models to be improved.

With respect to the current scale of GEMs, we have shown how modelling of unicellular model organisms can be beneficial. *Chlamydomonas* is arguably more complex than yeast and the bacterium *Escherichia coli,* which tend to attract more interest. Here the greater scope of understanding how *Chlamydomonas* can regulate photosynthesis is a means towards increasing biofuel production. We have seen how acetate induces activation of the oxidative pentose phosphate pathway (OPPP), which channels excess reductant into the chloroplast whilst providing carbon skeletons for nucleotide synthesis. As a result, photosynthesis switches from a linear mode to a cyclic mode to counteract the excess NAPDH provided by the OPPP yet contributing to a heightened biomass. For algal biofuel yields to be viable, growth strategies that complement current policies to reduce atmospheric carbon must be adhered to. Phototrophic cultures that naturally obtain carbon from the atmosphere for growth remain the natural choice, as they eliminate the cost of supplying inorganic carbon to produce combustible carbon whilst extracting atmospheric CO_2. Knowledge of how supplementary acetate can regulate photosynthesis can lead to novel manipulation strategies that aim to enhance the growth rate of phototrophic cultures of *C. reinhardtii* and improve algal biofuel yields.

With these results in mind, possible manipulation strategies to develop efficient phototrophic processes of biofuel production must be sought. For algal biofuel production to be viable, increased assimilation rates of photosynthetically fixed CO_2 into the Calvin–Benson cycle and into TAGs must be achieved. Just how one can optimise metabolism to direct maximal carbon flux into TAGs whilst still maintaining cell fitness remains the key to this issue and will require a systems biology approach.

Future work should aim to look more closely at the variability and regulation of metabolism to achieve the high mixotrophic growth rates, albeit using CO_2 as a sole carbon source. Alternative metabolic routes that lead to an optimal phototrophic biomass should, in theory, mimic optimised mixotrophic metabolism. One method to investigate this further is with Flux Variability Analysis (FVA). In this study we used FVA to look at reaction essentiality, however FVA can also be used to search for alternative metabolic pathways that can give rise to optimal yields. Using FVA we would be able to investigate metabolic pathways that, active for mixotrophic metabolism, may be operable under phototrophic growth. Once identified, fluxes could be diverted along these pathways, with the addition of constraints to further streamline the flux of carbon into biomass and TAGs.

One such pathway is the Oxidative Pentose Phosphate Pathway (OPPP), which is active under a mixotrophic growth and inactive for phototrophic metabolism. The OPPP results in increased matter entering nucleotide synthesis, supporting an enhanced biomass (Kruger & Von Schaewen, 2003.) To achieve this an incresed partition of flux must first enter gluconeogenesis from the Calvin–Benson cycle. One way in which this can be achieved is through activation of Isocitrate Lyase (ICL) (Plancke et al., 2014). It is apparent that expression of ICL is essential to support a maximal algal growth and we have further predicted that biomass of cells can be increased as the capacity for ICL to carry flux increases (**Figure 4.10**); hence the importance of expression of this enzyme. If photosynthetically fixed carbon flux could be diverted from the Calvin–Benson cycle to biomass using the glyoxylate cycle, facilitated by ICL, more carbon would be retained within biomass. An increased retention of carbon would mean more carbon availability that could be channelled into TAG reserves since ICL bypasses two metabolic steps that release CO_2. Increased carbon fixation and gluconeogenesis would however place further metabolic demands onto the cell that has to be addressed.

To meet these demands, a constant linear electron flow has to proceed, to account for both the production of both reductant and ATP. The challenge here would be to stop the cycling of electrons around photosystem I in which only ATP is produced, as this would be insufficient to meet the demands imposed. To achieve this, the accumulation of reductant would have to be prevented, with the transport of any excessive newly synthesised NAPDH to distinct locations within the cell. This could be further investigated with use of a validated GEM, by

including reactions that account for the traffic of excess NADPH away from where it is produced to sites where it is needed, preventing the toxic build-up of reductant that may kick-start CEF.

Of course, only a truly validated model that takes into account a greater metabolic potential of the genome would be suited for this challenge. The current GEM represents ~6% of the genome, from the latest genome annotation, therefore we are still choosing to ignore ~94% of the known genome. These missing genes may play vital roles in metabolic regulation which are currently ignored. A more accurate and representitive model of algal metabolism would provide the ideal platform to perform the above analysis. To further enhance this model's reliability it should include elements of regulation.

By integrating 'omic data into the model, it is possible to get improved predictions and thereby gain a further insight into the regulation of photosynthesis. We have looked at the proteome of cells treated with and without acetate, yet several other approaches exist and should be explored. Integration of thermodynamic data would reveal which reactions are most likely to occur and in which direction and also presents a convenient way of relating metabolomic data with predicted fluxes. Integration of transcriptomic data, in the form of microarray data or RNA sequencing data, would present another effective way of relating the expression level of a gene to the flux that the corresponding enzyme catalyses. On a simple level, if genes are not expressed under a given condition, the corresponding enzyme flux can be constrained to zero or the gene can be knocked out prior to simulation. On a more advanced level, random sampling methods can be combined with transcriptomic data to find correlations between mRNA levels and associated flux values. With this approach reactions in which high gene expression corresponds with a high flux level can be identified as a transcriptionally controlled reaction and will give further clues about the down-regulation of photosynthesis with acetate. This methodology has been successfully applied to a yeast GEM to identify large subsets of responsible transcription factors that regulate glycolysis and ergosterol synthesis pathways (Österlund et al., 2013). A similar application of this methodology to the current model might identify key transcriptional regulators of photosynthesis. Simulations involving regulatory gene knockdown or over-expression whilst optimising biomass would dictate what 'wet' experiments to conduct. Identification of genes that can influence the growth rate and the reactions of photosynthesis would then require

experimental validation. It is only with a true systems biology approach that phototrophic algal biofuel production can be viable, due to the complexity of photosynthesis and its integrated role with metabolism at the level of the genome.

The aim of this thesis was to investigate the biological mechanisms underlying the down-regulation of photosynthesis as seen with *C. reinhardtii* by integrating genome-scale metabolic reconstructions with *in vivo* and *in vitro* experimental validations. In doing so, we wanted to address the assimilatory route of acetate using a combination of computational and experimental techniques and to identify key pathways of central carbon metabolism that appear to be regulated with acetate.

In **Chapter 1** a GEM of *Chlamydomonas* (*i*RC1080) was used to quantitatively predict the down-regulation of photosynthesis by acetate, using a combination of FBA and FVA to investigate the changes in metabolism that occur when cultures of the alga are grown phototrophically or mixotrophically. The model predicted that the assimilatory route of acetate involved the enzyme acetyl-CoA synthase in a glyoxylate-like TCA cycle within the mitochondria. With these predictions in mind, it is important to discuss if the model can or cannot accurately predict alternative routes for acetate assimilation. For meaningful predictions to be made about the assimilatory route of acetate, acetate must be present within the biomass reaction, as is the case for *i*RC1080. This means that acetate uptake by the model is proportional to the acetate contained within the biomass. However, FBA will not describe the alternative assimilatory routes of acetate assimilation due to the implementation of linear programming used to calculate the fluxes.

As such, FBA will always predict the shortest and simplest pathways to an objective function, presenting another limitation of this method. What can be addressed with FBA however, are the metabolic differences between cells grown with and without acetate. We have investigated this and the model has predicted an increased mitochondrial TCA metabolism facilitated through ICL, increased flux through the OPPP, and a cyclic electron flow associated to the reactions of light-driven photosynthesis with acetate metabolism.

The prediction that acetate induces a cyclic flow of electrons, which is otherwise linear for phototrophic cells, is a correct prediction as this has been experimentally observed (Johnson

et al, 2014). Importantly, the model suggested a non-essential role for cyclic electron flow, which does reflect the known biological response and as such, was able to answer a guiding question of this research project, i.e. it is the action of CEF which accounts for a down-regulation of photosynthesis when cells are supplemented with acetate.

In conclusion, we have successfully demonstrated how experimental and modelling techniques complement each other in addressing complex biological investigations. We have suggested a model that links acetate metabolism to a down-regulation of photosynthesis. We highlight the importance of the OPPP in conjunction with activation of CEF and the importance of ICL that limits cell biomass, although this result requires further experimentation. It is through the use of systems biology that we demonstrate the predictive capabilities of GEMs. Despite the present limitations of FBA, these approaches are essential to gain a further understanding of complex physiological traits that may increase algal biofuel yields.

6. References for Chapters 1 and 5

Allen, J. F. 2003. Cyclic, pseudocyclic and noncyclic photophosphorylation: new links in the chain. *Trends Plant Sci,* 8**,** 15-9.

Almaraz-Delgado, A. L., Flores-Uribe J., Peréz-España, V. H., Salgado-Manjarrez, E. & Badilo-Corona, J. A. 2014. Production of therapeutic proteins in the chloroplast of *Chlamydomonas reinhardtii*. *AMB Express,* 4**,** 57-57.

Alric, J. 2014. Redox and ATP control of photosynthetic cyclic electron flow in *Chlamydomonas reinhardtii*: (II) involvement of the PGR5-PGRL1 pathway under anaerobic conditions. *Biochim Biophys Acta,* 6**,** 825-34.

Baghalian, K., Hajirezaei, M.-R. & Schreiber, F. 2014. Plant metabolic modeling: Achieving new insight into metabolism and metabolic engineering. *The Plant Cell,* 26**,** 3847-3866.

Becker, S. A., Feist, A. M., Mo, M. L., Hannum, G., Palsson, B. O. & Herrgard, M. J. 2007. Quantitative prediction of cellular metabolism with constraint-based models: the COBRA Toolbox. *Nat Protoc,* 2**,** 727-38.

Beevers, H. (1982). Glyoxysomes in higher plants. *Annals of the New York Academy of Sciences*, *386*(1), 243-253.

Boschetti, A. & Schmid, K. 1998. Energy Supply for ATP-Synthase Deficient Chloroplasts of *Chlamydomonas reinhardii*. *Plant and Cell Physiology,* 39**,** 160-168.

Boyle, N. R. & Morgan, J. A. 2009. Flux balance analysis of primary metabolism in *Chlamydomonas reinhardtii*. *BMC Systems Biology,* 3**,** 4-4.

Bruggeman, F. J. & Westerhoff, H. V. 2007. The nature of systems biology. *Trends in Microbiology,* 15**,** 45-50.

Bukhov, N., Egorova, E. & Carpentier, R. 2002. Electron flow to photosystem I from stromal reductants in vivo: the size of the pool of stromal reductants controls the rate of electron donation to both rapidly and slowly reducing photosystem I units. *Planta,* 215**,** 812-820.

Calvin, M. 1962. The Path of Carbon in Photosynthesis. *Angewandte Chemie International Edition in English,* 1**,** 65-75.

Cardol, P., Forti, G. & Finazzi, G. 2011. Regulation of electron transport in microalgae. *Biochimica et Biophysica Acta (BBA) - Bioenergetics,* 1807**,** 912-918.

Chang, R. L., Ghamsari, L., Manichaikul, A., Hom, E. F., Balaji, S., Fu, W., Shen, Y., Hao, T., Palsson, B. O., Salehi-Ashtiani, K. & Papin, J. A. 2011. Metabolic network reconstruction of *Chlamydomonas* offers insight into light-driven algal metabolism. *Mol Syst Biol,* 7**,** 52.

Chen, P., Min, M., Chen, Y., Wang, L., Li, Y., Chen, Q., Wang, C., Wan, Y., Wang, X. & Cheng, Y. 2010. Review of biological and engineering aspects of algae to fuels approach. *International Journal of Agricultural and Biological Engineering,* 2**,** 1-30.

Dal'Molin, C. G., Quek, L. E., Palfreyman, R. W. & Nielsen, L. K. 2011. AlgaGEM-a genome-scale metabolic reconstruction of algae based on the *Chlamydomonas reinhardtii* genome. *BMC Genomics,* 22**,** 1471-2164.

De Oliveria, Dal'Molin, C. G., Quek, L. E., Palfreyman, R. W., Brumbly, S. M. & Nielsen, L. K. 2010. AraGEM, a genome-scale reconstruction of the primary metabolic network in *Arabidopsis*. *Plant Physiol,* 152**,** 579-89.

Dang, K. V., Plet, J., Tollether, D., Jokel, M., Cuine, S., Carrier, P., Auroy, P., Richaud, P., Johnson, X., Alric, J., Allahverdiyeva, Y. & Peltier, G. 2014. Combined increases in mitochondrial cooperation and oxygen photoreduction compensate for deficiency in cyclic electron flow in *Chlamydomonas reinhardtii*. *Plant Cell,* 26**,** 3036-50.

Dent, R. M., Han, M. & Niyogi, K. K. 2001. Functional genomics of plant photosynthesis in the fast lane using *Chlamydomonas reinhardtii*. *Trends in Plant Science,* 6**,** 364-371.

Durot, M., Bourguignon, P.-Y. & Schachter, V. 2009. Genome-scale models of bacterial metabolism: reconstruction and applications. *Fems Microbiology Reviews,* 33**,** 164-190.

Engel, B. D., Schaffer, M., Kuhn Cuellar, L., Villa, E., Plitzko, J. M., & Baumeister, W.

(2015). Native architecture of the *Chlamydomonas* chloroplast revealed by in situ cryo-electron tomography. *eLife*, *4*, e04889. http://doi.org/10.7554/eLife.04889

Ghirardi, M. L., Zhang, L., Lee, J. W., Flynn, T., Seibert, M., Greenbaum, E. & Melis, A. 2000a. Microalgae: a green source of renewable H2. *Trends in Biotechnology,* 18**,** 506-511.

Grovenstein, P. B., Wilson, D. A., Lennox, C. G., Smith, K. P., Contractor, A. A., Mincey, J. L., Lankford, K. D., Smith, J. M., Haye, T. C. & Mitra, M. 2013. Identification and molecular characterization of a novel *Chlamydomonas reinhardtii* mutant defective in chlorophyll biosynthesis. *F1000Res,* 2**,** 2-138.

Gudmundsson, S. & Thiele, I. 2010. Computationally efficient flux variability analysis. *BMC Bioinformatics,* 11**,** 489.

Hankamer, B., Morris, E., Nield, J., Gerle, C. & Barber, J. 2001. Three-Dimensional Structure of the Photosystem II Core Dimer of Higher Plants Determined by Electron Microscopy. *Journal of Structural Biology,* 135**,** 262-269.

Hannon, M., Gimpel, J., Tran, M., Rasala, B. & Mayfield, S. 2010. Biofuels from algae: challenges and potential, *Biofuels*. 2010 Sep;1(5):763-84.

Hanson, D. T., Franklin, L. A., Samuelson, G. & Badger, M. R. The *Chlamydomonas reinhardtii* cia3 mutant lacking a thylakoid, *Plant Physiol*. 2003 Aug;132(4):2267-75. doi:10.1104/pp.103.023481.

Harris, E. H. 2001. *Chlamydomonas* as a Model Organism. *Annu Rev Plant Physiol Plant Mol Biol,* 52**,** 363-406.

Hayashi, Y., Sato, N., Shinozaki, A. & Watanbe M. 2015. Increase in peroxisome number and the gene expression of putative glyoxysomal enzymes in *Chlamydomonas* cells supplemented with acetate. *J Plant Res,* 128**,** 177-85.

Heifetz, P. B., Forster, B., Osmond, C. B., Giles, L. J. & Boynton, J. E. 2000a. Effects of acetate on facultative autotrophy in *Chlamydomonas reinhardtii* assessed by photosynthetic measurements and stable isotope analyses. *Plant Physiol,* 122**,** 1439-45.

Henry, C. S., Jankowski, M. D., Broadbelt, L. J. & Hatzimanikatis, V. 2006. Genome-scale thermodynamic analysis of *Escherichia coli* metabolism. *Biophys J,* 90**,** 1453-61.

Herrgård, M. J., Lee, B. S., Portnoy, V. & Palsson, B. Ø. 2006. Integrated analysis of regulatory and metabolic networks reveals novel regulatory mechanisms in *Saccharomyces cerevisiae. Genome Research,* 16**,** 627-635.

Hill, R. & Bendall, F. A. Y. 1960. Function of the two cytochrome components in chloroplasts: A Working Hypothesis. *Nature,* 186**,** 136-137.

Houille-Vernes, L., Rappaport, F., Wollman, F. A., Alric, J., & Johnson, X. (2011). Plastid terminal oxidase 2 (PTOX2) is the major oxidase involved in chlororespiration in *Chlamydomonas*. *Proceedings of the National Academy of Sciences*, *108*(51), 20820-20825.

Johnson, G. N. 2011. Physiology of PSI cyclic electron transport in higher plants. *Biochim Biophys Acta,* 3**,** 384-9.

Johnson, G. N., Cardol, P., Mingawa, J. & Finazzi, G. 2014a. Regulation of Electron Transport in Photosynthesis. *In:* Theg, S. M. & Wollman, F.-A. (eds.) *Plastid Biology.* Springer New York.

Johnson, X. & ALRIC, J. 2012. Interaction between starch breakdown, acetate assimilation, and photosynthetic cyclic electron flow in *Chlamydomonas reinhardtii. J Biol Chem,* 287**,** 26445-52.

Johnson, X. & Alric J. 2013. Central carbon metabolism and electron transport in *Chlamydomonas reinhardtii*: metabolic constraints for carbon partitioning between oil and starch. *Eukaryot Cell,* 12**,** 776-93.

Johnson, X., Steinbeck, J., Dent, R. M., Takahashi, H., Richaud, P., Ozawa, S., Houille-Vernes, L., Petroutsos, D., Rappaport, F. *et al*, J. 2014b. Proton gradient regulation 5-mediated cyclic electron flow under ATP- or redox-limited conditions: a study of DeltaATpase pgr5 and DeltarbcL pgr5 mutants in the green alga *Chlamydomonas reinhardtii*. *Plant Physiol,* 165**,** 438-52.

Juergens, M. T., Deshpande, R. R., Lucker, B. F., Park, J.J., Wang, H., Gargouri, M., Holguin, F. O., Disbrow, B., Schaub, T., Skepper, J. N. *et al*., 2015. The Regulation of Photosynthetic Structure and Function during Nitrogen Deprivation in *Chlamydomonas reinhardtii*. *Plant Physiology,* 167**,** 558-573.

Kennedy, C. J., Boyle, P. M., Waks, Z. & Silver, P. A. 2009. Systems-Level Engineering of Nonfermentative Metabolism in Yeast. *Genetics,* 183**,** 385-397.

Klein, U., Chen, C. & Gibbs, M. 1983. Photosynthetic Properties of Chloroplasts from *Chlamydomonas reinhardii*. *Plant Physiology,* 72**,** 488-491.

Kruger, N. J. & Von Schaewen, A. 2003. The oxidative pentose phosphate pathway: structure and organisation. *Curr Opin Plant Biol,* 6**,** 236-46.

Machado, D., Cpsta, R., Rocha, M., Ferreira, E., Tidor, B. & Rocha, I. 2011. Modeling formalisms in Systems Biology. *AMB Express,* 1**,** 45.

Mehler, A. H. 1951. Studies on reactions of illuminated chloroplasts: I. Mechanism of the reduction of oxygen and other hill reagents. *Archives of Biochemistry and Biophysics,* 33**,** 65-77.

Merchant, S. S., Prochnik, S. E., Vallon, O., Harris, E. H., Karpowicz, S. J., Witman, G. B., Terry, A., Salamov, A., Fritz-Laylin, L. K., Marechal-Drouard, L., et al. 2007. The *Chlamydomonas* genome reveals the evolution of key animal and plant functions. *Science,* 318**,** 245-50.

Morales-Sanchez, D., Martinez-Rodriguez, O. A., Kyndt, J. & Martinez, A. 2015. Heterotrophic growth of microalgae: metabolic aspects. *World J Microbiol Biotechnol,* 31**,** 1-9.

Orth, J. D., Thiele, I. & Palsson, B. O. 2010. What is flux balance analysis? *Nat Biotech,* 28**,** 245-248.

Osbourne, C. P., Drake, B. G., Laroche, J. & Long, S. P. 1997. Does Long-Term Elevation of CO2 Concentration Increase Photosynthesis in Forest Floor Vegetation? (Indiana Strawberry in a Maryland Forest). *Plant Physiology,* 114**,** 337-344.

Österlund, T., Nookaew, I., Bordel, S., & Nielsen, J. (2013). Mapping condition-dependent regulation of metabolism in yeast through genome-scale modeling. *BMC systems biology*, *7*(1), 36.

Paul, M. J. & Foyer, C. H. 2001. Sink regulation of photosynthesis. *Journal of Experimental Botany,* 52**,** 1383-1400.

Plancke, C., Vigeolas, H., Hohner, R., Roberty, S., Emonds-Alt, B., Larosa, V., Willamme, R., Duby, F., Onga Dhali, D., Thonart, P. *et al.,* 2014. Lack of isocitrate lyase in *Chlamydomonas* leads to changes in carbon metabolism and in the response to oxidative stress under mixotrophic growth. *Plant J,* 77**,** 404-17.

Pospíšil, P. 2009. Production of reactive oxygen species by photosystem II. *Biochimica et Biophysica Acta (BBA) - Bioenergetics,* 1787**,** 1151-1160.

Radakovits, R., Jinkerson, R. E., Darzins, A., & Posewitz, M. C. (2010). Genetic engineering of algae for enhanced biofuel production. *Eukaryotic cell*, *9*(4), 486-501.

Raines, C. A. 2003. The Calvin cycle revisited. *Photosynth Res,* 75**,** 1-10.

Raman, K. & Chandra, N. 2009. Flux balance analysis of biological systems: applications and challenges. *Briefings in Bioinformatics,* 10**,** 435-449.

Resat, H., Petzold, L. & Pettigrew, M. F. 2009. Kinetic Modeling of Biological Systems. *Methods in molecular biology (Clifton, N.J.),* 541**,** 311-335.

Roach, T., Sedoud, A. & Krieger-Liszkay, A. 2013. Acetate in mixotrophic growth medium affects photosystem II in *Chlamydomonas reinhardtii* and protects against photoinhibition. *Biochim Biophys Acta,* 10**,** 17.

Saha, R., Suthers, P. F. & Maranas, C. D. 2011. *Zea mays* iRS1563: A comprehensive genome-scale metabolic reconstruction of maize metabolism. *PLoS ONE,* 6**,** 6.

Santos, F., Boele, J. & Teusink, B. 2011. Chapter twenty-four - A practical guide to Genome-Scale metabolic models and their analysis. *In:* Daniel Jameson, M. V. & Hans, V. W. (eds.) *Methods in Enzymology.* Academic Press.

Sargent, M. C. 1940. Effect of light intensity on the development of the photosynthetic mechanism. *Plant Physiology,* 15**,** 275-290.

Scheibe, R. 2004. Malate valves to balance cellular energy supply. *Physiologia Plantarum,* 120**,** 21-26.

Segrè, D., Vitkup, D. & Church, G. M. 2002. Analysis of optimality in natural and perturbed metabolic networks. *Proceedings of the National Academy of Sciences,* 99**,** 15112-15117.

Smalbone, K., Messiha, H. L., Carroll, K. M., Winder, C. L., Malys, N., Dunn, W. B., Murabito, E., Swainston, N., Dada, J. O., Khan, F. *et al.,* 2013. A model of yeast glycolysis based on a consistent kinetic characterisation of all its enzymes. *FEBS Lett,* 587**,** 2832-41.

Smith, A. M. & Stitt, M. 2007. Coordination of carbon supply and plant growth. *Plant, Cell & Environment,* 30**,** 1126-1149.

Spreitzer, R. J. & Mets, L. 1981. Photosynthesis-deficient mutants of *Chlamydomonas reinhardii* with associated light-sensitive phenotypes, Plant Physiol. 1981 Mar;67(3):565-9.

Steinberg-Yfrach, G., Rigaud, J. L., Durantini, E. N., Moore, A. L., Gust, D. & Moore, T. A. 1998. Light-driven production of ATP catalysed by F0F1-ATP synthase in an artificial photosynthetic membrane. *Nature,* 392**,** 479-82.

Strizh, I. 2008. The Mehler Reaction as an essential link between environmental stress and chloroplast redox signaling. *In:* Allen, J., Gantt, E., Golbeck, J. & Osmond, B. (eds.) *Photosynthesis. Energy from the Sun.* Springer Netherlands.

Stroebel, D., Choquet, Y., Popot, J. L. & Picot, D. 2003. An atypical haem in the cytochrome b(6)f complex. *Nature,* 426**,** 413-8.

Sweetlove, L. J., Beard, K. F., Nunes-Nesi, A., Fernie, A. R. & Ratcliffe, R. G. 2010. Not just a circle: flux modes in the plant TCA cycle. *Trends Plant Sci,* 15**,** 462-70.

Varma, A., & Palsson, B. O. (1994). Metabolic Flux Balancing: Basic Concepts, Scientific and Practical Use. *Bio/technology*, *12*.

Vu, T. T., Stolyar, S. M., Pinchuk, G. E., Hill, E. A., Kucek, L. A., Brown, R. N., Lipton, M. S., Osterman, A., Fredrickson, J. K., Konopka, A. *et al* 2012. Genome-scale modeling of light-driven reductant partitioning and carbon fluxes in diazotrophic unicellular cyanobacterium *Cyanothece sp*. ATCC 51142. *PLoS Comput Biol,* 8**,** 5.

Westerhoff, H. V., Winder, C., Messiha, H., Simeonidis, E., Adamczyk, M., Verma, M., Bruggerman, F. J. & Dunn, W. 2009. Systems Biology: The elements and principles of Life. *FEBS Letters,* 583**,** 3882-3890.

Yizhak, K., Benyamini, T., Liebermeister, W., Ruppin, E. & Shlomi, T. 2010. Integrating quantitative proteomics and metabolomics with a genome-scale metabolic network model. *Bioinformatics,* 26**,** i255-i260.

Zhang, C., Zhang, Y., Zhuang, B. & Zhou, X. 2014. Strategic enhancement of algal biomass, nutrient uptake and lipid through statistical optimization of nutrient supplementation in coupling *Scenedesmus obliquus*-like microalgae cultivation and municipal wastewater treatment. *Bioresource Technology,* 171**,** 71-79.

Zhu, X. G., Wang, Y., Ort, D. R. & Long, S. P. 2013. e-Photosynthesis: a comprehensive dynamic mechanistic model of C3 photosynthesis: from light capture to sucrose synthesis. *Plant Cell Environ,* 36**,** 1711-27.